

## Proceedings of the METNET Seminar 2015 in Budapest



METNET Annual Seminar in Budapest, Hungary, on 13 – 14 October 2015

**Kuldeep Viridi and Lauri Tenhunen (Editors)**

Editors:  
Kuldeep Viridi, Aarhus University  
Lauri Tenhunen, Häme University of Applied Sciences (HAMK)

**Proceedings of the METNET Seminar 2015 in Budapest**

PRINTED

ISBN 978-951-784-762-9  
ISSN 1795-4231  
HAMKin julkaisuja 15/2015

ELECTRONIC

ISBN 978-951-784-763-6 (PDF)  
ISSN 1795-424X  
HAMKin e-julkaisuja 30/2015

© Häme University of Applied Sciences and writers

**PUBLISHER**

Häme University of Applied Sciences (HAMK)  
PO Box 230  
FI-13101 Hämeenlinna, FINLAND  
tel. +358 3 6461  
julkaisut@hamk.fi  
www.hamk.fi/julkaisut

Hämeenlinna, December 2015

# INDEX

Kuldeep Virdi & Lauri Tenhunen <b>PREFACE</b> .....	4
András Jakab, Kinga Nehme & Salem Georges Nehme <b>STABILITY OF CENTRALLY LOADED GLASS COLUMNS</b> .....	7
Markku Heinisuo, Kristo Mela, Teemu Tiainen, Timo Jokinen, Jolanta Baczkiewicz & Marsel Garifullin <b>SURROGATE MODEL FOR ROTATIONAL STIFFNESS OF WELDED TUBULAR Y-JOINTS</b> ....	18
I.M. Kuzmenko, S.N. Markov & V. M. Friedkin <b>BELARUSIAN-RUSSIAN INNOVATION: CREATION OF ENGINEERING STRUCTURES OF THE XXI CENTURY</b> .....	40
László Horváth, Balázs Kövesdi & László Dunai <b>FIRE BEHAVIOUR OF STEEL INDUSTRIAL HALL</b> .....	52
D'yachkov V.V., Devyatov V.V. & Vershinin V.P. <b>EVOLUTION TREND OF REINFORCEMENT CONNECTIONS IN CONCRETE STRUCTURES</b> ...	62
Anatoly Perelmutter & Vitalina Yurchenko <b>ON THE ISSUE OF STRUCTURAL ANALYSIS OF SPATIAL SYSTEMS FROM THIN-WALLED BARS WITH OPEN PROFILES</b> .....	68
Tarja Meristö & Jukka Laitinen <b>RESOURCE-WISE SOLUTIONS – A KEY TO SUCCESSFUL FUTURE BUSINESS</b> .....	81
Lukáš Ledecký, Yvonne Ciupack, Hartmut Pasternak, Christoph Mette, Elisabeth Stammen & Klaus Dilger <b>ADHESIVE BONDED STEEL STRUCTURES UNDER CYCLIC LOADING</b> .....	90
Mikko Långvik, Kauko Jyrkäs, Antti Markkula & Meri Rosenberg <b>NEW T-BEND TESTING METHOD TO EXAMINE FORMABILITY OF COLOR COATED STEEL SHEET IN DIFFERENT TEMPERATURES</b> .....	102
Marsel Garifullin, Alexey Sinelnikov, Maria Bronzova & Nikolai Vatin <b>BUCKLING BEHAVIOR OF PERFORATED COLD-FORMED COLUMNS</b> .....	112
Alexander Danilov & Olga Tusnina <b>THE EFFECT OF RIVETS APPLICATION ON THERMAL CHARACTERISTICS OF SANDWICH PANEL ROOFINGS</b> .....	124
Kuldeep S. Virdi <b>COLUMN BUCKLING CURVES FOR HIGH STRENGTH STEEL</b> .....	131
Olli Ilveskoski <b>STABILIZATION OF STEEL STRUCTURES BY SANDWICH PANELS</b> .....	139

## PREFACE

The knowledge-based innovation network (METNET) was established to strengthen the regional innovation systems on engineering applications of metals and fostering economic growth in Europe.

The aims of the METNET network are:

1. to consolidate the expertise and efforts of the regional steel construction and technology industries in research and development, and
2. to share knowledge and technology services as well as new production-related solutions and operating models among the industry players.

Recognising the strength of international cooperation networks in contributing to regional innovation systems, the METNET knowledge-based network was first formally established by signing an agreement between eight foundation members in Berlin on 2 November 2006. The METNET knowledge-based network is based on voluntary cooperation and equality of rights for its members. Currently, the METNET network has over 40 members from 17 countries all over Europe including non-member states of the European Union such as Russia, Ukraine, Belarus and Turkey. These members are universities, higher education institutions and research institutions and enterprises who represent their regional innovation networks. Each regional innovation network has its own priorities and strengths.

The specific objectives of the METNET knowledge-based network are as follows:

- to build and maintain a large scale international innovation environment for the network members and their regions,
- to promote the exchange of information and best practices through the network to increase the know-how of companies and organisations operating in the European steel construction and technology industry,
- to support innovative processes aimed at developing new products, services and business processes by sharing capabilities, expertise and resources among network members,
- to prepare and launch joint international projects of common interest financed by companies, European Union, World Bank etc.,
- to hold international seminars, workshops, training programmes, and consultation and to seek funding for these activities.

Cooperation in research and innovation activities has become the highest priority issue for the regional development authorities in many EU countries. The completion of the European Research Area (ERA) by 2014 was at the top

of the political and legislative agenda of the European Union (EU), as it would be an area of free movement and exchange of research, scientific knowledge and technology (Chou, 2014).

Planning, preparing and managing joint international projects are the most important and most demanding activities of the METNET network. The network members have prepared and submitted several project applications for the EU funding. One recently completed international project is called Ruoste (financed by the Research Fund of Coal and Steel RFCS). A current project is called UNICO (financed by the Nordic-Russian program of EU). New projects in the same technical area are under preparation. Additionally, METNET members have participated in several Finnish national projects managed by HAMK.

International networking facilitates learning that promotes innovation. Through the channels of the METNET network, network members are able to use more of the information available in their research and development work. Importantly, enterprises are able to acquire new knowledge, new development and business opportunities and access to resources outside their regions. (Boekema et al., 2000).

Interpersonal relationships are of particular importance in the exchange of information between the network members. The achieved long-term trustful relationships stimulate interactive learning and inspire joint development work. In turn, joint projects developed by the members of the network maintain the METNET cooperation.

The METNET annual conferences and workshops have taken place in different countries and have been organised in cooperation with the regional network members. The Budapest University of Technology and Economics (BME) hosted the Tenth METNET International Conference in October 2015.

Papers presented at the seminar covered aspects of analysis, design and experimental investigations of metal structures and structural elements. One paper developed the stiffness matrix of a thin-walled member using an extra degree of freedom in setting up the stiffness matrix. Another paper dealt with the defining of the moment-rotation characteristics of connections in welded tubular Y-joints so as to speed up the optimisation process of structures using tubular members. Fire behaviour of entire steel frame of an industrial hall was discussed in the presentation from the host organisation. Instability and buckling was the topic of several papers covering perforated cold form columns and beams, centrally loaded glass columns, as well columns made of very high strength steel. Among the papers describing experimental results were one dealing with formability of paint-coated steel sheets and one dealing with adhesive bonding of metal structures focusing on the fatigue behaviour. Another paper considered use of stressed skin approach towards stabilising steel frames using sandwich panels. A number of innovative applications of metal structures were described in yet another paper.

The cumulative effects of utilising the possibilities of an international cooperation network, instead of the regional innovation network only, will produce significant increases in the economic value added of enterprises (Tenhunen, 2007). One paper considered the warping of thin-walled members using an extra degree of freedom, relating

Kuldeep Viridi and Lauri Tenhunen

## REFERENCES

Boekema, F., Morgan, K., Bakkers, S. & Rutten, R. (2000). Introduction to Learning Regions: A New Issue for Analysis? In F. Boekema, K. Morgan, S. Bakkers, & R. Rutten (Eds.), *Knowledge, Innovation and Economic Growth. The Theory and Practice of Learning Regions*. Cheltenham, UK: Edward Elgar.

Chou, M.H. (2014). The evolution of the European research area as an idea in European integration. In *Building the knowledge economy in Europe: New constellations in European research and higher education governance* (pp. 27-50). Cheltenham, UK: Edward Elgar.

Tenhunen, L. (2007). How international collaboration benefits companies – Evaluation of the scale effects of an expanding innovation environment. Cases InnoSteel and Metnet. In T. Similä-Lehtinen (Ed.), *InnoSteel – True Stories Made Out of Steel*. HAMK Publications, 10.



# STABILITY OF CENTRALLY LOADED GLASS COLUMNS

**András Jakab**

PhD Student, Department of Construction Materials and Technologies,  
Budapest University of Technology and Economics, Budapest, Hungary  
jakab.andras@epito.bme.hu

**Kinga Nehme**

Associate Professor, Department of Civil Engineering, University of Debrecen, Debrecen, Hungary;  
Owner of Struktúra Ltd, Budapest, Hungary

**Salem Georges Nehme**

Associate Professor, Head of the Laboratory, Department of Construction Materials and Technologies,  
Budapest University of Technology and Economics, Budapest, Hungary

## ABSTRACT

Although glass can be applied in load bearing structures due to the development of glass strengthening procedures, it remains still fragile. Glass walls can be supported by glass fins against wind load, as well as a slab can be supported by glass columns. However the appropriate question is where can be found the limit of the load bearing capacity of the glass columns. This paper focuses on the stability issues. More than 120 scaled-size specimens were loaded under compression to study the buckling behaviour of glass columns with flat shaped cross-section. Laboratory experiments were carried out at the BME, Department of Construction Materials and Technologies. Laminated glass consisted of different glass layers (e.g. variable thicknesses, type of glass layers etc.) were compressed by concentrated load. The loading force and displacements were measured. Increment method was applied to study and determine the Serviceability Limit State (SLS) based on horizontal displacement results. The experimental results were studied to find the relationship between the type of buckling and the glass columns. Based on laboratory experiments and theoretical calculations the influencing factors on critical force and buckling behaviour of glass columns were studied. The authors draw attention to the difficulties of design of glass columns.

**Keywords:** glass column, buckling, load bearing glass, stability, transparency, compression

## INTRODUCTION

Glass is called also the material of the third millennium. Although glass is a brittle material, its brittleness has been a well-known property alongside its transparency (Pankhardt et al. 2012 – [8]). This paper focuses on the buckling behaviour of the load bearing glass elements, especially glass

columns. Laboratory tests were carried on axially compressed glasses in the BME, Department of Construction Material and Technologies. Based on the laboratory experimental results, influence of several physical properties of glass columns were compared to each other e.g. effect of the rate of loading, heat strengthening, effect of the different height of the specimen and the effect of the lamination with total thickness of 12 mm (single layer glasses, and laminated glasses consist two, and three layers) on the behaviour of glass columns. Three different stages were determined and introduced in the buckling behaviour of glass columns. The critical buckling force was studied based on the international theoretical results and the laboratory tests (Nehme and Jakab and Nehme 2013 [6]).

Continuing the previous laboratory research, the stability and design methods of glass columns were studied based on the existing calculation method for reinforced concrete. Hence the described topic is reviewed according to the book of prof. László Palotás – The Theory of Reinforced Concrete (Palotás 1973 – [7]).

## LABORATORY TESTS

### Test parameters

Laboratory experiments were carried out to study the buckling behaviour of single and laminated glass columns. The specimens were tested using an Instron 5989 testing machine. The scale of the geometry of specimens (height, thickness, width) was selected on the basis of existing glass columns from international and Hungarian realized projects. Test parameters of glass specimens were the following:

Constants: test arrangement, the type of support; width of glass (80 mm); interlayer material (EVA foil with thickness of 0.38 mm); edgework; temperature ( $+23 \pm 5$  °C). Variables: type of glass layers: HSG/ non heat-treated Float; height of specimens: 1000 mm; 920 mm; 840 mm; number of glass layers and the thickness of specimens: single layer: 8 mm; 12 mm, laminated: 4.4 mm; 6.6 mm; 8.4 mm, laminated: 4.4.4 mm; The rate of loading: 0.5 mm/min; 1 mm/min. Support: Height of fixing: 95 mm; rubber plate (Shore A 80) was used between the steel supports and the glass. Simplified designation is used to distinguish the studied specimens, these are e.g. H\_2(4.4)\_2\_920\_0.5: ~ H, F: Type of glass: H – HSG; F – non heat-treated float glass; 2(4.4): Number of glass layers ex.: 4.4 mm laminated glass; 2: The number of specimen; 920: Nominate height of specimen [mm]; 0.5: Rate of loading [mm/min]. Abbreviations are used for the float laminated glass VG and for heat-strengthened laminated glass VSG. (Nehme and Jakab and Nehme 2013 – [5]).



### Experimental test set-up

The load and vertical displacement of the upper cross-head of the Instron 5989 universal testing machine were continuously measured. At three different heights the buckling displacement (horizontal displacement) of all specimens were continuously measured with HBM displacement transducers during the tests. Strains at centre point on the surface of the glass panels were measured with HBM LY11-10/120 strain gauges. The tests were carried out at a room temperature ( $+23 \pm 5$  °C). At least three specimens were tested for each testing combination. Laminated specimens were loaded until all glass layers were fractured. In total, 120 specimens were tested.



Figure 1. Illustrates the test set-up. (Nehme and Jakab and Nehme 2013 – [5])

## PHENOMENON OF FLEXURAL BUCKLING

### Flexural Buckling in Principle

Axially loaded columns start to deform without horizontal displacement at the beginning of the loading process. Damping material (rubber min. SHORE 80) is recommended to apply between the glass and the supporting steel surfaces. Therefore, the vertical displacement contains the deformation of the glass and the damping material as well. When the compression load reaches a critical value, the buckling of the column begins. This force is called critical buckling force ( $N_{cr}$ ). In the first stage of the buckling process the loaded element can be unloaded without visible residual deformations. It should be noted that, in case of glass single layer columns, residual deformations do not occur after the critical buckling force. Until the loading force is increased up to the

critical buckling force, it is mainly a stability problem (SLS- Serviceability Limit State of the columns). After reaching the critical buckling force, post-critical stages follow. In the case of further increase of the loading force, the column reaches the Ultimate Limit State (ULS), where the risk of the whole construction failure is significant. Significant displacements can be observed between SLS and ULS, which serves as a reserve of the glass column in the post-critical stages. The critical buckling force calculated with the application of the Euler formula was used as follows:

$$N_{cr} = \frac{\pi^2 EI}{(\nu L)^2} \quad (1)$$

This formula includes physical properties of the structural element. However, the critical buckling force is sensitive to variation in the effective length factor. This factor can have different values depending on the shape of the buckled elements. Figure 2 introduces general buckled shape with the value of the effective length factor. (Jakab and Nehme and Nehme 2014 – [3]).

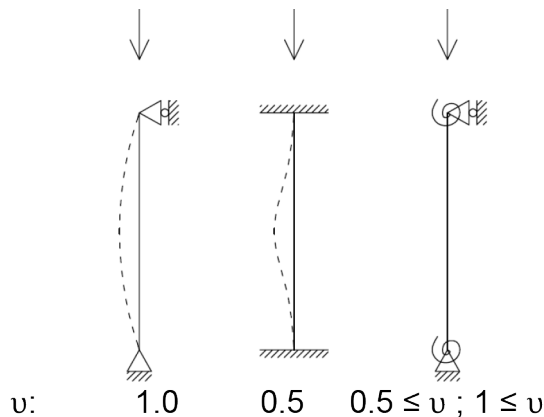


Figure 2. Critical buckling shape and the effective length factor.

The effective length factor in real glass columns is about 1.0. The damping material causes displacement in the supports in case of glass, - and functions like a spring in the fixings – hence the real effective length factor can be more than the value 1.0. The effective length factor varies during the loading process. Until the SLS the effective length factor approaches the value 1.0 (it functions rather like a pinned support) and after the SLS it reduces. The buckling of the specimen causes more fixity in the supports, that is, it functions rather like a fixed support.

### Grouping of the Glass Specimens

Characteristic curves are represented as loading force vs. displacement (vertical, horizontal and deformations) diagrams to study the laboratory experimental results. Curves are categorized in three separate groups according to the experimental results. Variation can be noticed in case of loading force vs. horizontal displacement diagrams. In case of the categorization, the variables are not considered e.g.: different heights, thickness etc. The grouping depends on the stages of the loading history of the specimens. The names of stages are:

1. First stable stage;
2. Unstable stage;
3. Second stable stage.

The first Group contains all of previously mentioned stages. Specific buckling point cannot be determined in case of the second Group, the unstable stage does not appear. Only one stable stage can be observed in case of the third stage. The load histories of the different Groups are introduced in the Figure 3.

The critical buckling forces can be determined by the incremental method, where the horizontal displacement increments are studied. The distribution of the groups are shown in percentage terms in Figure 4. The second Group occurs in the most cases. (Jakab and Nehme and Nehme 2015 – [4]).

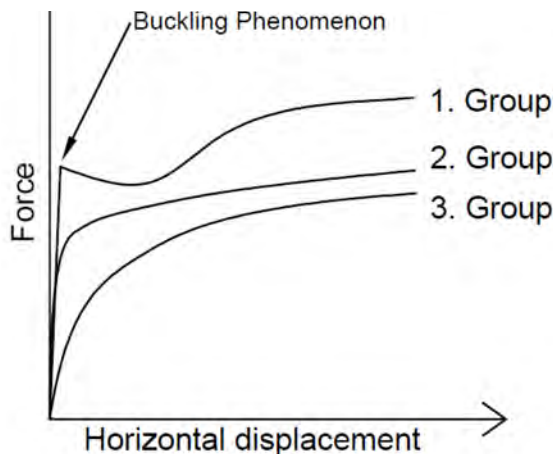


Figure 3. Horizontal displacement vs. Force diagram of the Groups.

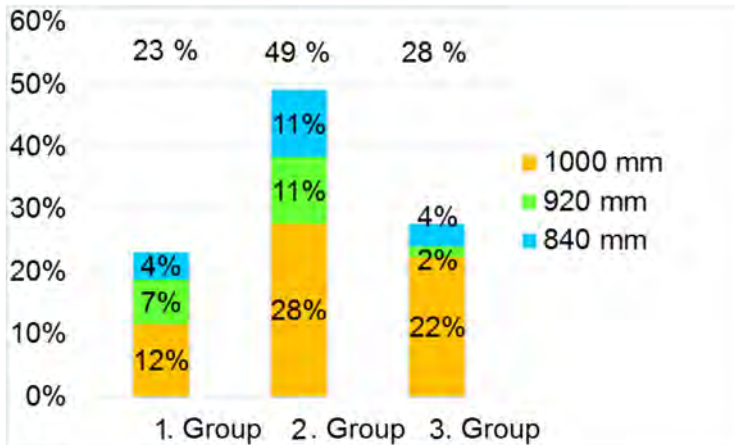


Figure 4. Grouping of the glass columns in aspect of the buckling phenomenon.

### Basic Principles of Stability

According to Palotás, the first problem is the Young's modulus in case of reinforced concrete, because at the starting moment the diagram of  $\sigma$ - $\epsilon$  is curved so it must be treated rather as a plastic state. However, this diagram of glass is a straight line, that is, the behaviour is ideally elastic. After the critical buckling force, the flat shaped column starts to buckle when one side starts to unload while the other is more loaded. The first will be the tension side, the second will be the compression side. In case of concrete the unloading and the loading will occur by different Young's modulus, however due to the equilibrium equations the two sides have to be balanced according to Engesser-Jaszinszkij-Kármán (Figure 5.). This equation provides an upper limit of critical buckling force. (Palotás 1973 – [7])

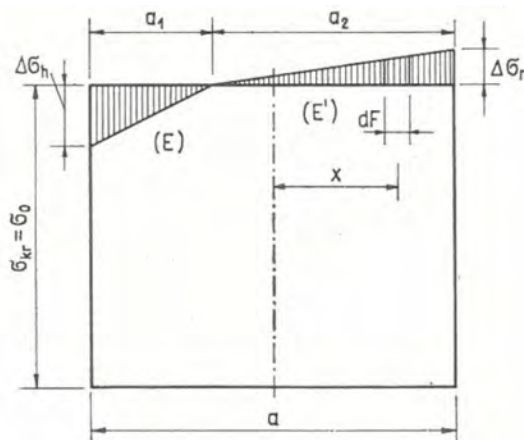


Figure 5. Stress distribution in the middle of the specimen at the cross-section after buckling according to Engesser-Jaszinszkij-Kármán (Palotás 1973 – [7]).

$$N_{cr,E-J-K} = \frac{\pi^2 T I}{(\nu L)^2} \quad (2)$$

Equation 2 is similar to the basic Euler critical buckling force formula (1), however  $T$  is a substitute buckling Young's modulus, which contains the loading and the unloading Young's modulus. According to Engesser-Shanley, immediately after the buckling moment a small bending stress appears before the stress changing (unloading at the tension side). The stress distribution is shown in Figure 6, where  $\sigma_0$  is the basic compressive stress, " $a$ " is the width of the column, the infinitesimal bending stress is  $\Delta\sigma$  and the  $E'$  is the actual and corresponding Young's modulus (Formula 3). This method provides a lower limit for critical buckling force. (Palotás 1973 – [7])

$$N_{cr,E-S} = \frac{\pi^2 E' I}{(\nu L)^2} \quad (3)$$

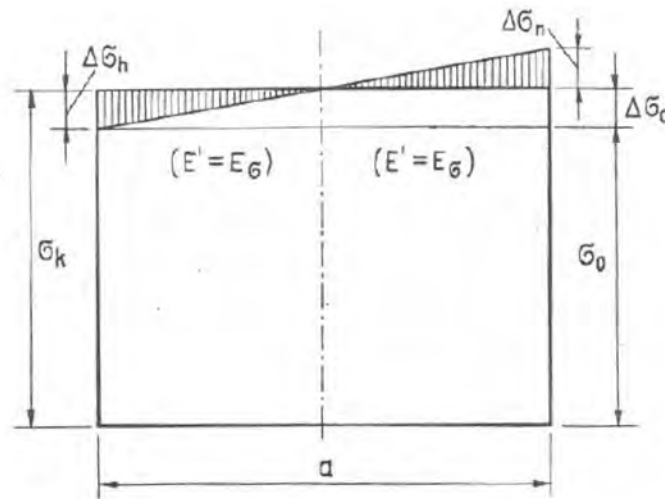


Figure 6. Stress distribution in the middle of the specimen at the cross-section after buckling according to Engesser-Shanley (Palotás 1973 – [7]).

In the case of single layer glass the Young's modulus is the same at the loading and unloading processes, hence the formula is the same as the basic Euler formula (1). From the buckling moment the bending stress increases faster than the basic compressive stress.

## EFFECT OF THE INITIAL ECCENTRICITY

The initial curvature of the glass columns can influence significantly the critical buckling forces according to the earlier studies of the authors (Jakab and Nehme and Nehme 2015 – [4]). Engineers cannot neglect the effect of the initial eccentricity of the structures in the design. The incidence of buckling increases with the increase in the initial eccentricity that is magnified due to the effect of loading. The reinforced concrete structures have also initial eccentricity, regardless of being pre-cast or monolithic structure. In the case of glass the float glass also contains minimal initial eccentricity, however the heat strengthening processes increase it due to the specific procedure.

The critical buckling force decreases in case of more slender ( $\lambda$ ) reinforced concrete columns and the decreasing of the concrete quality (the strength of the applied concrete). It is justified by the different Young-module of different concretes. However the quality (or Young's modulus) of the glass can change due to the glass imperfections and the raw materials. The Equation 4 introduces the relative initial eccentricity:

$$m_0 = A + B \left( \frac{\lambda}{100} \right)^2 \quad (4)$$

Where  $m_0$  ( $m_0 = \frac{e_0}{k}$ , where  $e_0$  is the initial eccentricity, and  $k$  is distance of the core point) is the eccentricity of the core point. "B" is a random eccentricity from the non-slender shape. "A" depends from the material quality and inhomogeneity. The critical buckling force barely changes in the range 60-80 of the slenderness of reinforced concrete column according to Gehler 1938. In case of glass are more slender columns for instance the specimens tested (Figure 8-9). The buckling reduction factor ( $\alpha_0$ ) is needed for the calculation:

$$\alpha_0 = \frac{1}{1+v_0^2} \quad (5)$$

Where  $v_0$  contains the effect of the slenderness, permanent loads and the initial eccentricity. The diagram of the buckling reduction factor and slenderness is needed to simplify the calculation method for the buckling structures, where the buckling reducing factor ( $\alpha_0$ ) decreases if the initial eccentricity factor ( $m$ ) increases. In the future the authors would like to determine this diagram for glass columns. (Figure 7, Palotás 1973 – [7])



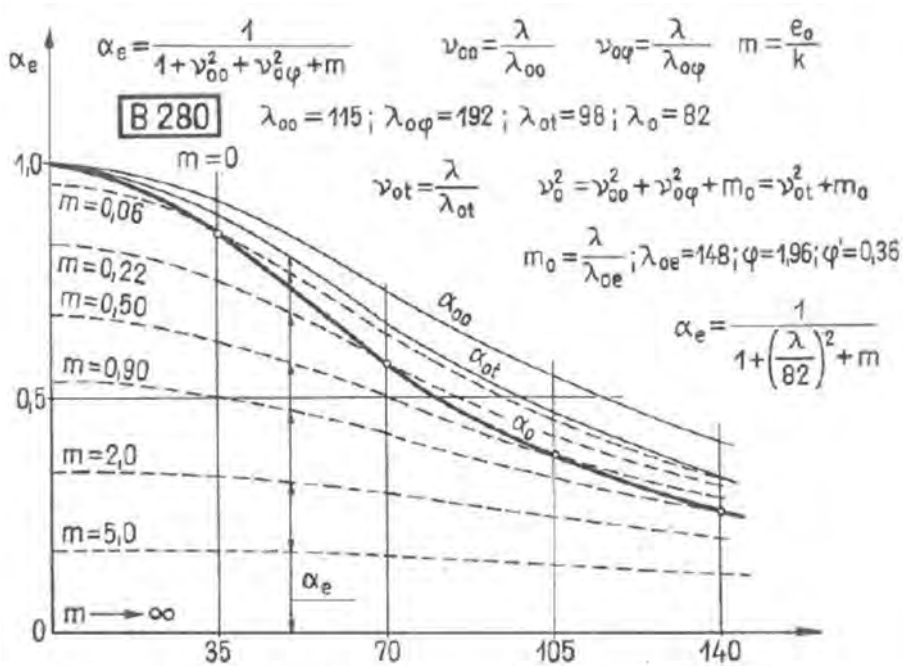


Figure 7. Critical buckling shape and the effective length factor (Palotás 1973 – [7]).

## CALCULATION RESULTS

### Slenderness and the Critical Buckling Force

The critical buckling forces were not well determined values in each case according to earlier studies (Jakab and Nehme and Nehme 2015 – [4]). Hence the critical buckling force of the third group cannot be taken into account to compare the experimental and calculated values. For instance the authors prefer to ignore the 10 mm thick specimens in case of single layer glass.

### Single Layer Float Glass

To compare the experimental results a common effective length factor must be determined. 1.0 value was chosen in the present paper. The theoretical calculation of the effective length factor is comparable in the case of single layer glass and laminated glass based on the experimental results (Nehme and Jakab and Nehme 2013 – [6]). Figure 8 indicates the slenderness of the tested glass columns vs. critical buckling force. The mean results of specimens are in same position as the results which correspond to the effective length factor value 1.0, which means that the supports are rather pinned. The nominal thicknesses are also indicated in Figures 8 and 9.

### Laminated Float Glass

In the case of laminated glass, significant difference can be observed in the buckling behaviour. The laboratory experimental results of laminated glass consist of two glass layers, - thickness of 4.4; 6.6; 8.8 mm - indicating a more fixed supporting state. Although it means the supports are stiffer, the test set-up did not vary. The changes are justified by the effects of the interlayer material. When calculating the limit curve of the critical buckling load, the effect of the interlayer material cannot be taken into account and the border curve will be lower located than the experimental mean results. When the inertia decreased the slenderness increased due to the interlayer material if it is compared to the single layer glasses. In the laboratory experiments short term loading was applied (loading rate of 0.5 mm/min). In the future it is suggested to study the stress sharing effects in the case of long term loading (Figure 9).

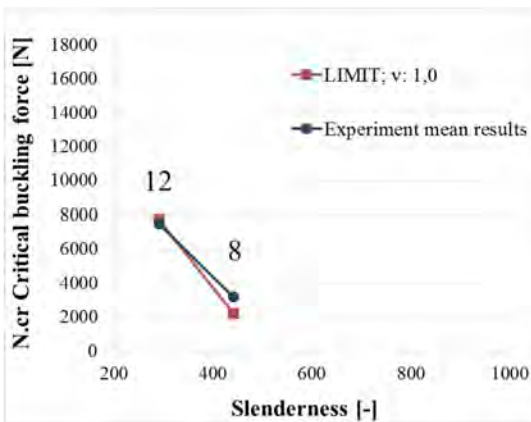


Figure 8. Slenderness vs. Critical buckling force in case of single layer glasses.

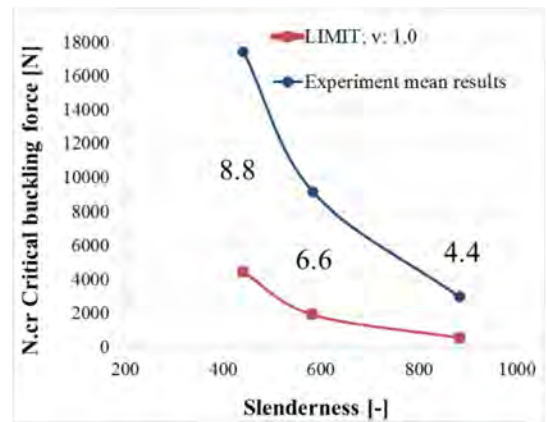


Figure 9. Slenderness vs. Critical buckling force in case of laminated glasses.

## CONCLUSIONS

Three different stages can be distinguished in the buckling behaviour of glass columns. However, the 2<sup>nd</sup> Stage may be missing depending on the initial shape and stiffness of the supporting system. At the buckling moment the stress distribution is similar to the Engesser-Shanley theorem, that is, it is linear. The critical buckling force decreases in case of more slender columns and the decreasing of the glass quality (e.g. the strength of the applied glass). The range of the effective length factor in the reality of a glass columns varies about 1.0. Although the damping material causes displacement in the supports, the real effective length factor can be taken as 1.0. The critical buckling forces of the single layer glass are closer to the calculated values because the basic Euler formula does not calculate with the effect of interlayer foil.

## ACKNOWLEDGEMENT

Authors express their gratitude to Rákosy Glass Ltd. for providing the specimens. Authors are thankful to the Department of Construction Materials and Technologies, BME and Mr. A Eipl (Struktúra Ltd.) and Mr. P Molnár (Struktúra Ltd.) for their technical support.

## REFERENCES

- [1] Gehler, W. 1938: Hypotesen u. Grundlagen f. d. Schwinden u. Kriechen d. Betons. Baut. 1938. 5. 16.
- [2] Jakab A, Nehme K, Nehme S G 2014 Fracture Behaviour of Glass columns (Düsseldorf: Glasstec Engineered Transparency, ISBN:978 3 86780 402 8)
- [3] Jakab A, Nehme K, Nehme S G 2014 Fracture Behaviour of Glass Columns. Experimental Study of Axial Loaded Glass Columns (Iccmtp3 – Abstract)
- [4] Jakab A, Nehme K, Nehme S G 2015 Laboratory Experiments of Centrally Loaded Glass Columns (GPD – Glass Performances Days 2015, Tampere, Finland, ISBN: 978-952-5836-03-5)
- [5] Nehme K, Jakab A, Nehme S G 2013 Experiments on the Buckling Behaviour of Glass Columns Part 1. (Budapest: Építőanyag 65/3 <http://dx.doi.org/10.14382/epitoanyag-jsbcm.2013.13>)
- [6] Nehme K, Jakab A, Nehme S G 2013 Experiments on the Buckling Behaviour of Glass Columns Part 2. (Budapest: Építőanyag 65/4 <http://dx.doi.org/10.14382/epitoanyag-jsbcm.2013.21>)
- [7] Palotás L. 1973: The Theory of Reinforced Concrete (A Vasbeton Elmélete – Akadémiai Kiadó), Budapest
- [8] Pankhardt K 2012 Load Bearing Glasses. Testing of Constuction Glasses (Saarbrücken: Lap Lambert, ISBN: 978 3 8473 2191 0)

# SURROGATE MODEL FOR ROTATIONAL STIFFNESS OF WELDED TUBULAR Y-JOINTS

**Markku Heinisuo, Kristo Mela, Teemu Tiainen, Timo Jokinen**

Tampere University of Technology

**Jolanta Baczkiewicz**

Poznan University of Technology

**Marsel Garifullin**

Peter the Great St.Petersburg Polytechnic University

When designing tubular structures using semi-rigid joints between members, the rotational stiffness is the most important stiffness parameter of the joint. The initial in-plane rotational stiffnesses with different layouts of the welded tubular Y-joints are defined using the surrogate model (meta model). The sample and validation points are defined using comprehensive non-linear finite element analysis in ABAQUS. The ABAQUS models were validated with the tests of K-joints of high strength steel (HSS) cold-formed tubular members. Several brace/chord combinations are studied and the goal is to cover the most important practical cases appearing in buildings. The local joint rotations were derived from the ABAQUS results by subtracting the rotations due to the beam deformations from the ABAQUS rotations. Finally, DACE toolkit of Matlab was used to define the surrogate model.

## INTRODUCTION

Tubular structures with welded joints are used in the wide range of structural applications. The most typical application is tubular trusses. The structural analysis model is frequently constructed using beam finite elements, and the braces are connected to the chords using hinges. In reality, the welded joint does not behave as a hinge when it is loaded by the moment. The joint has resistance against the moment, but in the joint area deformations may occur both at the brace and at the chord, so the stiffness against the moment has to be taken into account in the global analysis of the structure. In the Eurocode (EN 1993-1-8) only the moment resistance is given for the joint where the angle between the brace and the chord is 90 degrees. In (Grotmann and Sedlacek 1988) there is the equation which can be used to calculate the initial rotational stiffness for the same case, angle 90 degrees.

When aiming to economic and environmental friendly design the stiffness of the joints must be taken into account. This is especially true when using high strength steel in structures, because then buckling at the ultimate limit state and deflections and vibrations in the serviceability limit state are often critical.

In (Boel 2010) and (Snijder et al. 2011) it has been shown that the rotational stiffness of the welded tubular joint is the main parameter when considering buckling of members of tubular trusses. However, this information is very limited, as given above.

In design it is possible to define the rotational stiffness for the joint using comprehensive finite element analysis (FEA). In practice, this is impossible, especially when performing optimization of structures when the structural analysis must be done thousands and thousands times. In order to avoid these computationally heavy calculations so called surrogate models (or meta models) have been developed. Surrogate models have been used widely in the aerospace applications (Roux et al. 1998), (Jin et al. 2001), (Queipo et al. 2005), (Kleijnen 2008), (Müller 2012). Civil engineering applications can be found, too (Mukhopadhyay et al. 2015). In (Díaz et al. 2012) there are 9 references presented (Yun et al. 2008), (Jadid and Fairbairn 1996), (Anderson et al. 1997), (Stavroulakis et al. 1997), (De Lima et al. 2005), (Guzelbey et al. 2006), (Pirmoz and Gholizadeh 2007), (Salajegheh et al. 2008), (Kim et al. 2010) dealing with steel structures using surrogate models. In (Díaz et al. 2012) the optimum design of steel frames is presented using semi-rigid joints and surrogate models.

The standard steps in the construction of the surrogate model are:

- Design of experiments (DOE);
- Surrogate model construction;
- Surrogate model validation.

Moreover, the fourth step is the fidelity validation, but it is not needed here.

## DESIGN OF EXPERIMENTS

The method for determining the sample points to carry out an analysis is called Design of Experiments (DOE). The location of the sample points is very important for generation of an accurate surrogate model. It consists of a compromise between the usage of a reasonable number of sample points to build an accurate model. Several DOE methods are described in (McKay et al. 1979), (Fang et al. 2006) and (Montgomery 2012). The Latin Hypercube Sampling (LHS) proposed by (McKay et al. 1979) is the most popular space filling sampling technique. In this research engineering justification is used for the definition of the sample points. This technique may mean satisfactory results because the graphs of the initial rotational stiffness indicate rather smooth behavior. The sample points cannot violate any of the requirements of the standards (EN 1993-1-8) and the values are rounded to the nearest possible value, for e.g. member size. In this research Eurocodes are used and give rather strict rules for the variables of the problem.

## SURROGATE MODEL CONSTRUCTION

In the surrogate model construction we replace the computationally expensive function  $f(x)$  by a sum of two other functions ( $x$  is the vector of the variables (Müller 2012)):

$$f(x) = s(x) + \varepsilon(x) \quad (1)$$

where  $s(x)$  is the surrogate model at the point  $x$  and  $\varepsilon(x)$  is the difference between the two. The idea is to use the function  $s(x)$  during the calculations or optimization instead of the function  $f(x)$ . The function  $s(x)$  is chosen so that it is cheap to evaluate, and thus the computation times can be reduced considerably.

We can start with a quadratic regression model:

$$s_p(x) = \beta_0 + \sum_{i=1}^k \beta_i x_i + \sum_{i=1}^k \beta_{ii} x_i^2 + \sum_{i=1}^{k-1} \sum_{j=i+1}^k \beta_{ij} x_i x_j \quad (2)$$

or with linear regression ( $\beta_{ij} = 0$ ) or with constant, only  $\beta_0 \neq 0$ . If this gives good results (see later criteria) then we can add to the regression a *predictor*  $Z(x)$  (stochastic process) and end up to Kriging.

Kriging is named after the pioneering work of D.G. Krige (a South African mining engineer), and was formally developed by (Matheron 1963). In (Sacks, Schiller, et al. 1989; Sacks, Welch, et al. 1989) and (Jones et al. 1998) it was made well-known in the context of the modelling, and optimization of deterministic functions, respectively. The Kriging models consist of two components. The first component is some simple model that captures the trend in the data, and the second component measures the deviation between the simple model and the true function. An example of the surrogate model  $\bar{f}(x)$  using Kriging with one variable  $x$  with  $n$  sample points is:

$$\bar{f}(x) = \frac{\sum_{j=1}^n x_j}{n} + Z(x) \quad (3)$$

where the zero order regression is used and the predicted value  $\bar{f}(x)$  is given scaled to  $[0;1]$ . The real values  $f(x)$  can be calculated from the normalized data  $\bar{f}(x)$ . In the construction of  $Z(x)$  we need a *correlation function* between points. Define  $R$  as the matrix  $R$  of stochastic-process correlations between the sample points  $x_i$  and  $x_j$ :



$$R_{ij} = R(\theta, x_i, x_j), \quad i, j = 1, \dots, n \quad (4)$$

and let  $\bar{r}(x)$  be a vector of correlation between sample points and untried points  $x$ :

$$\bar{r}(x) = [R(\theta, x_1, x) \dots R(\theta, x_n, x)]^T \quad (5)$$

The mostly preferred correlation function is the Gaussian correlation:

$$R(x_i, x_j) = \exp \left[ - \sum_{k=1}^m \theta_k |x_i^k - x_j^k|^2 \right] \quad (6)$$

where

- $\theta_k$  are unknown correlation parameters,  $k = 1, \dots, m$ ;
- $m$  is the number of design variables;
- $x_i^k$  and  $x_j^k$  are components of samples  $x_i$  and  $x_j$ .

After this the surrogate model can be defined, see e.g. (Müller 2012).

## SURROGATE MODEL VALIDATION

The validation process uses a new sample size approximately equal to one third of the sample size used to build the surrogate model (Lee and Jung 2006). The validation process consists of comparing the results of the surrogate model with those of the real response. This is a specific problem which depends on the accuracy required of the fitted model. If this accuracy is too low, then the surrogate model must be modified by the introduction of more sample points or by the modification of the surrogate model variables.

The accuracy of the surrogate model can be checked (Díaz et al. 2012) using  $R^2$  value. It consists of calculating the square of the difference between the real response and surrogate model results divided by the difference between the real response results and the mean of the observed values. The larger the value of  $R^2$ , the more accurate is the surrogate model. The validation process consists of using a new set of sample points, but excluding the original sample point set.

$$R^2 = 1 - \frac{\sum_{i=1}^r (y_i - \bar{y}_i)^2}{\sum_{i=1}^r (y_i - \bar{y})^2} \quad (7)$$

where  $y_i$  is the real response value,  $\bar{y}_i$  is the surrogate predicted value at the  $i$ th validation point,  $\bar{y}$  is the mean of the validation point values, and  $r$  is number of validation points.

No single rule exists that specifies a minimum  $R^2$  value which guarantees a good fitting surrogate model. In (Díaz et al. 2012) only the surrogate models with  $R^2$  values larger than 0.85 are considered.

## REQUIREMENTS OF EUROCODES

In this research the Eurocodes are used meaning EN 1993-1-8 for joints and extension for steel grades up to S700 (EN 1993-1-12). The variables of the welded T-joint are:

- Chord member dimensions  $b_0, t_0$ ;
- Brace dimensions  $b_1, t_1$ ;
- Angle  $\theta$  between the brace and the chord;
- Weld type  $w_f$  or  $w_b$ , can be either fillet weld ( $w_f$ ) or butt weld ( $w_b$ );
- Relative axial load of the chord  $n_0$ .

Our goal is to predict typical practical cases and this means the chord sizes  $b_0$  are between 300x300x12.5 and 100x100x4, and only squares are considered. This limits the sizes of braces, because:

$$0.25 \leq \frac{b_1}{b_0} = \beta \leq 0.85 \quad (8)$$

The ratio  $b_1/t_1$  is limited  $b_1/t_1 \leq 35$  and in compression to cross-section class 1 or 2. The ratio  $b_0/t_0$  is limited  $35 \geq b_0/t_0 \geq 10$  and moreover to the cross-section class 1 or 2. We consider also HSS up to S700 and this limits the range of the cross-sections. The member sizes are discrete and follow those of Ruukki, meaning cold-formed tubes. The angle  $\theta$  between the brace and the chord is due to welding in the range  $30 \text{ degrees} \leq \theta \leq 90 \text{ degrees}$ .

The butt weld is modeled as “no weld” by using TIE constraint of ABAQUS. The fillet weld is modeled as steel and using TIE constraint where the weld is in contact with steel. The full strength weld is used for the fillet weld and the size  $a$  is defined as:

$$a \geq \sqrt{2} \cdot \beta_w \frac{\gamma_{M2}}{\gamma_{M0}} \frac{f_{y1}}{f_{u1}} t_1 \quad (9)$$

where the correlation factor  $\beta_w = 0.9$  for S355 and 1.0 for greater steel grades and material factors are  $\gamma_{M2} = 1.25$  and  $\gamma_{M0} = 1.0$ . The index 1 refers to the brace. In practice this means very large weld sizes for HSS as is given in the following table (Ongelin and Valkonen 2012).

Table 1. Fillet weld sizes

Brace material	Weld size
S355	$1.16t_1$
S460N	$1.50t_1$
S500N	$1.60t_1$
S550M	$1.62t_1$
S700M	$1.64t_1$

## FINITE ELEMENT ANALYSIS

The ABAQUS model was made by using C3D8 brick elements both for the tubes and for the welds. All sections were modeled with round corners, according to EN 10219-2. Meshing of the truss members was created with solid hexahedral elements as shown in Figure 1.

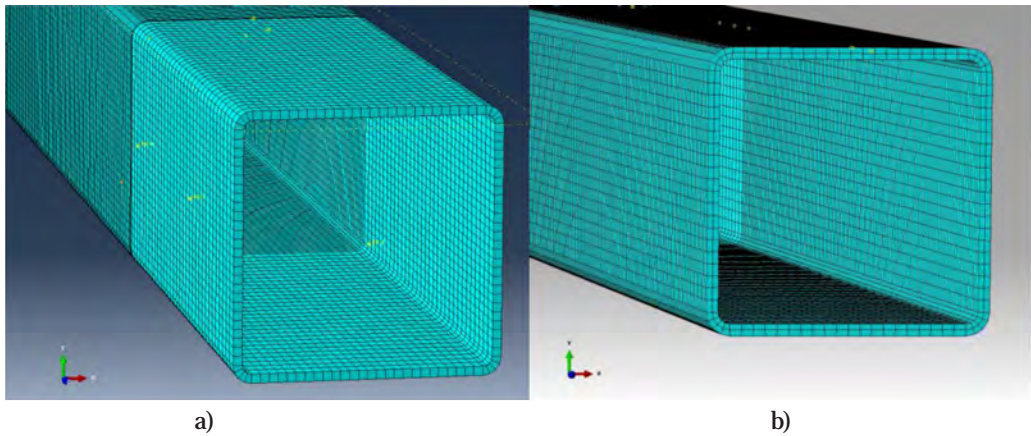


Figure 1. FEM meshes of the tubes: a) far away from the joint, one layer; b) near the joint, two layers.

Meshing of fillet weld is shown in Figure 2.

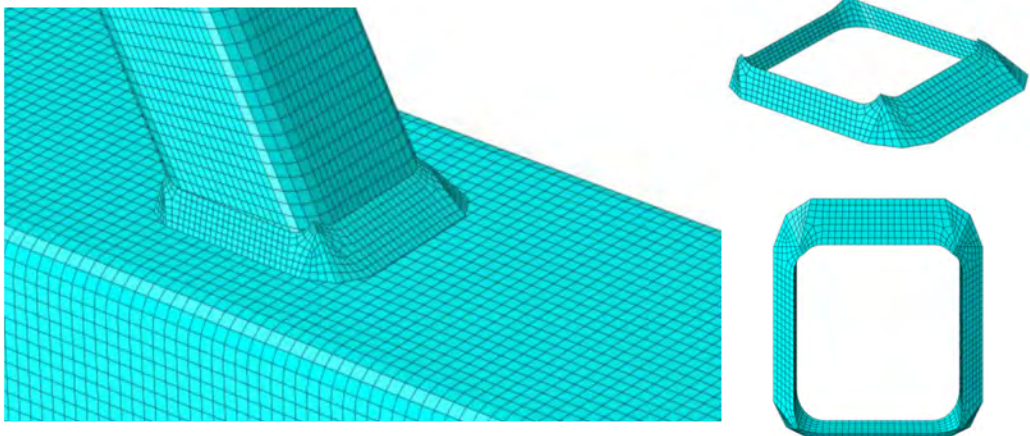


Figure 2. Meshing the fillet weld.

The material model for S355 steel grade is shown in Figure 3. The meshing and the material model were the same as in (Haakana 2014).

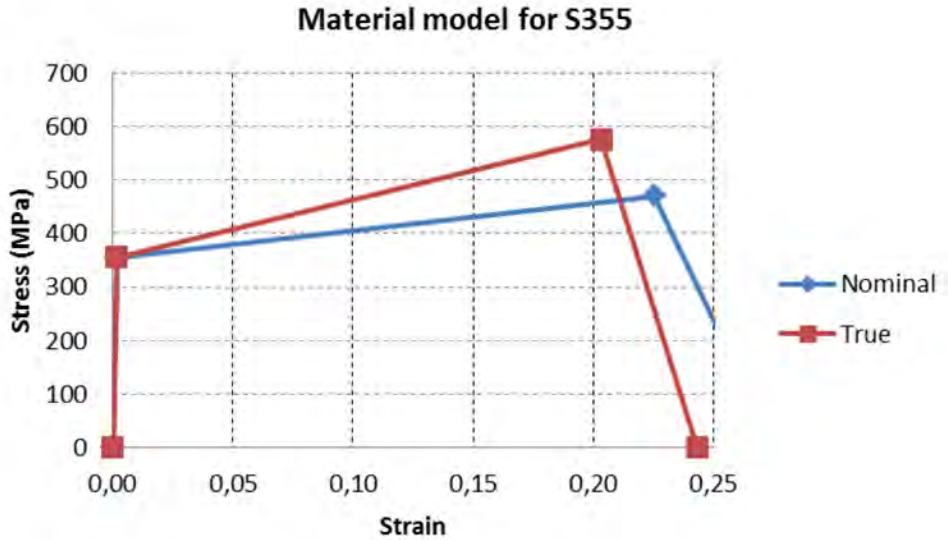


Figure 3. Material model for S355.

Similar models were used for all steel grades. The input material models are given in Table 2. The material does not have influence on the stiffness with butt welds. But, with the fillet welds the material of the brace has influence on the stiffness due to the weld sizes which are given in Table 1.

Table 2. Material data

Nominal S355		Nominal S460		True, S355		True, S460	
$\epsilon$	$\sigma$ , [MPa]	$\epsilon$	$\sigma$ , [MPa]	$\epsilon$	$\sigma$ , [MPa]	$\epsilon$	$\sigma$ , [MPa]
0	0	0	0	0	0	0	0
0,00169	355	0,00219	460	0,00169	356	0,00219	461
0,2255	470	0,2593	540	0,20335	576	0,23058	680
0,2755	0,522222222	0,3093	0,6	0,24334	1	0,26952	1
Nominal S500		Nominal S550		True, S500		True, S550	
$\epsilon$	$\sigma$ , [MPa]	$\epsilon$	$\sigma$ , [MPa]	$\epsilon$	$\sigma$ , [MPa]	$\epsilon$	$\sigma$ , [MPa]
0	0	0	0	0	0	0	0
0,00238	500	0,00262	550	0,00238	501	0,00262	551
0,2643	550	0,2883	600	0,23451	695	0,25335	773
0,3143	0,611111111	0,3383	0,666666667	0,27329	1	0,29143	1
Nominal S700 t>8mm		Nominal S700		True, S700 t>8mm		True, S700	
$\epsilon$	$\sigma$ , [MPa]	$\epsilon$	$\sigma$ , [MPa]	$\epsilon$	$\sigma$ , [MPa]	$\epsilon$	$\sigma$ , [MPa]
0	0	0	0	0	0	0	0
0,00324	680	0,00333	700	0,00323	682	0,00333	702
0,3604	750	0,3605	750	0,30776	1020	0,30783	1020
0,4104	0,833333333	0,4105	0,833333333	0,34386	1	0,34393	1

The analyses were force controlled, and the load step was calculated with “Static, Riks” procedure. Figure 4 illustrates the FEM mesh for the Y-joint with butt welds using 8-noded brick elements.

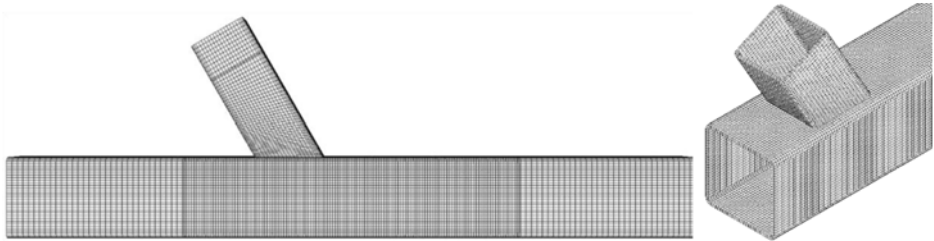


Figure 4. FEM mesh for Y-joint.

The welds were modeled as is shown in Figure 5.

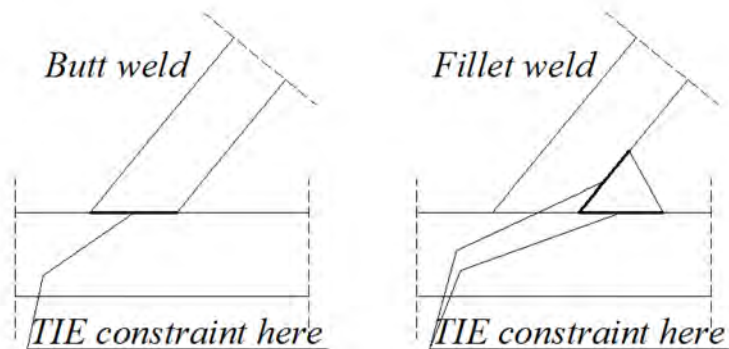


Figure 5. Weld modeling.

## VALIDATION OF FEM

The described ABAQUS model was validated with the tests of LUT (Tuominen and Björk 2014) in (Haakana 2014). The validation was done for K-joint with nominal S500/S500 steel grades. In this case the constant axial load was acting at the chord and the tensile force was increasing at one brace and the other brace was supported axially so there was compression when the tensile was increasing in the test. Figure 6 presents the testing apparatus, node sets where displacement differences were measured and one validation result.



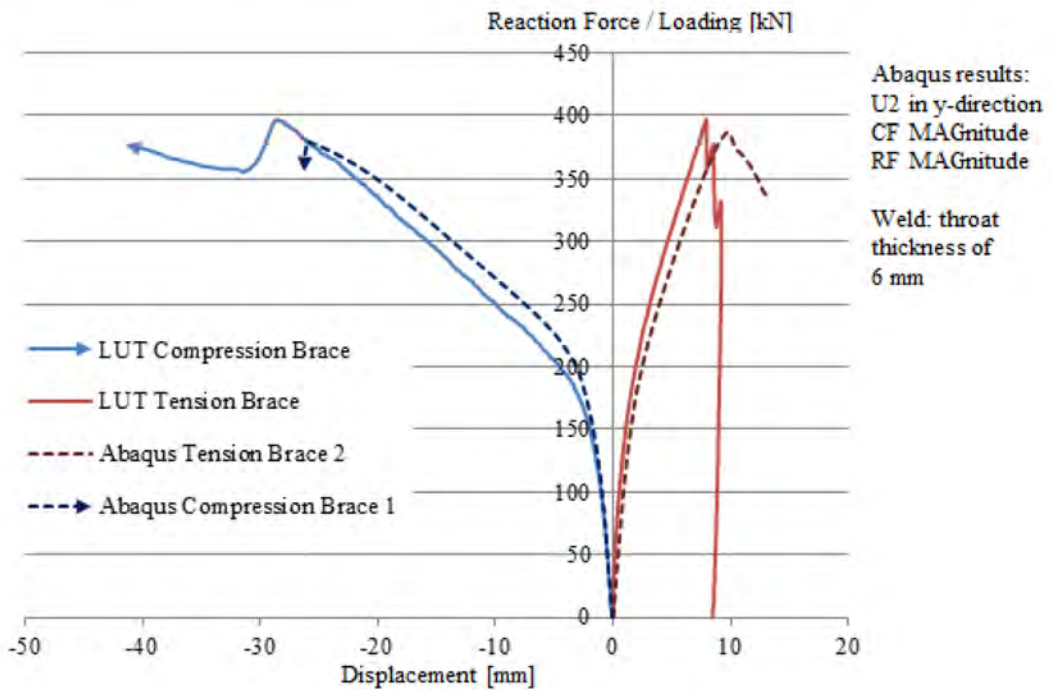
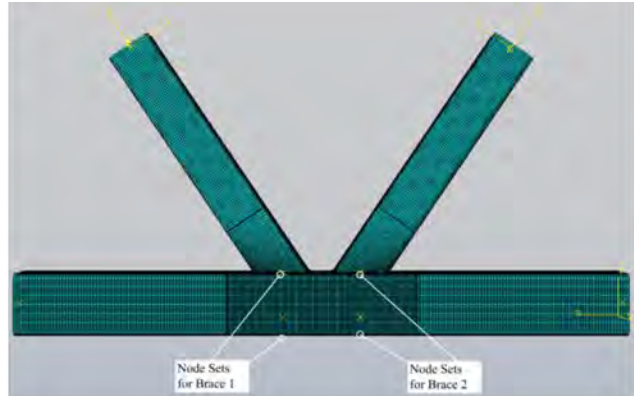
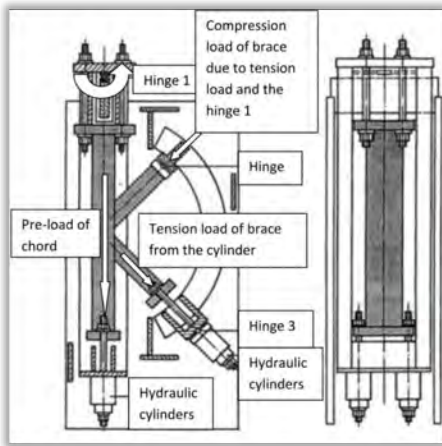


Figure 6. Validation of the ABAQUS model (Haakana 2014).

It can be seen, that the ABAQUS model predicts rather well the test results in this case.

## VERIFICATION OF FEM

The first verification was done for the Y-joint where the moment load was acting at two opposite directions. The expected result was that there would not be large difference in the moment resistance and initial rotational stiffness. This verification was done with the Y-joint and:

- Steel grades of chord and brace S500;
- Chord size 150x150x6;
- Two braces sizes 60x60x5 and 110x110x5;
- Angle 60 degrees.

The results are shown in Figure 7.

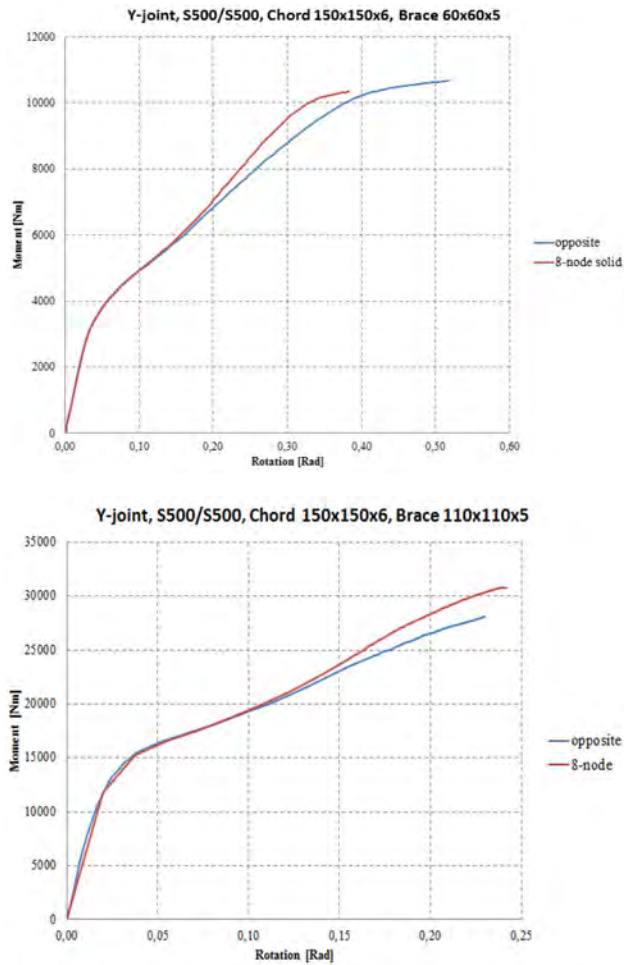


Figure 7. Verification case: two opposite moments.

It can be seen that the maximum moment and the initial rotations are very similar in both cases in Figure 7. The differences in response curves occur at very large rotations, say after 100 mrad.

Next verification was done using shell elements S4R of ABAQUS, as is shown in Figure 8. The case was as the previous Y-joint with the brace size 60x60x5, angle 60 degrees. Two shell models were constructed: one along the mid lines of tubes and one along the outer surfaces of the tubes.



Figure 8. Shell element model.

The computing time required for this model is about the same as for that with 8-noded brick elements. The results are shown in Figure 9 in one case (angle 30 Degrees). In this figure the rotation is the rotation at the end of the brace, the point where the moment is acting.

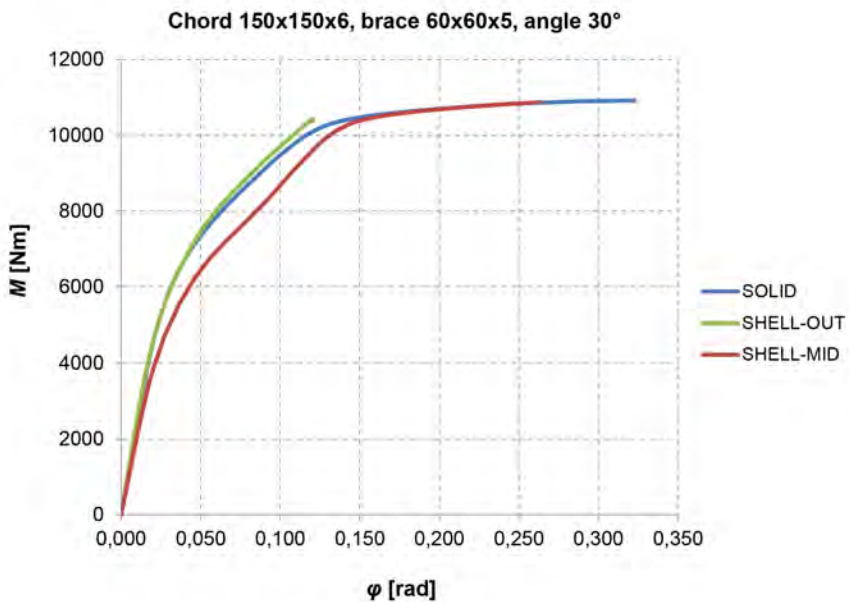


Figure 9. Shell model vs brick model.

It can be seen, that the stiffness of the brick model (8-node solid) is about same as the stiffness of the shell model. The runs were also done using the shell elements for the same case, chord 150x150x6, brace 60x60x5 and with angles 60 and 90 degrees. The results are shown in Figures 10-12 for the moment below 1000 Nm.

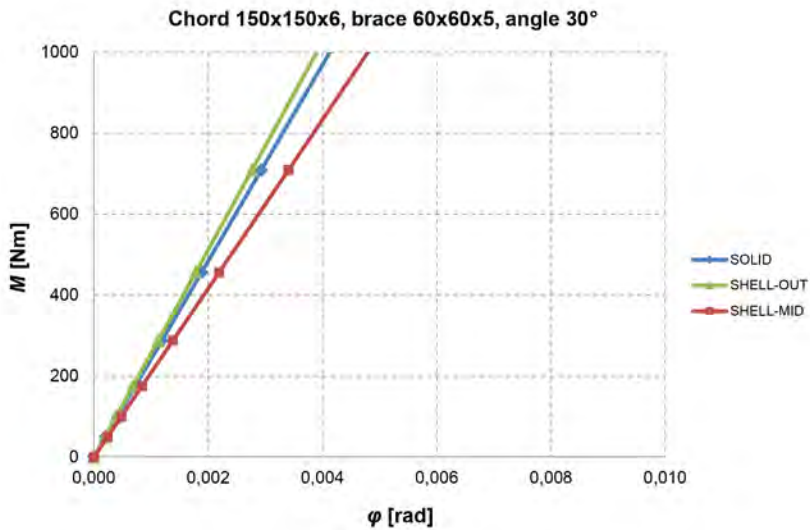


Figure 10. Stiffness of Y-joint, angle 30 degrees.

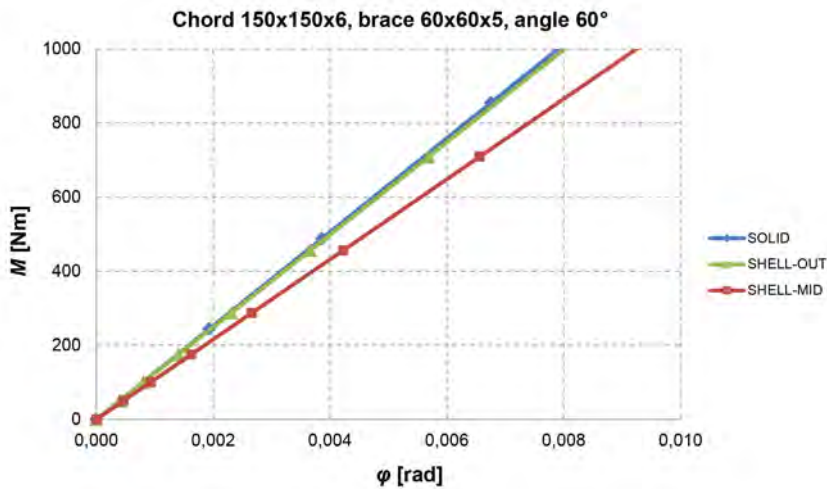


Figure 11. Stiffness of Y-joint, angle 60 degrees.

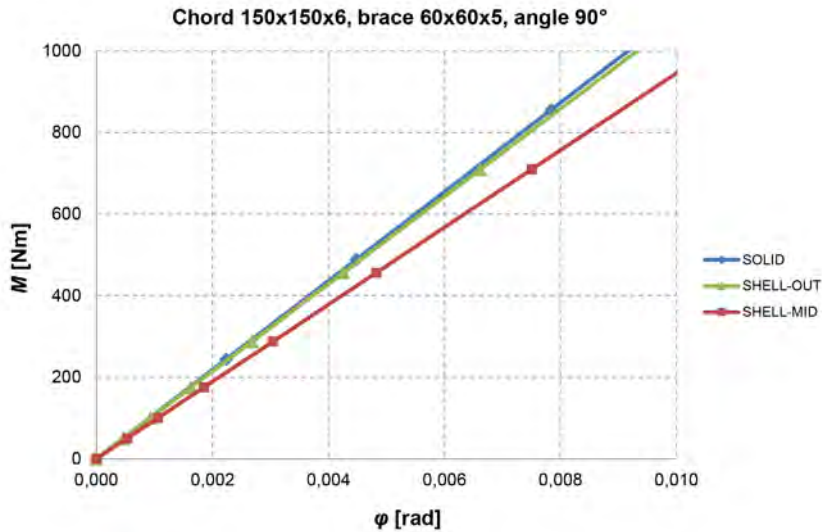


Figure 12. Stiffness of Y-joint, angle 90 degrees.

It can be seen that the difference between the solid model and the shell model is very small, practically zero, if the shell model is made along the outer surface of the tubes. The shell model along the mid surface is shown for the comparison, because that technique has been used in some papers. It can be seen in the figure how the initial stiffness increases when the angle between the brace and the chord decreases.

Sample and validation points were defined using the solid model because the maximum moment was obtained using the solid model rather than using the shell model and the modeling of fillet welds could be done based on the exact geometry of the weld. Some tests were done using four layers of 8-noded solid elements near the joints and the 20-noded solid elements, but the results were about the same as using two layers of solid elements.

## SURROGATE MODELING

The sample points were defined so that:

- they cover the wide range of variables;
- they can be used for the steel grades in the range from S355 to S700;
- the failure of the brace was not critical.

Based on the engineering judgement the total number of sample points was set as 80. The sample points are given in Table 3. In the table the values of the initial rotational stiffness are also given using (Grotmann and Sedlacek 1988).

Table 3. Sample points, butt welds

No	Chord		Brace		$\varphi$ [deg]	C [kNm/rad]	
	$b_0$ [mm]	$t_0$ [mm]	$b_1$ [mm]	$t_1$ [mm]		ABAQUS	CIDECT
1	100	4	40	4	30	92	-
2	100	4	80	4	30	1827	-
3	100	5	60	4	30	617	-
4	150	6	60	5	30	264	-
5	150	6	110	5	30	2881	-
6	200	8	150	6	30	7601	-
7	200	10	120	5	30	4468	-
8	200	12.5	120	7.1	30	8229	-
9	300	12.5	180	7.1	30	9279	-
10	300	12.5	220	10	30	25950	-
11	100	4	40	4	60	44	-
12	100	4	80	4	60	676	-
13	100	5	60	4	60	241	-
14	150	6	60	5	60	126	-
15	150	6	110	5	60	1071	-
16	200	8	150	6	60	2833	-
17	200	10	120	5	60	1755	-
18	200	12.5	120	7.1	60	3310	-
19	300	12.5	110	6	60	979	-
20	300	12.5	180	7.1	60	3502	-
21	300	12.5	220	10	60	8697	-
22	100	4	40	4	90	38	34
23	100	4	80	4	90	532	492
24	100	5	60	4	90	197	230
25	150	6	60	5	90	109	117
26	150	6	110	5	90	843	999
27	200	8	150	6	90	2231	2692
28	200	10	120	5	90	1434	1914
29	200	12.5	120	7.1	90	2724	3520
30	300	12.5	110	6	90	852	896
31	300	12.5	180	7.1	90	2726	3819
32	300	12.5	220	10	90	7117	8976
33	100	4	40	4	45	56	-
34	100	4	80	4	45	921	-
35	100	5	60	4	45	313	-
36	150	6	60	5	45	212	-

<b>37</b>	150	6	110	5	45	1521	-
<b>38</b>	200	8	150	6	45	3965	-
<b>39</b>	200	10	120	5	45	2266	-
<b>40</b>	200	12.5	120	7.1	45	4474	-
<b>41</b>	300	12.5	110	6	45	1131	-
<b>42</b>	300	12.5	180	7.1	45	4264	-
<b>43</b>	300	12.5	220	10	45	11180	-
<b>44</b>	100	4	40	4	75	39	-
<b>45</b>	100	4	80	4	75	543	-
<b>46</b>	100	5	60	4	75	194	-
<b>47</b>	150	6	60	5	75	112	-
<b>48</b>	150	6	110	5	75	892	-
<b>49</b>	200	8	150	6	75	2366	-
<b>50</b>	200	10	120	5	75	1437	-
<b>51</b>	200	12.5	120	7.1	75	2850	-
<b>52</b>	300	12.5	110	6	75	813	-
<b>53</b>	300	12.5	180	7.1	75	2856	-
<b>54</b>	300	12.5	220	10	75	7489	-
<b>55</b>	140	6	80	4	45	414	-
<b>56</b>	160	7.1	120	6	45	2591	-
<b>57</b>	220	8	180	7.1	45	7100	-
<b>58</b>	260	10	200	8	45	8126	-
<b>59</b>	140	6	80	4	75	277	-
<b>60</b>	160	7.1	120	6	75	1669	-
<b>61</b>	220	8	180	7.1	75	4552	-
<b>62</b>	260	10	200	8	75	5192	-
<b>63</b>	110	4	50	4	45	72	-
<b>64</b>	110	6	60	4	45	330	-
<b>65</b>	180	8	140	6	45	4591	-
<b>66</b>	250	10	160	6	45	2894	-
<b>67</b>	250	10	180	7.1	45	5380	-
<b>68</b>	110	4	50	4	75	52	-
<b>69</b>	110	6	60	4	75	228	-
<b>70</b>	180	8	140	6	75	2947	-
<b>71</b>	250	10	160	6	75	1909	-
<b>72</b>	250	10	180	7.1	75	3354	-
<b>73</b>	120	5	80	4	45	526	-
<b>74</b>	120	5	100	5	45	2147	-
<b>75</b>	180	10	150	6	45	12173	-
<b>76</b>	260	10	220	8	45	16668	-
<b>77</b>	120	5	80	4	75	317	-
<b>78</b>	120	5	100	5	75	1265	-
<b>79</b>	180	10	150	6	75	7322	-
<b>80</b>	260	10	220	8	75	10764	-

Firstly, we tried the first order polynomial regression, Eq. (2). In that case the error term was about  $R^2 = 0.75$ . Next, we used DACE toolkit of Matlab (Lophaven et al. 2002). We found soon, that the limit 0.85 of the error term  $R^2$  is not the good criterion for this case. We could exceed it but still the errors at the validation points were over 10%. Using Kriging and zero order regression the errors at the validation points were reduced below 10%, which we set as the acceptance criterion. The validation points and errors between ABAQUS results and surrogate model are provided in Table 4 using zero order regression and Kriging with the Gaussian correlations.

Table 4. Validation of the surrogate model

№	Chord		Brace		$\varphi$ [deg]	C [kNm/rad]		%
	$b_0$ [mm]	$t_0$ [mm]	$b_1$ [mm]	$t_1$ [mm]		ABAQUS	SURROGATE	
1	140	6	80	4	50	367.52	357.80	2.6
2	160	7.1	120	6	50	2280.13	2192.70	3.8
3	220	8	180	7.1	50	6264.95	6222.90	0.7
4	260	10	200	8	50	7358.35	7028.20	4.5
5	140	6	80	4	80	271.24	263.70	2.8
6	160	7.1	120	6	80	1619.04	1629.40	0.6
7	220	8	180	7.1	80	4402.38	4300.40	2.3
8	260	10	200	8	80	5020.85	4766.30	5.1

The  $R^2$  error in this case is 0.99, as for linear and second order regression with Kriging. In those cases the maximum errors in the validation points were 22% and 29% respectively.

In this case the results are to:

- Use sample points of Table 3.
- Calculate the surrogate model using DACE toolkit (Kriging) of Matlab and the zero order regression with the Gaussian correlations.
- Predict the value of the initial rotational stiffness using DACE toolkit.

The Matlab operations needed to perform these tasks are:

```
theta = 10 ; lob = 1e-1; upb = 20;
[modelC, perfC] = dacefit(data, C, @regpoly1, @corrGauss, theta, lob, upb)
CC=predictor (VP, modelC)
C8=predictor ([260 10 200 8 80], modelC)
```

where



- $\theta$ ,  $lob$ ,  $upb$  are the parameters of the surrogate model,
- $data$  and  $VP$  are the sample points and the validation points respectively
- $C$  are the stiffness values of the sample points,
- $modelC$  is a surrogate model constructed
- $CC$  are the surrogate model values calculated for the validation points,
- $C8$  is the surrogate model value calculated for the #8 validation point (see Table 4)

## EXAMPLES

Next there are some examples of the application of the surrogate model. Surrogate model allows to realize how moment resistance and rotational stiffness depend on incoming parameters. i.e. chord and brace geometry, angle between a chord and a brace. Figure 13 illustrates the rotational stiffness-angle curve for a certain case.

It can be seen from the the figure that with the increase of the angle between a chord and a brace from 30 degrees to 90 degrees the rotational stiffness of the joint declines.

Figure 14 presents how rotational stiffness depends on brace width  $b_l$ .

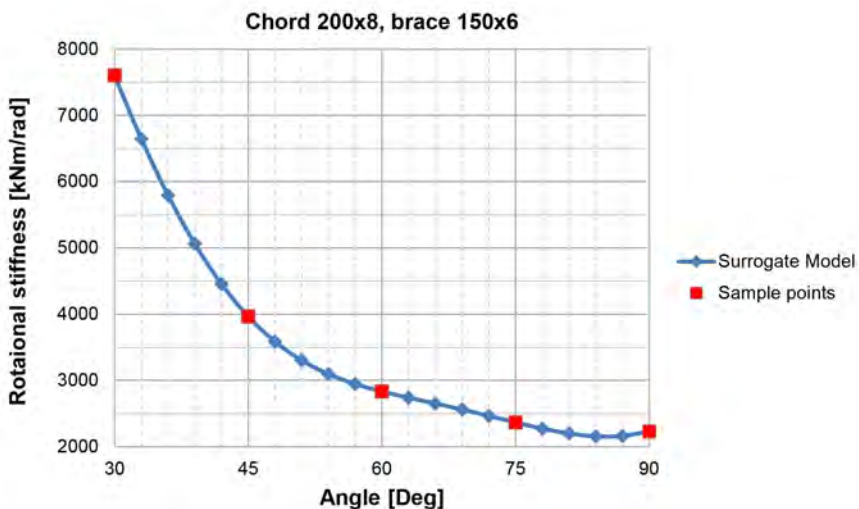


Figure 13. Rotational stiffness-angle curve,  $b_0=200$  mm,  $t_0=8$  mm,  $b_1=150$  mm,  $t_1=6$  mm.

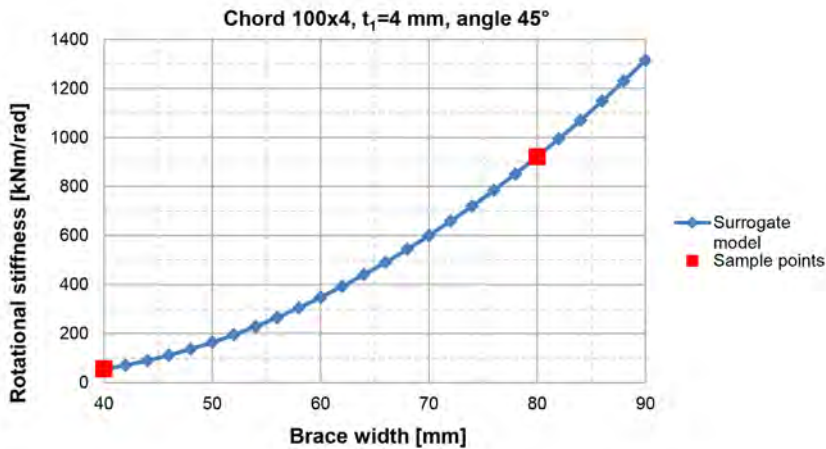


Figure 14. Rotational stiffness-brace width curve,  $b_0=100$  mm,  $t_0=4$  mm,  $t_1=4$  mm,  $\varphi=45^\circ$ .

It can be seen that the function of rotational stiffness behaves rather predictable, gradually increasing with the width of the brace.

## CONCLUSIONS

Initial rotation stiffness of welded tubular joint has been known for the case where the brace member is connected to the chord with the angle of 90 degrees. In this paper the initial rotational stiffness is defined using Kriging, including Gaussian correlation with the surrogate model for wide range of joint details and by taking into account the requirements of EN 1993-1-8. The stiffness values at sample and validation points were calculated using 3D finite element analysis using ABAQUS. The sample and validation points were defined using engineering judgement. The typical error criteria  $R^2 \geq 0.85$  was found to be not suitable for this case, but the criterion was set to be as: error in each validation point should be smaller than  $\pm 5\%$ . The error is the difference between the ABAQUS result and the result from the surrogate model prediction. The  $R^2$  error was then 0.99. The surrogate model was defined using DACE toolkit of Matlab. This technique seems to be suitable for the definition of the response of tubular joints and the results will be used in the optimization of HSS structures in the future.

Next steps in our research are to define the effects of weld sizes and axial forces of the chord to the stiffness. In previous studies we have found that the size of the fillet weld has considerable effect to the stiffness. After these studies we derive the surrogate model to the moment resistance of the joint.

## ACKNOWLEDGEMENTS

Financial support of TEKES/FIMECC/MANU/Digimap is gratefully acknowledged. Also, the support from Erasmus and Peter the Great St.Petersburg Polytechnic University made it possible to complete this research.

## REFERENCES

- Anderson, D., Hines, E.L., Arthur, S.J. and Eiap, E.L. 1997. Application of artificial neural networks to the prediction of minor axis steel connections. *Computers & Structures* 63(4): 685–692.
- Boel, H. 2010. Buckling Length Factors of Hollow Section Members in Lattice Girders, Ms Sci thesis. Eindhoven University of Technology.
- Díaz, C., Victoria, M., Querin, O.M. and Martí, P. 2012. Optimum design of semi-rigid connections using metamodels. *Journal of Constructional Steel Research* 78: 97–106.
- European Committee for Standardisation, (CEN). Eurocode 3. Design of steel structures, Part 1-12: Additional rules for the extension of EN 1993 up to steel grades S 700 (EN 1993-1-12:2007), Brussels, 2007.
- European Committee for Standardisation, (CEN). Eurocode 3. Design of steel structures, Part 1–8: Design of joints (EN 1993-1-8:2005), Brussels, 2005.
- Fang, K.-T., Li, R. and Sudjianto, A. 2006. Design and modeling for computer experiments, Chapman & Hall/CRC.
- Grotmann, D. and Sedlacek, G. 1988. Rotational stiffness of welded RHS beam-to-column joints. Cidect 5BB-8/98, RWTH Aachen.
- Guzelbey, I.H., Cevik, A. and Göğüş, M.T. 2006. Prediction of rotation capacity of wide flange beams using neural networks. *Journal of Constructional Steel Research* 62(10): 950–961.
- Haakana, Ä. 2014. In-Plane Buckling and Semi-Rigid Joints of Tubular High Strength Steel Trusses, Ms Sci thesis. Tampere University of Technology.
- Jadid, M.N. and Fairbairn, D.R. 1996. Neural-network applications in predicting moment-curvature parameters from experimental data. *Engineering Applications of Artificial Intelligence* 9(3): 309–319.
- Jin, R., Chen, W. and Simpson, T.W. 2001. Comparative studies of metamodeling techniques under multiple modelling criteria. *Structural and Multidisciplinary Optimization* 23(1): 1–13.

Jones, D.R., Schonlau, M. and Welch, W.J. 1998. Efficient global optimization of expensive black-box functions. *Journal of Global optimization* 13(4): 455–492.

Kim, J., Ghaboussi, J. and Elnashai, A.S. 2010. Mechanical and informational modeling of steel beam-to-column connections. *Engineering Structures* 32(2): 449–458.

Kleijnen, J.P.C. 2008. Simulation experiments in practice: statistical design and regression analysis. *Journal of Simulation* 2: 19–27.

Lee, T. and Jung, J. 2006. Metamodel-based shape optimization of connecting rod considering fatigue life. *Key Engineering Materials* 306-308: 211–216.

De Lima, L.R.O., Vellasco, P.C.G. da S., De Andrade, S.A.L., Da Silva, J.G.S. and Vellasco, M.M.B.R. 2005. Neural networks assessment of beam-to-column joints. *Journal of the Brazilian Society of Mechanical Sciences and Engineering* 27(3): 314–324.

Lophaven, S.N., Søndergaard, J. and Nielsen, H.B. 2002. DACE, A MATLAB Kriging Toolbox, Version 2.0, August 1, Technical University of Denmark.

Matheron, G. 1963. Principles of geostatistics. *Economic geology* 58(8): 1246–1266.

McKay, M.D., Bechman, R.J. and Conover, W.J. 1979. A Comparison of Three Methods for Selecting Values of Input Variables in the Analysis of Output From a Computer Code. *Technometrics* 21(2): 239–245.

Montgomery, D.C. 2012. *Design and Analysis of Experiments*, John Wiley & Sons.

Mukhopadhyay, T., Dey, T.K., Dey, S. and Chakrabarti, A. 2015. Optimization of fiber reinforced polymer web core bridge deck – A hybrid approach. *Structural Engineering International* 25(2): 173–183.

Müller, J. 2012. *Surrogate Model Algorithms for Computationally Expensive Black-Box Global Optimization Problems*, Tampere University of Technology. Publication 1092.

Ongelin, P. and Valkonen, I. 2012. *Structural hollow sections. EN 1993 - Handbook 2012*, Rautaruukki Oyj.

Pirmoz, A. and Gholizadeh, S. 2007. Predicting of moment--rotation behavior of bolted connections using neural networks, 3rd national congress on civil engineering.

- Queipo, N. V., Haftka, R.T., Shyy, W., Goel, T., Vaidyanathan, R. and Kevin Tucker, P. 2005. Surrogate-based analysis and optimization. *Progress in Aerospace Sciences* 41: 1–28.
- Roux, W.J., Stander, N. and Haftka, R.T. 1998. Response surface approximations for structural optimization. *International Journal for Numerical Methods in Engineering* 42(3): 517–534.
- Sacks, J., Schiller, S.B. and Welch, W.J. 1989. Designs for computer experiments. *Technometrics* 31(1): 41–47.
- Sacks, J., Welch, W.J., Mitchell, T.J. and Wynn, H.P. 1989. Design and analysis of computer experiments. *Statistical science*: 409–423.
- Salajegheh, E., Gholizadeh, S. and Pirmoz, A. 2008. Self-organizing parallel back propagation neural networks for predicting the moment-rotation behavior of bolted connections. *Asian Journal of Civil Engineering* 9(6): 625–640.
- Snijder, H.H., Boel, H.D., Hoenderkamp, J.C.D. and Spoorenberg, R.C. 2011. Buckling length factors for welded lattice girders with hollow section braces and chords. *Proceedings of Eurosteel 2011*: 1881–1886.
- Stavroulakis, G.E., Avdelas, A.V., Abdalla, K.M. and Panagiotopoulos, P.D. 1997. A neural network approach to the modelling, calculation and identification of semi-rigid connections in steel structures. *Journal of Constructional Steel Research* 44(1-2): 91–105.
- Tuominen, N. and Björk, T. 2014. Ultimate Capacity of Welded Joints Made of High Strength Steel CFRHS, Eurosteel 2014, 7th European Conference on Steel and Composite Structures, September 10-12, 2014, Naples, Italy.
- Yun, G.J., Ghaboussi, J. and Elnashai, A.S. 2008. Self-learning simulation method for inverse nonlinear modeling of cyclic behavior of connections. *Computer Methods in Applied Mechanics and Engineering* 197(33-40): 2836–2857.

# BELARUSIAN-RUSSIAN INNOVATION: CREATION OF ENGINEERING STRUCTURES OF THE XXI CENTURY

**I.M. Kuzmenko**

Ph.D., Associate Professor, "Belarusian-Russian University", Mogilev, Republic of Belarus

**S.N. Markov,**

Head of the design department, OAO "Mostostroy", Minsk, Republic of Belarus

**V. M. Friedkin**

Professor, "Moscow State University of Railway Transport" (MIIT), Moscow, Russian Federation

## INTRODUCTION

The State Institution of Higher Professional Education "Belarusian-Russian University" (hereinafter BRU) about 20 years ago, initiated studies in perspective, in our opinion, direction: the development of a fundamentally new innovative design and manufacture of advanced constructions for various industries. Its level should correspond to the priority areas of modernization and technological development of economy of the Republic of Belarus and the Russian Federation. Theoretical and experimental studies have allowed creating a *composite (steel-concrete) bearing element of constructions (KNESK)*.

The scientists of BRU and the Federal State Budget Institution of Higher Professional Education "Moscow State University of Railway Transport" (the MIIT) take direct part in this work. Design and construction works are carried out jointly with specialists of "Mostostroy" and then holding company "Protos group of companies."

The innovative manufacturing technology based on KNESK includes a number of complex measures: the design of the construction, adapting of KNESK to the projected construction, project development and production technology of KNESK, the development of designs and manufacturing techniques of field joints and transport modules, the development of installation technology.

The wide variety of possible constructive forms and designs of KNESK allows its use as a basic element for a variety of purposes and structures with desired properties.

Design and technological solutions were used in the construction of some objects of bridge building in Mogilev, Minsk and Gomel.

The composition (KNESK) is flexible and perfect in manufacturing and installation technology, has achieved effective implementation in bridge construction of the Republic of Belarus, and can get a wide field of use in creating highly reliable and long exploited engineering structures of the XXI century.

## DEFINITIONS OF KEY TERMS

Some terms used in this article require clarification. More details are discussed in the monographs [1, 2]. Here we present only the interpretation of key terms in the wording of the author of the above-mentioned monographs.

One of the promising areas of establishing effective civil engineering constructions in the XXI century is the development of innovative technical solutions *based on the principles of forming building structures*: a set of criteria for the selection of a set of structural forms the most advanced and effective solutions.

*Shaping* - the creation and development of structural forms: the creation of new and improvement of known structural materials and the creation of new techniques and high-efficiency technologies on their basis, updating of regulatory requirements for qualitative and quantitative criteria for the selection of structural form.

*The structural form* is understood as a set of constructions with a uniform set of materials and the same geometrical structure of bearing elements and relationships with the environment. Thus, quantitative characteristics of structures are ignored: their scale, aspect ratio, etc., but not the physical and mechanical properties of materials.

*The bearing element* - located in static or dynamic equilibrium a solid deformable body, perceiving external influences and reactions of relationships with other bodies. The bearing element may be homogeneous or composed of separate discrete components and perhaps these components may be surrounded by continual deformable solid medium (matrix), and the connection of the components determines the geometric dimensions of the element.

*The detail* - in the construction industry is, for example, the steel frame, fittings, base etc.

*The matrix* - reinforced concrete or some other aggregate.

The creation of new forms of design is largely driven by information technologies, the development of mechanics, mathematics, and experimental methods.



## COMPOSITE BEARING CONSTRUCTION ELEMENT

### Design features of the element

Several patents of the Republic of Belarus and the Russian Federation [3 - 5] protect the design KNESK. The options of constructive and factory KNESK performances are presented in Figure 1.

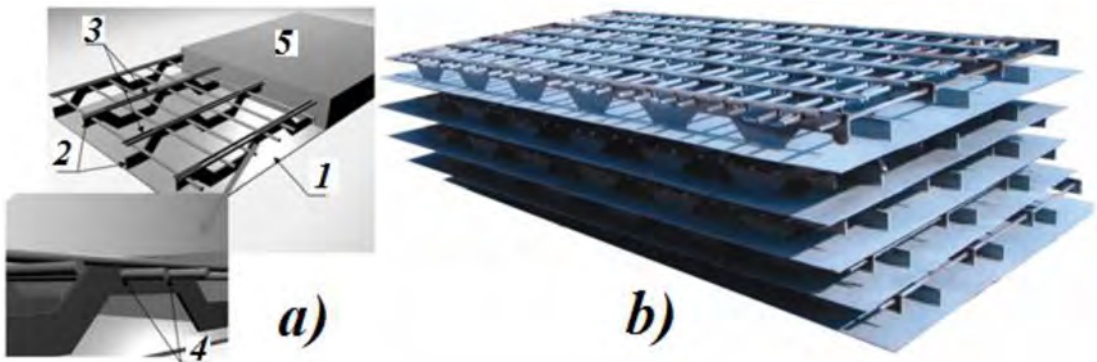
*The forming sheet 1* provides implementation of mounting on high-strength bolts or welding and reducing the complexity of grouting of installation joints; tightness up to the vacuum; operation in harsh environments; explosion and fire resistance.

*Steel reinforcement 2* (ribbed reinforcing element - virtually waste-free cutting of flat steel) allows to increase the load-carrying ability of structures, to ensure the readiness of the erected structure bear load without aggregate and scaffolding, to reduce the tendency of the aggregate to crack, to improve the level of industrialization in structure fabrication.

The use of *reinforcing rods 3, 4* allows you to increase the grip of a shell reinforcement with an aggregate, to simplify the creation of prestressed structures.

The use of an *aggregate 5* (concrete and other materials - the *matrix*) provides increased resistance of a structure to the loss of bearing capacity and effective corrosion protection of a shell reinforcement.

Items 1 - 4 are combined by welding into a *steel component* KNESK (following terminology adopted above - *detail*), which is shown in Figure 1 b. Concreting was carried out after the installation of the metal structure of the overpass.



1 – shape-generating sheet; 2 – foliated reinforcement; 3 - rod longitudinal reinforcement; 4 – rod transverse reinforcement; 5 - aggregate (usually - modified concrete with additives of multifunctional action).

Figure 1. Options for the embodiment (a) and factory performance (b) of KNESK

### **Competitive advantages of KNESK**

The features of element design and use of modern technologies provide:

- the ability to perform the installation on the high-resistant bolts or by welding, and as a result, relatively quick erection of structures;
- the minimum length of erection weld;
- to simplify the creation of complex three-dimensional shapes;
- the execution of shell reinforcement the function of permanent shuttering and retaining systems;
- to minimize the drawbacks of steel-reinforced concrete and welded shell structures;
- a high level of production industrialization.

KNESK has high resistance to thermal shocks, water resistance and tightness, increased adhesive properties, radiation shielding. It allows you to create a prefabricated structure with the same specific properties.

The broad scope of KNESK applications are due to the versatility of the materials used therein. The principal novelty lies in the fact that KNESK is a composite structure uniting hardening aggregate, especially a modern concrete, with a metal by connecting rod reinforcement and rolled steel sheet along with various types of aggregate. The proposed technology is superior to the existing analogues in terms of efficiency and technology, including the support of environmental and anti-terrorist security system.

### **The effectiveness of KNESK**

Composite bearing elements are particularly cost-effective, in our opinion, when they are used for the construction of unique, complex structures. Examples of the implementation of the above-mentioned principles of formation, which are used by the authors in bridge construction practice, set out in a number of publications [6 - 10].

The effectiveness of use is proved by the implementation of KNESK in load-bearing structures of the deck of highway overpasses. On the territory of Belarus, four objects of bridge construction with KNESK application are designed, built and successfully operated. In 2005 a pedestrian bridge over the river Dubrovenka Mogilev (Figure 2a) was built. Unique road overpasses were built in 2008 in Minsk (Figure 2 b), and in 2011-2015 in Gomel (Figure 2 c). The leadership of holding "Protos Group" showed strong interest in the practical growth of the topic of the industrial use of the development. The company is working successfully in the Mogilev region.

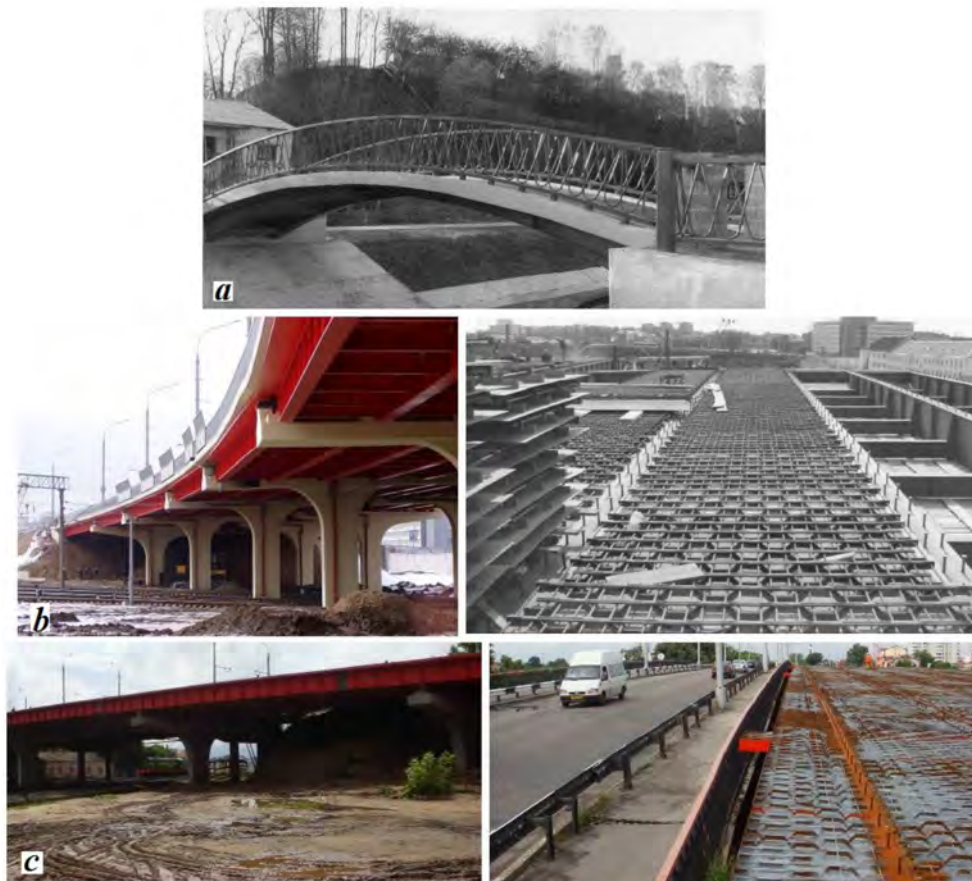


Figure 2. Examples of KNESK in load-bearing structures of the overpass: a) pedestrian bridge in Mogilev; b) road overpasses in Minsk and c) Gomel.

Basing on the experience of designing for roadway of overpasses, geometrical parameters of structural components of steel component KNESK are recommended to prescribe, depending on the particular design of the overpass and conditions of operation, within the following limits:

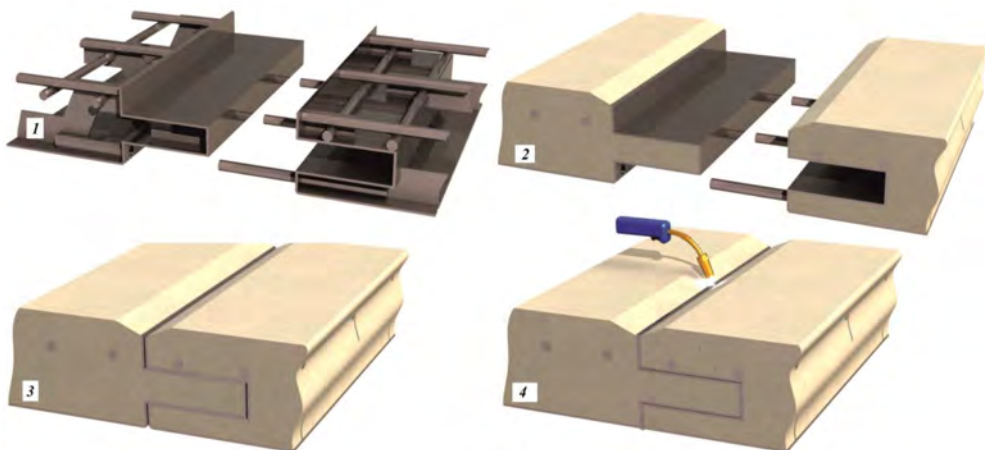
- thickness of the forming plate - 4 . 12 mm;
- thickness of a sheet of reinforcement - 4 . 16 mm;
- height of a sheet of reinforcement - 70 . 170 mm;
- wave height of a sheet reinforcement - 30-50 mm;
- angle of a sheet reinforcement wave - 45°;
- diameter of longitudinal rod reinforcement - 12 . 22 mm;
- diameter of the transverse rod reinforcement - not less than 10 mm.

It should be emphasized that in the concrete part of KNESK – in *matrix* during concreting special cavities and channels for placing sensors and fiber optic cables for transmission of information can be formed.

### Quickly erected structures based on KNESK

The usage of a common technology of monolithic and precast-monolithic construction of composite reinforced concrete structures, including ones based on KNESK is limited to low level of industrialization of the installation technology as it is defined by the hardening period of concrete, time of mounting and time of achieving technological strength by field connections.

The BRU developed and investigated the variants of design of field joints to ensure quick installation with the use of welding, without “wet” concrete processes [11 - 14]. Figure 3 shows factory fabricated field joint of quickly erected construction.



1 - mounted steel components of KNESK; 2 - filling with the hardening material (concrete); 3 - start of installation: assembling of the embedded details; 4 - the completion of installation: welding of field joint.

Figure 3. The procedure of factory fabrication of field joint of quickly erected construction

The production of the dimensional welded reinforcement KNESK (steel components) and subsequent filling with concrete are transferred to the shop floor. At the stage of the construction the mounting of the integrated segments (modules) is carried out, which are manufactured in the factory, already with a concrete component.

The proposed construction of field joints with welded connections for quickly erected segments based on KNESK, provide a sufficient bearing capacity, rapid welding assembly and ability to accept operational loads immediately after their implementation. Erection time is significantly reduced. The possibility of failure of the shuttering and retaining systems through the installation

of ready-made segments that can take the load, both of its own weight and the weight of the personnel involved in the installation, reduces the cost of installation and reduce the additional costs arising from the use of formwork, retaining systems and organization of bypass roads.

The developments of Belarusian scientists were highly appreciated in Russia. Figure 4 shows the diploma and a gold medal of the IX Moscow Salon of Innovations and Investments (Moscow, 2009) and the St. Petersburg Technical Fair (St. Petersburg, 2013).



a) IX Moscow Salon of Innovations and Investments; b) St. Petersburg Technical Fair.

Figure 4. Diploma and a gold medal for the development of KNESK

### The creation of engineering barriers for the safety of underground nuclear power stations

One of the major problems that must be solved in the construction of underground nuclear power stations is the creation of a highly reliable complex of engineering barriers for the safety of nuclear power stations. This fully applies to the storage of radioactive waste (RW): high-level waste (HLW) and spent nuclear fuel (SNF). The problem is relevant for Belarus in connection with the prospects of the development of nuclear power in the Republic. It is also necessary to ensure an adequate level of security of such plants in the event of accidents. It is also necessary to take into account the possibility of a military or terrorist attack that can cause not only a great material damage, but also lead to an environmental disaster.

Leading Russian scientists, in collaboration with BRU, proposed the construction of composite membranes based on KNESK placed inside the trunk space created in the areas of a reactor and storage [15 - 17].

A complete encapsulating of the space is provided with the shells based on KNESK. Completely seal the space around all sides of the shells KNESK.



Such shells may be with a gap nested within each other, creating a highly reliable barrier of any desired degree of long-term protection from radiation. The barrier in the form of a shell KNESK creates favorable conditions for thermodynamic dissipation of local one-sided thermal field.

Using KNESK also facilitates the construction of prefabricated anti-radiation and protective shelters that protect personnel engaged in assembly, from dangerous radiation exposure and the lowest possible length of welds and volume of assembly operations.

### **Use of the basic elements of KNESK in designs of vertical cylindrical tanks**

One promising area of development is the use of basic elements or segments of KNESK in the construction of tanks and gas tanks [18]. Reservoirs of different structural performance up to 200 thousand m<sup>3</sup> for storage of aggressive oil or flammable liquids and gases, may be regarded as relatively quickly erected buildings.

The size of the segment of KNESK limited to bearing capacity of the equipment for installation, transportation and manufacturing sections, space limitations of production facilities and the expected route of transportation. The use of large basic elements simplifies installation and eliminates the need for welding sheets of large thickness. The main part of the welding work is carried out only inside of the tank. The walls of tanks constructed of KNESK have an increased fire and explosion-proof. Concrete aggregate ensures reliable protection of steel components from aggressive atmosphere or weather changes and shaping steel plate seals and allows the tank to operate in hostile environments, destroying the concrete. Due to the use of KNESK metal content can be lowered compared to tanks manufactured by traditional technology.

### **The composite bearing block and the field joint of bearing blocks for prefabricated buildings**

The MIIT has developed and patented in Russia [19] new carrying prefabricated concrete and steel-reinforced concrete building elements, including ones using KNESK.

The invention relates to the construction of engineering structures with supporting framework in the form of prefabricated composite structures with shell, plate or shell-plate large-sized structure, which can be single- or multi-connected, including cellular. These include the installation of reinforced concrete blocks with steel or non-metallic reinforcing rods, with the possible inclusion in the shells and plates thin-walled shell elements made of steel sheet metal with embedded metal parts forming the connection between the mounting blocks and other building structures.

The proposed structure is recommended for applications in many fields of construction, for example, such as bridge building, demersal and overhead tunneling, and construction of tanks. They can be used in the construction of retaining walls, transportation galleries, columns, walls and floors of industrial buildings, high-rise buildings, toroidal tanks, domed, cylindrical and conical vaulted structures, including underground and underwater at depths up to 500 m, fixed and mobile bases platforms for the production of hydrocarbons offshore. They will also be useful in the construction of ventilation pipes and chimneys, cooling towers, sea and river piers and terminals; the use of such structures in shipbuilding is possible.

## CONCLUSIONS

1. Increased use of KNESK in the future leads to the development of the famous and the creation of new forms of engineering structures design, which will generate long-term technical solutions and determine the potential core innovations for composite reinforced concrete in the field of civil engineering of the XXI century.
2. The design features of a steel component of KNESK allow you to create *quickly erected constructions* on their basis for various industries. The developed basic structures of welded field joints have up to 80% of bearing capacity of the base material and provide a framework assembly without the use of “wet” technology of concreting directly into the installation process.
3. Based on the results of the studies the thesis and three thesis for a master’s degree in technical sciences were done and defended.
4. The authors worked out new technical solutions for the various structures using this innovative development [20 - 25]:
  - for transport construction, including the approaches to the bridge through challenging obstacles and extensive overpasses, foundations and intermediate supports of bridges, demersal tunnels;
  - for the construction of toroidal tanks;
  - for underground structures – complex barrier such as vertical shafts of small nuclear power plants (NPPs) and storage of high level waste (HLW) and spent nuclear fuel (SNF);
  - for shipbuilding and marine underwater fishing platforms for shore protection, artificial islands, etc.



## REFERENCES

- [1] Friedkin V.M. Principles in the theory of forming linearly extended structures: monograph / Friedkin V.M. - M.: Lad'ya, 2006. - 512 p: ill. (in Russian)
- [2] Friedkin V.M. Shaping of building structures: monograph / Friedkin. – Ministry of Education and Science. Russian Federation “Moscow State Building. Univ. “ M.: MSBU, 2011. - 171 p: ill. (in Russian)
- [3] Pat. 4082 RB MPK7 E 04 C 2/28. The composite bearing element of constructions / Friedkin V.M., Nosarev A.V., Kuzmenko I.M., Pavlyuk S.K., Semenov A. V., Popkovsky V.A., Filatenkov A.A.; applicant and patentee Mogilev Engineering Institute. - № 970421; appl. 07/29/97; publ.19.04.01, Bul. № 3. - 3 p.: ill. (in Russian)
- [4] Pat. 2181406 RF MPK7 E 01 D 12/00, E 04 C 2/24. The composite bearing element of constructions / Friedkin V.M., Nosarev A.V., Kuzmenko I.M., Pavlyuk S.K., Semenov A.V., Popkovsky V.A., Filatenkov A.A.; applicant and patentee Mogilev Mechanical Engineering. Inst. - № 97121947; appl. 07/29/97; publ. 20.04.02, Bul.№ 11. - 6 p: ill. (in Russian)
- [5] Pat. 4352 RB, IPC E 04S 2/00. The composite bearing element of constructions / Friedkin V.M., Kuzmenko I.M., Nosarev A.V., Maksimenko L.B., Markov S.N., Basharimova V.N., Medvedev V.N.; applicant and patentee Belarus. Rus. Univ. and JSC “Mostostroy.” - № u20070512; appl. 11.07.2007; publ. 30.04.08, Bul. Number 2 - 5 p.: ill. (in Russian)
- [6] Kuzmenko I.M. New trends in the design of composite structures with high economic efficiency and load carrying capacity / Kuzmenko I.M., Popkovsky V.A., Semenov A.V., Friedkin V.M. // «Nove smery vo vyrobnych technologiach» Col. Articles IV Int. Conf. - Prešov, 1999, p. 83-86. (Slovak)
- [7] Kuzmenko I.M. The use of welded bearing elements in composite construction of new structures / Kuzmenko I.M., Pavlyuk S.K., Friedkin V.M. // “Welding Production», № 9, 2003, pp. 47-50. (in Russian)
- [8] Kuzmenko I.M. Aspects of the design of the composite bearing elements with the help of CAD / Kuzmenko I.M., Friedkin V.M., Podymako M.E., Leonenko O.V., Medvedev V.N.// Herald BRU, №4, 2006, p. 198-202. (in Russian)
- [9] Kuzmenko I.M. Impact of loading of the rolling stock (SC-80 and A-11) on the bridge deck made of KNESK / Kuzmenko I.M., Medvedev V.N.// “Vestnik Polotsk gov't. univ. “. Series F. J. Appl. science. Construction, №12. - Publ PSU, 2007.- 180 p. S.63-67. (in Russian)

- [10] Kuzmenko I.M. Innovative design solutions of roadway bridges spans / Kuzmenko I.M., Friedkin V.M., Markov S.N., Podymako M.E., Leonenko O.V., Medvedev V.N., Bogdanov S.V.// "Roads and bridges", Minsk, №1, 2008.-142 pp., Pp 37-41. (in Russian)
- [11] Bogdanov S.V. The use of composite load-bearing elements for prefabricated building structures assembled by welding / Bogdanov S.V., Kuzmenko I.M., Pavlyuk S.K. // Herald BRU, №4, 2009.-166 p., P. 68-75. (in Russian)
- [12] Bogdanov S.V. The rational use of composite load-bearing elements of building structures on economic performance and strength / Bogdanov S.V., Kuzmenko I.M. // Scientific and technical magazine "Construction Science and Technology." Official. inf. ed. Min. of Architect. and p. RB, №4, 2011. - 64 p., p. 33-36. (in Russian)
- [13] Pat. 15480 RB, IPC 23 K 1/00. Welded butt joint of building blocks / Bogdanov S.V., Pavlyuk S.K., Kuzmenko I.M.;applicant and patentee Belarus. Ros. Univ. - № a20090951; appl. 26.06.2009; publ. 28.02.2012, Bull. № 1. - 4 p.: ill. (in Russian)
- [14] Bogdanov S.V. Ensuring the continuity and cohesion of an aggregate and metal reinforcement made of KNESK when the field joint welds / Bogdanov S.V., Kuzmenko I.M. // Herald BRU, №3, 2013.-p. 13-22. (in Russian)
- [15] Friedkin V.M. Environmental engineering, construction and technological problems of creating engineering barriers for long-term storage and final disposal of spent nuclear fuel in the interior of the Earth / Friedkin V.M., Chesnokov S.A., Tsernant A.A., Kuzmenko I.M., Nosarev A.V., Maksimenko L.B., Pisarev I.L., Kokosadze A.E. // Mountain information-analytical bulletin. Publishing house of the Moscow State Mining University, Moscow, №4, 2005 pp.88-94. (in Russian)
- [16] Friedkin V.M. Ensuring the safety of underground nuclear power plants based on the use of complex barriers made of KNESK / Friedkin V.M., Kuzmenko I.M., Nosarev A.V. // 6th International Scientific and Technical Conference "Safety, Efficiency and Economics of Nuclear Energy (ISTC-2008)." Moscow, 2008, pp 912-915. (in Russian)
- [17] Kedrovsky O.L. New approaches to design solutions to create the underground nuclear power facilities / Kedrovsky O.L., Dmitriev S.A., Friedkin V.M., Chesnokov S.A., Kuzmenko I.M., Malkova O. V., Kokosadze A.E.// Science and technology in the industry, Moscow, №1, 2009.-120 pp., Pp 94 – 97. (in Russian)
- [18] Bogdanov S.V. Preserving the field joints of welded structures made of composite elements with supporting metal shell fittings: Author's abstract. Scientific Work Advisor Kuzmenko I.M. - Mogilev: 2013 – 23 p. ill. (in Russian)

[19] Pat. 22519021 RF IPC E04S 1/00 Composite bearing block and the field joint of bearing blocks of prefabricated buildings / Friedkin V.M., Tokarev P.M., Zenin A.V., Zamuhovsky A.V., Savkin D.A., Grudskii V.A., Ponomarev I.V., Tsomaeva K.A.; applicant and patentee VPO "Moscow State University of Railway Engineering(MIIT). " - № 2012128146; appl. 06. 07. 2012; publ. 10/06/2014.Number 16 - 28 p.: ill. (in Russian)

[20] An application for a patent for the invention № a20121717 "The composite carrier of metal structures and metal structures based on it" / Friedkin V.M., Tsomaeva K.A., Kuzmenko I.M., Markov S.N., Basharimova V.N., Sysa N.S., Kuzmenko D.O., Bogdanov S.V.; the applicant Belarus. Rus. Univ. - Application by 07.12.12. (in Russian)

[21] Kuzmenko I.M. Composite carrier element - the basis of the creation of new forms of design for structures of various purpose / Kuzmenko I.M., Friedkin V.M., Markov S.N., Bogdanov S.V.// Herald BRU, №4, 2011. - 180 p., P. 144-156. (in Russian)

[22] Kuzmenko I.M. Perspective directions of innovative development of design and manufacturing of metal structures / Kuzmenko I.M., Friedkin V.M., Sysa N.S. // Coll. materials Belor.-Litovsk. Fair of Business Relations "Trends in the integration of education, science and business." Research Edition / Minsk: Belarus Min. of Edu. 2014. - 120 p., P. 52-54. (in Russian)

[23] Kuzmenko I.M. Experience of the Republic of Belarus in the use of new design solutions for spans of road bridges / Kuzmenko I.M., Friedkin V.M., Markov S.N., Sysa N.S., // Naukovedenie (electronic mag.). Number 2 014 5 (24). [Electronic resource]. M-2014. - Access mode (free): <http://naukovedenie.ru/PDF/21KO514/pdf>. (in Russian)

[24] Friedkin V.M. Innovative concepts of solving problems of providing complex security measures of the Republic of Dagestan of the natural effects of the Caspian Sea level change / Friedkin V.M., Kharlamova U.A., Kuzmenko I.M. // Fifth international scientific and practical conference "Transport and industrial potential of the Caspian region: the state, problems and prospects of integration - 2015". - The Institute of Oriental Studies; May 28, 2015 - 5 pages. (in Russian)

[25] Friedkin V.M. CONSTRUCTIVE-TECHNOLOGICAL DECISIONS OF DESIGN ENGINEERING AND MANUFACTURING OF BEARING ELEMENTS OF THE LOWERED STEEL INTENSITY / Friedkin V.M., Kuzmenko I.M., Sysa N.S., Kuzmenko D.O., Bogdanov S.V. Proceedings of the METNET Seminar 2014 in Moscow. HAMK University of Applied Sciences. Hameenlinna, FINLAND, December, 2014. Pp 153 - 164. ELECTRONIC: ISBN 978-784-694-3 (PDF) HAMKin e-julkaisuja 35/2014. [julkaisut@hamk.fi](mailto:julkaisut@hamk.fi); [www.hamk.fi/julkaisut](http://www.hamk.fi/julkaisut). (English)

# FIRE BEHAVIOUR OF STEEL INDUSTRIAL HALL

László Horváth, Balázs Kövesdi, László Dunai

Budapest University of Technology and Economics, Department of Structural Engineering, 1111.  
Budapest, Műegyetem rkp. 3, Hungary

## ABSTRACT

Welded steel frame is one of the most widely used traditional engineering structures, but its economical fire design is still an important topic nowadays. The aim of the current investigation is to study the complex structural behaviour of a single storey industrial hall structure in fire. The paper focuses on the applicable advanced numerical techniques to make the fire resistance determination more economical. Coupled thermo-mechanical and structural analysis makes possible to simulate the real structural behaviour of the whole analysed structure including the interacting behaviour of the steel members and the joints. The application method and the benefits using coupled thermo-mechanical and structural analysis is discussed in the current paper and its application is presented for an existing steel frame structure. The executed research program is part of an R&D research project called HighPerFrame of the Budapest University of Technology and Economics, Department of Structural Engineering.

Keywords: fire design, steel frames, numerical simulation, industrial halls

## INTRODUCTION

The current Eurocode standard gives valuable support to the designers to calculate the overall performance of steel structures in fire, and to calculate the fire resistance of the structural steel members. However it gives only limited information to design or to evaluate the structural behaviour of the joints in fire. The focus of the current paper is to study the complex structural behaviour of a single storey steel industrial hall in fire including the interacting behaviour of the steel members and the joints. Coupled thermo-mechanical and structural analysis is performed on the analysed structure using advanced numerical models and software tools to determine the structural behaviour and the load carrying capacity at predefined time increments in fire. The application aim of the coupled analysis method is to use the same numerical model to investigate the static behaviour of the frame structure under static loads and under fire actions.

The current engineering praxis usually applies separate models to determine the temperature distribution in the structure by thermo-mechanical analysis, and separated models are used to determine the stresses and the

resistances by mechanical analysis based on the calculated temperatures. The coupled analysis makes possible to join these two analysis types. The main advantage of the coupled analysis is the automatic update of the temperature dependent material properties of the steel and the automatic generation of the temperature distribution with the structure in all the investigated time steps. The application of the coupled analysis method makes possible to predict the load bearing capacity of the joints, structural elements or the whole frame structure by GMNIA simulations and it is also able to make the GMNI analysis using fire actions coming from the detailed thermo-mechanical analysis.

In frame of the current research program local numerical models are developed to investigate the structural behaviour of the joints separately. The local models are built using volume elements modelling the bolts and the contact elements between the header plates. The results of the investigations are used to determine the bending moment – rotation characteristics for all the analysed joints which gives the reductions in the initial stiffness and load carrying capacity in specific predefined time steps (5, 10, 15, 20, 30 sec, etc...). Using this analyses method the structural behaviour of the joints can be characterised in different time steps after the fire start or the utilisation ratio can be directly determined.

Numerical model is also develop for the global frame structure to investigate the interaction behaviour of the steel members and joints under fire. The coupled thermo-mechanical and structural analyses are executed on the complex models by two numerical software tools (SAFIR and ANSYS). For the complex system two models are developed (i) using beam elements and (ii) using volume elements for the whole system. The aim of the two modelling levels are to evaluate the efficiency and accuracy of the modelling level using beam elements which can lead to much faster results during the design of frames than the models with volume elements. The structural behaviour and the load carrying capacity of the complex frame structure under fire is determined on the beam models with and without considering the effect of the joints. The differences between the results are evaluated and the effect of the joints on the fire resistance is discussed.

## DEVELOPED NUMERICAL MODELS

### Investigated Hall Structure

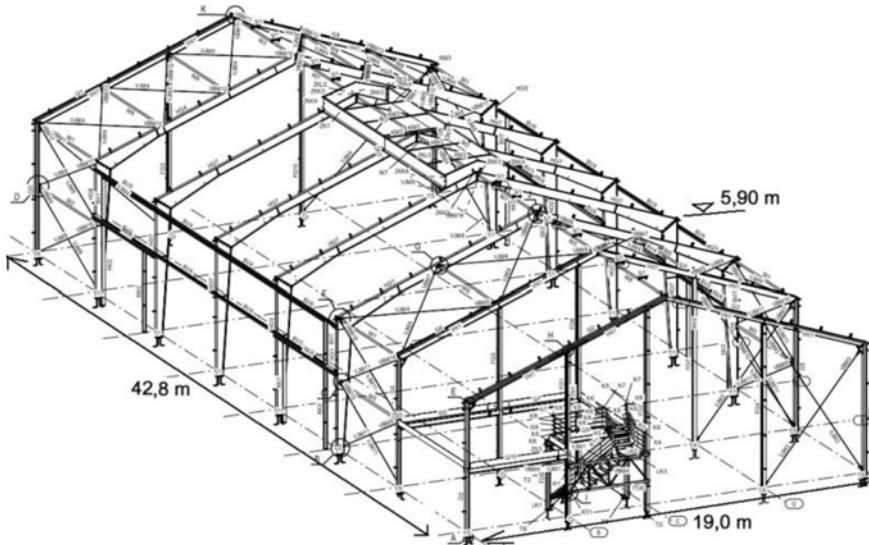


Figure 1. Investigated frame structure

The base of the current investigation is a real frame structure manufactured by the Rutin Ltd, shown in Figure 1. This is a typical one module industrial frame with duopitch roof. The span is 19,0 m, the distance between the frames varies between 6,0 - 6,8 m. The eave height of the structure is 5,9 m with the peak height of 9,36 m. The roof slope is 20°. The roof and the wall systems are also covered by thermo-isolated cladding system. The secondary bearing systems (purlins and girts) are manufactured from cold-formed steel sections. The beams and columns of the internal frames are made from welded I-girders with tapered webs using steel grade of S355J2. The frame has pinned column base joints and fixed peak and beam-to-column bolted joints. The bracing system is made from tie rods using diameters of Ø16- Ø24 mm and from tubes having dimensions of Ø76,1\*2,9 mm - 101,6\*3,6 mm. The fire requirements for the analysed structure are relative high coming from the function of the building. The main bearing system (internal frames and bracing system) is classified in the category R45, and the secondary bearing elements and the sheeting are classified into the category R30.

The executed and currently presented numerical simulations and the developed joints models refer to this existing structure.

### Numerical Model of the Joints and the Applied Material Model

Detailed numerical models are developed using volume elements for all the structural details as well as for the complex structural system. Material models are used in the simulations which can handle large plastic deformations, cumulative damage and fracture mechanism. The developed numerical models are able to handle coupled analysis methods to make the design possible for static loads and fire actions in the same model by updating all the material properties and the solution settings between the two analysis types. The joints are investigated using the Finite element software Ansys 14.5 (e.g. Ansys). The geometry and the finite element mesh of three typical joint models are presented in Figure 2, which are investigated in the current research project.

To model the failure of the bolts and the steel plates the applied material model should handle large plastic deformations and failure criterion. Volume elements are used in the FE analysis which can follow large plastic deformations and a multi-linear - hardening plastic material model is used containing cumulative damage model. The principle of the applied material models can be seen in Figure 3 for the bolts and plates, respectively. By large plastic deformations and using volume elements in the numerical model the application of the true stress-strain curve is more relevant and gives better fit to the real structural behaviour. In the applied material model softening rules are defined after reaching the failure limit point. If a state of stress is found to lay outside of the yield surface a backward-Euler algorithm is used to return the stress to the failure surface. The resulting inelastic increment in strain is then accumulated as crack strain. The maximum stress that can be sustained in an element is then reduced as a function of crack strain (e.g. Ansys). This is called as cumulative damage material model, which is used in the current investigations.

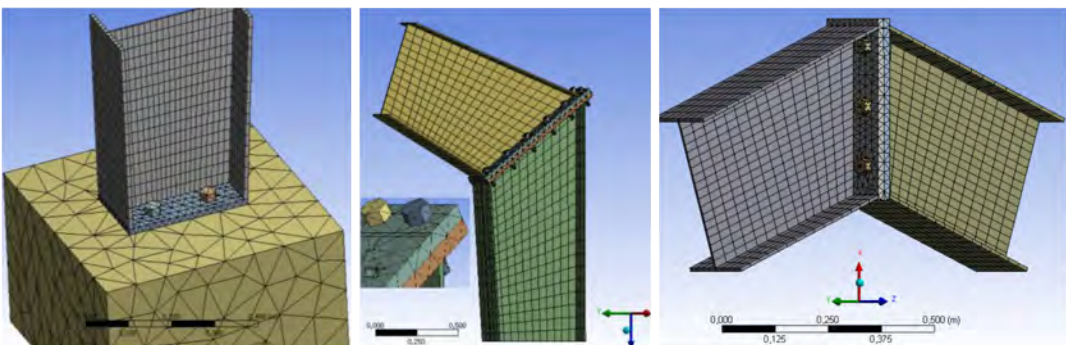


Figure 2. Numerical model of the analysed joints



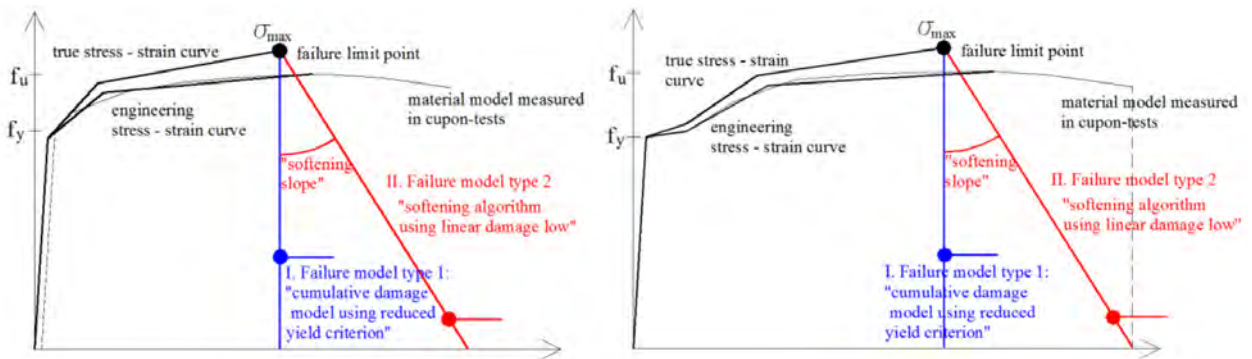


Figure 3. Applied material models

### Numerical Model of the Complex Structure

To study the structural behavior of the complex frame structure and to investigate the joint effect on the behaviour under fire three different modelling levels are used, as follows:

- beam model of one internal frame using supports representing the bracing system, as shown in Figure 4/a,
- 3D model of one frame using volume elements and supports representing the bracing elements,
- complex 3D model of the whole structure modelling the cladding and bracing systems as well, as shown in Figure 4/b.

### STRUCTURAL BEHAVIOUR OF THE JOINTS

The studied joints are subjected by the standard fire action based on the ISO834 (e.g. EN1991-1-2 2002). The temperature distributions in the studied joints are determined and evaluated at different time steps.

The typical temperature distributions after 15 minutes fire are presented in Figure 5. It can be seen that the temperature in the thinner plates (webs) are significantly larger than in the flanges. It can be also observed in the diagrams, that the header plates have also a significant cooling effect on the surrounding plates and on the bolts. This cooling effect can be the main advantage which can be considered in the design of the joints and the complex structure.

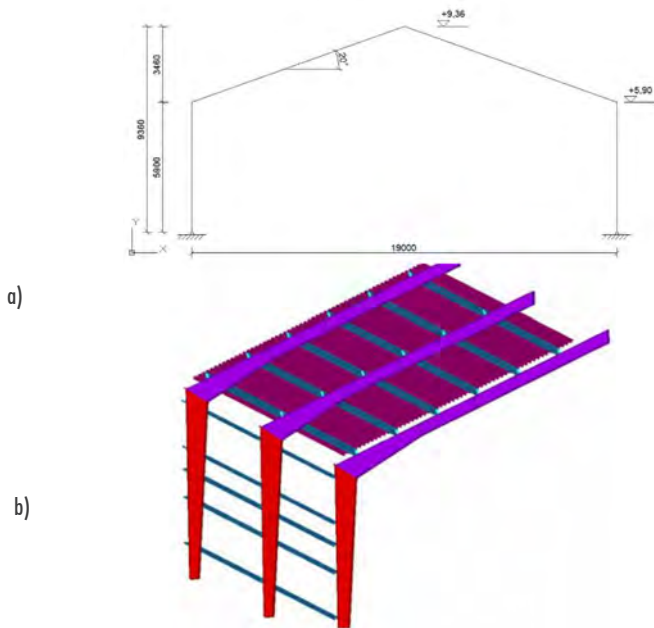


Figure 4. Applied material models using a) beam elements and b) volume elements.

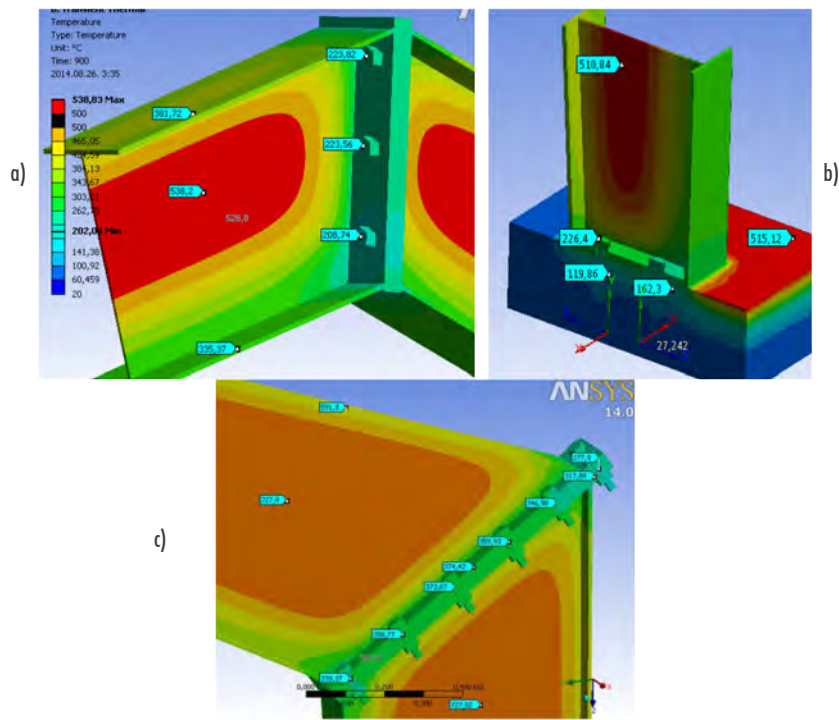


Figure 5. Typical temperature distributions in the analysed joints a) ridge joint b) column base c) frame corner

The largest temperature differences within the joints are observed in case of the column base joint, where the concrete foundation has also a significant cooling down effect. The numerical calculations showed, that the temperature of the concrete base reaches 500 °C after 15 sec fire, but under the base plate the temperature will be only 160°C, which can have positive effect on the joint behaviour in fire. On the other side the temperature in the anchor bolts are also significantly smaller than in other steel parts of the joints.

The structural behaviour of the ridge joint and the beam-to-column joints showed similar temperature distributions. Thus the web plate in the investigated beam and column belongs to Class 4 cross section, the local plate buckling is a relevant optional failure mode of the girder. Thus the increase in the temperature is the largest in the webs, the elongation will be the largest here also, which results in additional compression stresses coming from the supporting and pushing effect of the flanges. It means that by increasing the temperature in the web, the buckling susceptibility increases as well and after the local buckling the stiffness and the load carrying capacity of the joint decreases rapidly.

The final result for all the investigated joints are the moment – rotation curves regarding different time steps and temperature distributions. The typical curves representing the structural behaviour of the beam-to-column joint is presented in Figure 6. The initial stiffness of the joint and the load carrying capacities can be determined for all the analysed joints using the coupled analysis method.

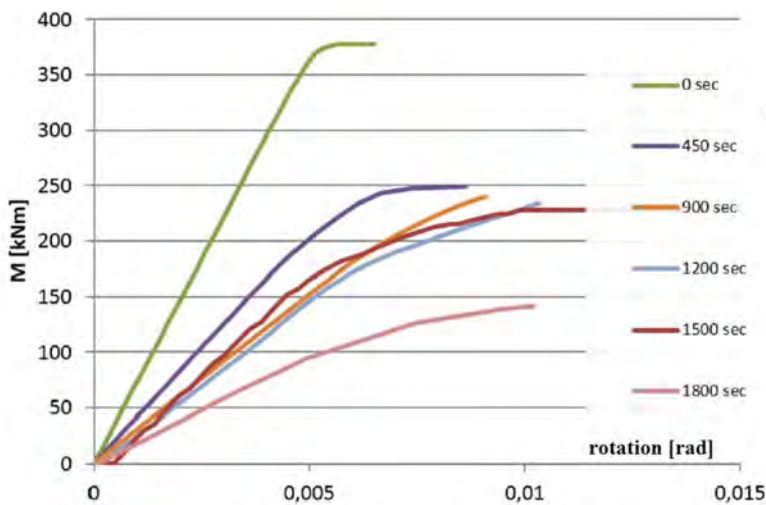


Figure 6. Moment – rotation curves of the beam-to-column joint in different time steps.

## STRUCTURAL BEHAVIOUR OF THE COMPLEX FRAME

The time (temperature) dependent joint characteristics are implemented into a global model to be able to analyse the effect of the joints on the complex structural behaviour under fire action. The global model using beam element is developed with the FE program SAFIR (e.g. *Safir*). The joint characteristics cannot be defined as time dependent values, its properties are handled as a constant within the whole calculation process in the software. Therefore a short virtual element is added to the model at the location of the joints with the time dependent characteristic taken from the local sub-models. The simulations are executed on the global model and the fire life time is determined for both models by neglecting the joint behaviour and by considering them. The results showed that the consideration of the time dependent joint characteristic can lead in the presented case to a 10% longer computed fire life time. The typical failure modes with and without modelling the time dependent joint characteristics can be seen in Figure 7. The increased life time can be explained by the base joint characteristic, thus the cooling effect of the concrete base can have significant effect on the column resistance.

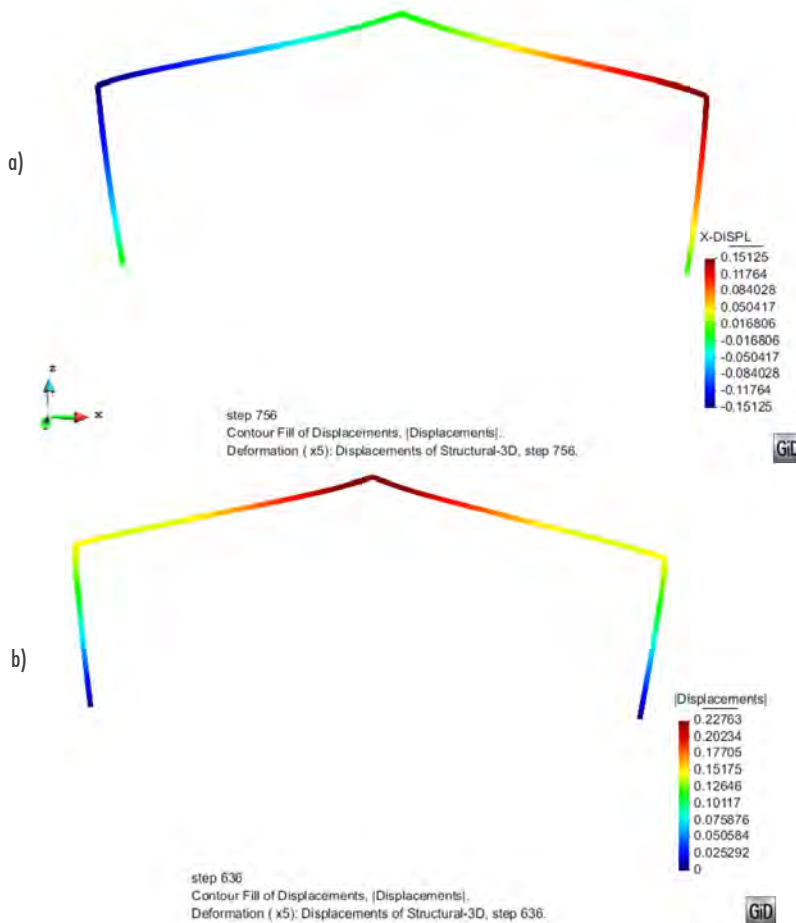


Figure 7. Global failure mode of the frame a) with and b) without modelling the joint effects.

In frame of the current research a complex 3D model in Ansys software (e.g. Ansys) is also developed for one frame structure using volume elements and with detailed joint models which can handle the coupled thermo-mechanical and mechanical analysis types. The typical temperature field after 15 minutes fire can be seen in Figure 8 for the complex structure and for the beam-to-column joint. In this model the calculated temperatures are automatically converted to the mechanical model where all the material properties are defined as temperature dependent values and the numerical model updates the exact material properties for all elements in each time steps. Furthermore the calculated temperature field is applied as a mechanical load on the model, to determine its effect on the internal forces and deformations of the frame. After the thermo-mechanical analysis and the conversion of the results to the mechanical analysis the load carrying capacity of the structure can be determined by GMNI analysis using the temperature dependent mechanical properties. A typical failure mode can be seen in Figure 8 b) after 16 minutes fire and under static loads in the accidental load case combination.

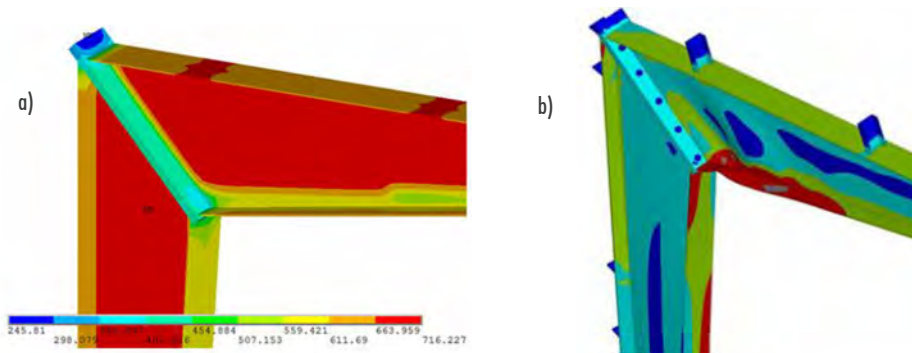


Figure 8. a) Temperature distribution after 15 minutes fire; b) failure mode under combined fire action and static loads in accidental load case combination.

## SUMMARY

The paper gives an outline on a complex research program with the aim to improve the FEM based design method of steel frames loaded by fire action. Application possibility of the coupled analysis methods and its advantages are presented and discussed in the paper which can make the design of steel frames for the static loads and fire action in the same time easier and faster. The paper presents two modelling levels to analyse steel frames under fire action and to consider the time dependent joint characteristics, which can lead to a more accurate approximation of the real structural behaviour. The combined analysis method makes possible to determine the load carrying capacity and the maximum utilization ratio of the structure in different time

steps (e.g. after 5, 15, 30, or 90 minutes fire) and the expected collapse time can also be predicted based on the numerical simulations.

## ACKNOWLEDGMENTS

The presented research program is part of the “*HighPerFrame*” Hungarian national R&D project No. GOP-1.1.1-11-2012-0568, supported by the *New Széchenyi Project, Hungary*. The financial support is gratefully acknowledged.

## REFERENCES

ANSYS® v14.5, Canonsburg, Pennsylvania, USA.

EN 1991-1-2 Eurocode 1: Actions on Structures- Part 1-2.: General actions. Actions on structures exposed on fire. 2002

HighPerFrame research project, Research report, BME Department of Structural Engineering, 2015.

SAFIR: <http://www2.argenco.ulg.ac.be/logiciels/SAFIR/what.html>

# EVOLUTION TREND OF REINFORCEMENT CONNECTIONS IN CONCRETE STRUCTURES

**D'yachkov V.V.**

Ph.D., deputy chief of Reinforcement Laboratory; Research Institute of Concrete and Reinforced Concrete; 6 Vtoraya Institutskaya str, Moscow 109428, Russia d-w@mail.ru

**Devyatov V.V.**

Ph.D., professor of the Structural Steel Faculty; Moscow State University of Civil Engineering; 26 Yaroslavskoe shosse, Moscow 129337, Russia, witalijdeviatow3@gmail.com

**Vershinin V.P.**

Ph.D., associate professor of the Structural Steel Faculty; Moscow State University of Civil Engineering; 26 Yaroslavskoe shosse, Moscow 129337, Russia, vlodya\_91@mail.ru

## ABSTRACT

In the present paper evolution trend of reinforcement connections in concrete structures is considered. A retrospective review and modern techniques of reinforcement connection are presented. Results of tension and fatigue tests of mechanical connections are given. These results revealed strength balance between mechanical connection and reinforcement rod itself. Corresponding development of existing Standards and Codes to be consistent with the experimental data is described.

## INTRODUCTION

Growing volume of construction necessitates transition to more durable, efficient and effective construction techniques. During design and erection of cast-in-place structures a problem with reinforcement connection appears. It is induced by the rod length restricted to 12m due to special manufacturing, transportation and assembling aspects.

Nowadays welded and lapped rebar connections are commonly used. However, an increasing number of building companies intends to abandon welded connections since they are energy-consuming, require recruitment of highly qualified welding operators and more sophisticated quality control and connection of a large number of rods is inherent in high labour consumption.

The most simple rebar connection is the lapped one when force transmission between two rods is provided through rods bonding to concrete. Despite its simplicity, lapped rebar connection has several disadvantages: excessive consumption of steel due to rebar overlap, necessity for setting extra lateral reinforcement within the connection area, and difficulties with placing



concrete into densely reinforced structures that may cause increase of a member cross-section.

Existence of science-based standards and codes is critical for efficient use of a particular type of rebar connection. For instance, lap length according to Russian building code SP 63.13330.2012 [1] is twice as large as that specified by Russian building code SNiP 2.03.01-84\* [2]. This leads to even higher overconsumption of steel that may rise up to 40-50% and makes lapped connections economically unsound. Thus, research of new rebar connection techniques is highly important.

## MECHANICAL REBAR CONNECTIONS

An alternative rod connection is the mechanical one. It should be emphasized that utilization of mechanical connections primarily results in connection durability increase which is extremely important for high-rise structures, while material consumption saving is a secondary goal. That's why mechanical connections are used for joining together reinforcement rods of large diameter (25-40 mm) in a large number of countries, in Great Britain, United States and Germany in particular. One may single out connections that can withstand compressive loads only (Fig. 1) in which force transmission between two rods is realized through rod ends compression and connections that can withstand to both compressive and tensile loads (Fig. 2).

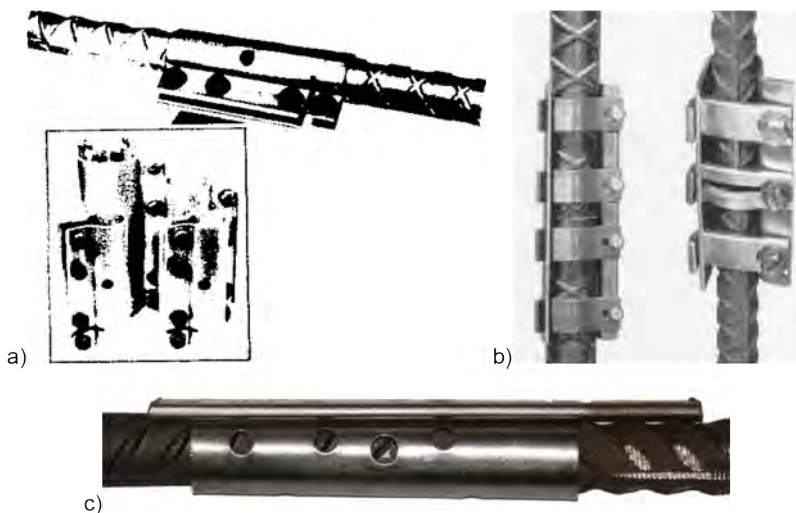


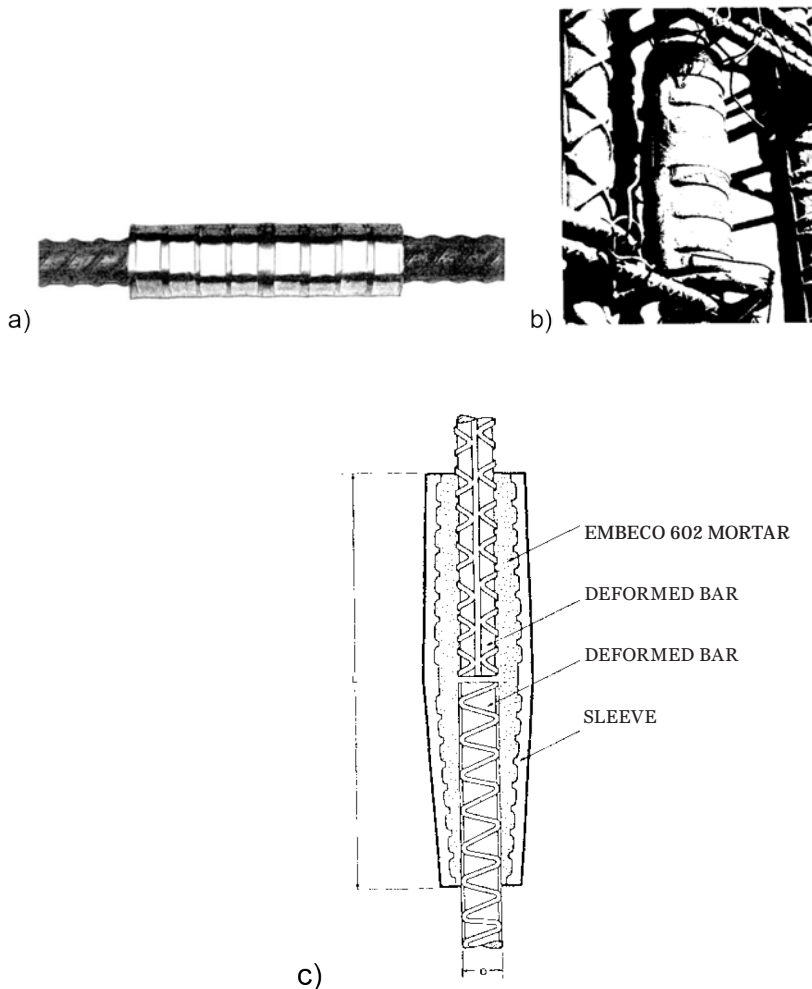
Figure 1. Mechanical rebar connections working in compression: a) rigid coupling; b) banded coupling; c) wedge-lock coupling

Since the mid-2000s Promstroykontrakt Ltd. has been offering a whole range of reinforcement connections: screwed (tapered and cylindrical), crimped and

others. Thereafter Research Institute of Concrete and Reinforced Concrete got into gear and performed an audit on manufacturers of mechanical rebar connections, developed regulatory technical documentation and executed certification. In 2004 essentially the first regulatory documentation RA-10-1-04 [3] appeared.

## EXPERIMENTAL TESTING

Along with documentation development Reinforcement Laboratory of the Research Institute of Concrete and Reinforced Concrete conducted analysis of work of mechanical connections under static and dynamic loading within concrete structure. Statistical processing of experimental data regarding tension of mechanical connections of class A500S rods (according to Russian codes) is presented in Table 1. A total of 986 samples were taken on various sites for certification and quality control and tested.



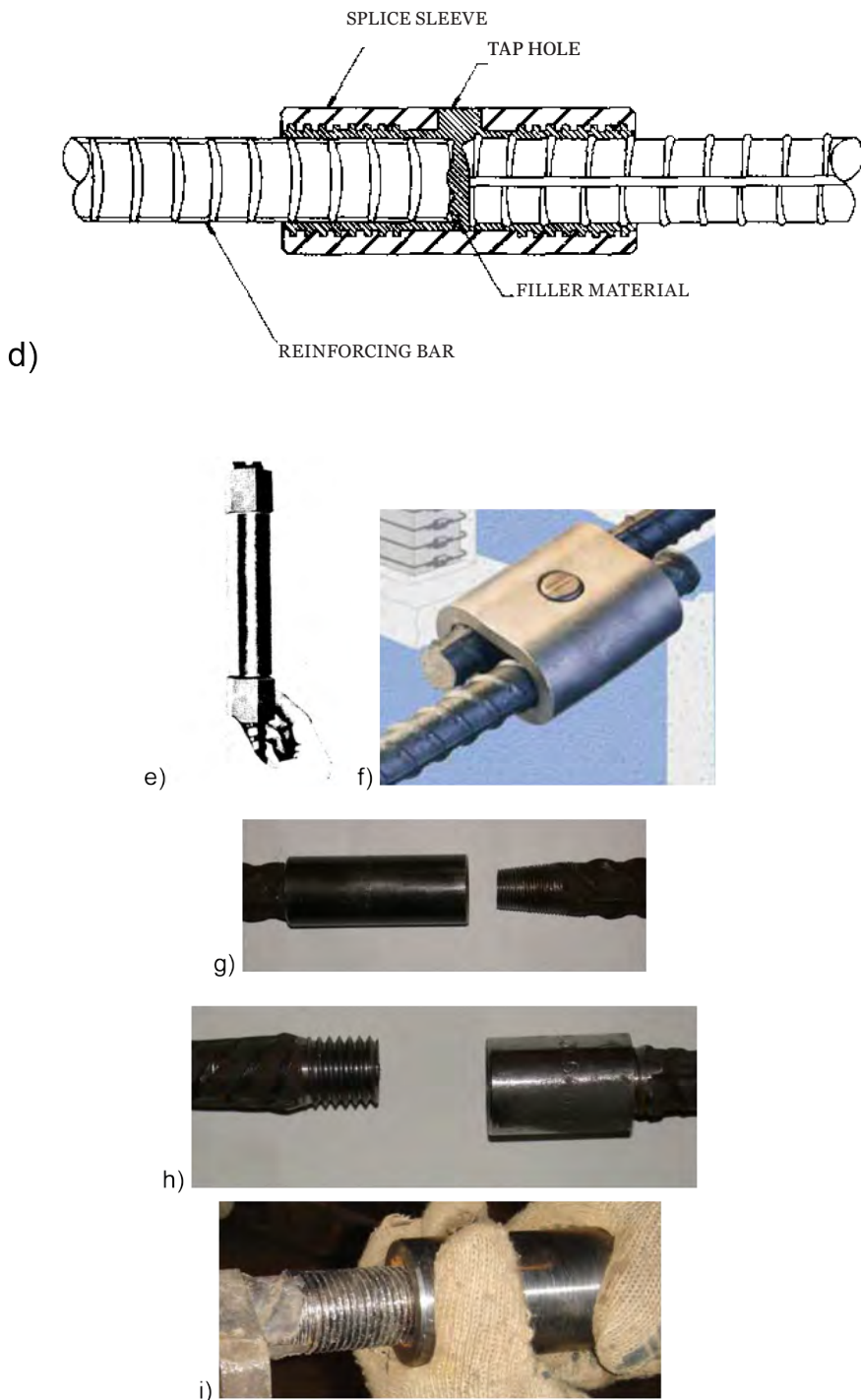


Figure 2. Mechanical rebar connections working in both tension and compression: a) crimped coupling; b) forged steel coupling; c) coupling filled with mortar; d) coupling filled with steel; e) connection of rods with specific screw; f) mechanical overlap rebar connection; g) tapered screwed connection; h) screwed connection with cut thread; i) screwed connection with rolled thread

With reliability of 0.95, tensile strength of mechanical connections of class A500S rods was determined to be 601.1 MPa, which is greater than rebar rejection value of 600 MPa. It should be mentioned that Russian codes are the strictest when concerning strength of such a connection. For instance, in foreign codes this value is prescribed to be greater than  $0.9\sigma_u$ , except nuclear power plants for which strength balance between mechanical rebar connection and rods themselves should be achieved. Average deformability value of screwed connections was determined to be equal to 0.038 mm, that testifies to no slide of rods within the coupling and, hence, no crack formation in the concrete. Determined rod uniform elongation after testing revealed high energy absorption capacity of rod-to-coupling contact. It is a very important property which increases structure durability, in particular its resistance to progressive failure.

Table 1. Results of experimental testing of mechanical rebar connections on tension

Mechanical properties	Mean value X	Standard deviation S	Coefficient of variation V, %	Value with reliability of 0.95
Tensile strength $\sigma_u$ , MPa	669.02	39.72	5.9	601.1
Rod uniform elongation after testing $\delta_u$ , %	7.8	2.1	26.9	4.2

To expand the range of applicability of mechanical rebar connections high-cycle fatigue tests and low-temperature strength tests were conducted. Fatigue tests carried out according to ISO 15835 [5] demonstrated that all types of mechanical rebar connections can withstand to 2 million loading cycles. Moreover, maximum number of loading cycles prior to failure achieved was 9-10 million cycles.

Foreign codes do not specify requirements for mechanical rebar connections under low temperature. Corresponding tests were conducted in the Reinforcement Laboratory of the Research Institute of Concrete and Reinforced Concrete. Samples were immersed into container with gasoline and carbon-dioxide ice and cooled up to  $-70^{\circ}\text{C}$ . When samples were tested in tension their surface temperature was equal to  $-50^{\circ}\text{C}$ . Experiments revealed that all types of mechanical rebar connections possess strength greater than 600 MPa under low temperature.

To assess influence of mechanical rebar connection deformability onto strength, resistance to cracking and deformability of reinforced concrete structures compression tests of axially and eccentrically loaded concrete columns were carried out. Rebar of these columns was connected through screwed couplings with various tightness and, thus, different deformability. The conducted research revealed that influence of mechanical rebar connection deformability onto strength, resistance to cracking and deformability of reinforced concrete columns is negligible [6, 7]. At the same time analysis of research conducted in Russia and other countries concerning work of mechanical rebar connections within bending concrete members was performed.

Hence, it was proposed to design reinforced concrete structures according to standards and codes in force and characteristic and design strength of rebar with couplings set equal to that of intact rods.

## CONCLUSIONS

During the last decade complex research of various types of mechanical rebar connections was performed, that made it possible to include the new data into the revised editions of Russian codes SP 63.13330.2012 [1] and SP 14.13330.2011 [8]. The next step was introduction of the technical requirements for such connections into the project of the new national standard GOST 10922, which is expected to be issued this year.

In summary it may be stated that mechanical rebar connections have become very popular in cast-in-place concrete construction and appeared to be durable, efficient and effective rebar connection technique. According to the existing trend utilization of mechanical rebar connections as a major technique for rods of classes A400 and A500S will increase steadily in Russia as well as in other countries.

## REFERENCES

- SP 63.13330.2012 “SNiP 52-01-2003 Concrete and reinforced concrete structures. Basic framework” (in Russian). – M.: FAU “FCS”, 2011. – 155 p.
- SNiP 2.03.01-84. Concrete and reinforced concrete structures. Design standards (in Russian). – M.: GUP CPP, 2000. – 76 p.
- Guidelines for mechanical rebar connections in reinforced concrete structures. RA-10-1-04 (in Russian). – M.: Association “Reinforced concrete”, 2004. – 22 p.
- Guidelines for utilization of mechanical rebar connections in reinforced concrete members of nuclear power plants. RD EO 0657-2006 (in Russian). – M.: 2006. – 48 p.
- ISO 15835-1:2009. Steels for the reinforcement of concrete – Reinforcement couplers for mechanical splices of bars – Part 1: Requirements.
- D'yachkov V.V. Properties and application features of screwed and crimped rebar couplings in reinforced concrete structures (in Russian). Ph.D. thesis, Moscow, Russia, 2009, 141 p.
- Madatyan S.A., D'yachkov V.V. Research of screwed rebar couplings in compressed reinforced concrete members (in Russian). Concrete and Reinforced Concrete. 2007. Vol. 4. p. 16-20.
- SP 14.13330.2011 “SNiP II-7-81 Building in earthquake-prone regions (in Russian)”. – M.: PLC “CPP”, 2010. – 83 p.

# ON THE ISSUE OF STRUCTURAL ANALYSIS OF SPATIAL SYSTEMS FROM THIN-WALLED BARS WITH OPEN PROFILES

**Anatoly Perelmutter**

Head of Department, Professor, Doctor of Science, Foreign Member of Russian Academy of Architecture and Construction Sciences, SCAD Soft 3a, Osvity str., of. 2, 03037, Kyiv, Ukraine, avp@scadsoft.com

**Vitalina Yurchenko**

Associate Professor, Candidate of Science, Steel and Timber Structures Department, Kyiv National University of Civil Engineering and Architecture, 31, Povitroflotskyj avenue, 03680, Kyiv, Ukraine, vitalina@scadsoft.com

## ABSTRACT

A working hypothesis relating to the structural analysis of the spatial structures from thin-walled bars with open profiles using seven degree of freedoms has been verified. The verification has been performed based on the results of the structural analysis of thin-walled bar systems. The behavior of which under the external loading has been simulated using design schemes with plate finite elements. Structural analysis has been realized using software package SCAD. Results of the performed investigation have indicated that the suggestion concerning to «joint warping» existence or, in other words, the equal warping for the each end member cross-section sided to the joint under consideration often is not true even for those design cases, where plane design models with spatial application of the structural loading are considered. Only the plate finite-element model of the thin-walled bar system can describe correctly the actual interaction of the thin-walled bars at the structural joint.

Key words: thin-walled bar, warping, bimoment, numerical simulation, finite element analysis, root-mean-square error

## PROBLEM STATEMENT

The problem of analysis of spatial structures from thin-walled bars has been of interest in the last few years. Thin-walled bar structures were the subject of investigation of different researchers, who used the finite element with seven degree of freedom at the both ends (Tusnin 2009, Bazant and Nimeiri 1973).

Strain and stress distribution in thin-walled bars with open profiles differs significantly from ordinary bars, as the Euler-Bernoulli's hypothesis of the plane sections as well as principal locality of the action of Saint-Venant's balanced system of forces (Vlasov 1940) are not valid partly or completely. There is considerable warping of cross-sections in thin-walled bars with

open profiles, which reflects appreciably on the structural behavior under the loading.

Structural analysis and calculation of internal forces in thin-walled structural members of open profiles accounting for bending torsion is a complicated task. Modern software packages for structural analysis use finite element types which take into account up to six degrees of freedom at the structural nodes, which corresponds to the linear and angular displacements in these nodes as for the rigid bodies. Structural analysis of thin-walled bar systems can be performed using the shell finite elements. In this case, accurate selection the finite element meshing for approximation of structural members is required. Besides, number of nodes and finite elements increases comparing to the bar approximation by several digits (Tusnin 2008).

At the same time, theory of thin-walled bars of open profile requires using the additional degree of freedom at the nodes adjoined to the thin-walled bars. The additional degree of freedom corresponds to the warping components of the total longitudinal node displacement. It should be noted, that it is necessary to determine correctly the support conditions of thin-walled finite element for this additional degree of freedom. Finally, the problem of strain compatibility conditions at the nodes of bar design model is left in abeyance, if there is additional degree of freedom which depends from the cross-section shapes of the bars sided to the joint under consideration.

Tusnin in his paper (Tusnin 2008) considered the problem of structural analysis of spatial thin-walled bar structures with open profiles and developed thin-walled bar finite element with seven degrees of freedom at the both ends (see Fig. 1). He also presented stiffness matrix for such thin-walled bars taking into account the bending torsion deformation as well as coordinate transformation matrix in order to transform from the local to the global system of coordinates.

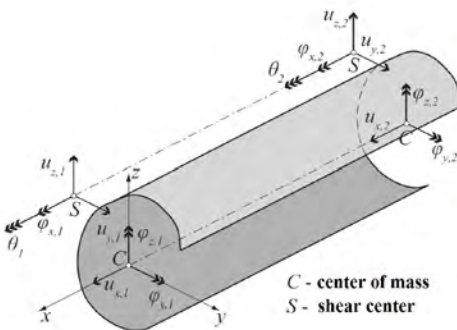


Figure 1. Thin-walled finite element with seven degree of freedom on each end

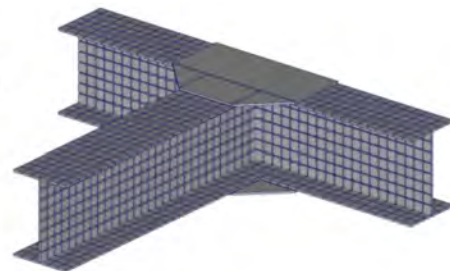


Figure 2. Plane rectangular frame according to (Horbunov and Strelbitckaja 1948)



In the last few years there were lots of scientists efforts to construct a universal algorithm for structural analysis of an arbitrary thin-walled bar system. Formulation of the boundary conditions at the ends of the thin-walled bar was the main problem in this context (Tchernyj 1996). In certain papers (Horodetckyj *et al.* 1976, Postnov and Kharhurim 1974) authors used the principle that at the end of the thin-walled bar the warping deformation either is absent completely (rigid support relative to the warping), or free (the hinge relative to the warping).

A hypothesis concerning to uniform warping for all end cross-sections of all thin-walled bars adjacent to the considered joint has been used by A. R. Tusnin in his paper (Tusnin 2009) for certain types of joint structural decisions. V. A. Postnov and I. Ya. Kharhurim also supposed that the spatial orientation of the thin-walled bar has no an influence on the warping, namely, warping deformation at the local and global system of coordinates has been assumed as equal (Postnov and Kharhurim 1974).

The approach mentioned above is sufficient, for example, for plane rectangular frames without eccentricities at the joints, when the bar axis passes through the shear centers, flanges of all bars at the considered joint are parallel to the frame plane, and gusset plates welded to the flanges have got an infinite in-plane stiffness and allow the warping in out-of-plane direction (Bychkov 1962, Horbunov and Strelbitckaja 1948) (see Fig. 2).

Different types of thin-walled finite elements and calculation techniques for structural analysis of thin-walled structural systems have been considered by authors of the following papers (Tchernov and Diyakov 2008, Gluck and Kalev 1972). Approaches applicable for only particular cases, which take into account warping compatibility conditions at the joints and focus on using seven node unknowns (six linear and angular displacements and warping) have been used in these papers (see Fig. 1). However, the hypothesis about availability of the unified warping at the node of truly space bar structures raises serious doubts and needs to be checked accurately.

## RESEARCH TECHNIQUE

Henceforth accurate finite-element models of the thin-walled bar systems loaded by an external torque moment with different support conditions have been considered. Besides, thin-walled bars for these models have been simulated by a set of plate finite elements. Longitudinal displacements of end cross-sections points  $\hat{u}_i$  of all thin-walled bars adjoined at the FE model, as well as axial stresses at these points  $\hat{\sigma}_i$  have been calculated for constructing finite-element models of the thin-walled bar systems. Comparison of the FE calculation results with the theoretical values of the longitudinal displacements  $u_i$  and axial stresses  $\sigma_i$  allows estimating the warping value and, in this way, calculating the bimoment value.

Let's consider base hypothesis of Vlasov's theory relating to the behavior of a thin-walled bar with open profile. Longitudinal displacement for each  $i^{\text{th}}$  point of the cross-section of such bar can be expressed using the following equation:

$$u_i(x, s) = \xi(x) - \eta'(x)y_i(s) - \zeta'(x)z_i(s) - \theta'(x)\omega_i(s), \quad i = 1, \dots, n, \tag{1}$$

where the first three summands of the equation correspond to the hypothesis of plane sections, namely:  $\xi(x)$  – longitudinal displacement of the center of mass C as function of axial coordinate  $x$  of the section under consideration;  $\eta(x), \zeta(x)$  – lateral displacements of the pole S of the section under consideration;  $y_i(s), z_i(s)$  – coordinate of the  $i^{\text{th}}$  section point under consideration as function of the angular position  $s$ . The last summand of the equation (1) corresponds to the warping component of the longitudinal displacements of section points at the direction of  $x - x$  axis, where  $\theta(x)$  and  $\omega_i(s)$  – rotation angle of the section under consideration about the pole S and sectorial coordinate for  $i^{\text{th}}$  section point accordingly (see Fig. 3).

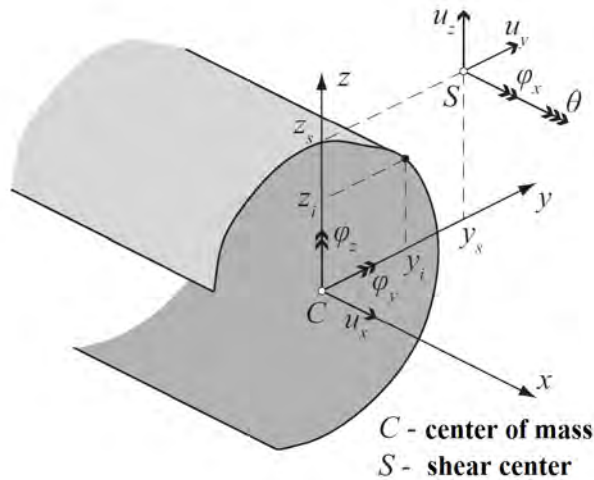


Figure 3. Cross-section of the thin-walled finite element with seven degree of freedom

Therefore, based on the sectorial geometrical properties of the cross-section and having the set of numerical values of longitudinal displacements  $\hat{u}_i, (i = 1, \dots, n)$  of  $n$  cross-section points as a result of FE structural analysis of plate finite-element model, we can calculate the warping  $\theta'(x)$  for each end cross-section of all thin-walled bars at the joint under consideration.

Deviations for the results of numerical calculation using equation (1) from the results of FE structural analysis for some  $i^{\text{th}}$  cross-section point can be written as,  $i = 1, \dots, n$ :

$$e''_i(x, s) = \xi(x) - \eta'(x)y_i(s) - \zeta'(x)z_i(s) - \theta'(x)\omega_i(s) - \hat{u}_i. \quad (2)$$

Using the least square technique the equation (2) formulated for each  $i^{\text{th}}$  cross-section point,  $i = 1, \dots, n$ , can be turned into the following problem of functional minimization:

$$\mathbf{E}_u = \sum_{i=1}^n (e''_i(x, s))^2 = \sum_{i=1}^n (\xi(x) - \eta'(x)y_i(s) - \zeta'(x)z_i(s) - \theta'(x)\omega_i(s) - \hat{u}_i)^2 \rightarrow \min. \quad (3)$$

Herewith, indispensable conditions for the minimum of the functional (3) give the system of linear equations relative to the unknown factors of the initial equation (1):

$$\left\{ \begin{array}{l} \frac{\partial \mathbf{E}_u}{\partial \eta'(x)} = -\eta' \sum_{i=1}^n (y_i)^2 - \zeta' \sum_{i=1}^n y_i z_i - \theta' \sum_{i=1}^n y_i \omega_i + \xi \sum_{i=1}^n y_i - \sum_{i=1}^n y_i \hat{u}_i = 0, \\ \frac{\partial \mathbf{E}_u}{\partial \zeta'(x)} = -\eta' \sum_{i=1}^n z_i y_i - \zeta' \sum_{i=1}^n (z_i)^2 - \theta' \sum_{i=1}^n z_i \omega_i + \xi \sum_{i=1}^n z_i - \sum_{i=1}^n z_i \hat{u}_i = 0, \\ \frac{\partial \mathbf{E}_u}{\partial \theta'(x)} = -\eta' \sum_{i=1}^n \omega_i y_i - \zeta' \sum_{i=1}^n \omega_i z_i - \theta' \sum_{i=1}^n (\omega_i)^2 + \xi \sum_{i=1}^n \omega_i - \sum_{i=1}^n \omega_i \hat{u}_i = 0, \\ \frac{\partial \mathbf{E}_u}{\partial \xi(x)} = -\eta' \sum_{i=1}^n y_i - \zeta' \sum_{i=1}^n z_i - \theta' \sum_{i=1}^n \omega_i + n\xi - \sum_{i=1}^n \hat{u}_i = 0; \end{array} \right. \quad (4)$$

Here, the indication of dependency from axial coordinate  $x$  or angular position  $s$  has been omitted and notations  $\eta$ ,  $\zeta$  and  $y_i$ ,  $z_i$  have been only used for the purpose of simplification.

Therefore, constructing and solving the system of linear algebraic equations (4) for each end cross-section of all thin-walled bars at the joint under consideration allows calculating the warping value  $\theta'(x)$  for these cross-sections. In turn, comparing the warping value  $\theta'(x)$  at the mentioned cross-sections gives the possibility to verify the hypothesis about its equality.

Verification of the static conditions at the node should be performed similarly comparing the values of the longitudinal (normal) stresses  $\hat{\sigma}_i$  ( $i = 1, \dots, n$ ) at the considered cross-section points of the plate finite-element model with the theoretical values of the stresses  $\sigma_i(x, s)$ . The latter has been calculated using the known formula for thin-walled bar taken into account the value of bimoment:

$$\sigma_i(x, s) = \frac{N(x)}{A} + \frac{M_y(x)}{I_y} z_i(s) + \frac{M_z(x)}{I_z} y_i(s) + \frac{B(x)}{I_\omega} \omega_i(s). \quad (5)$$

Deviations for the results of numerical calculation  $\hat{\sigma}_i$  ( $i=1, \dots, n$ ) using equation (5) from the results of FE structural analysis for some  $i^{\text{th}}$  cross-section point can be written as,  $i=1, \dots, n$ :

$$e_i^\sigma(x, s) = \sigma_i(x, s) - \hat{\sigma}_i = \frac{N(x)}{A} + \frac{M_y(x)}{I_y} z_i(s) + \frac{M_z(x)}{I_z} y_i(s) + \frac{B(x)}{I_\omega} \omega_i(s) - \hat{\sigma}_i. \tag{6}$$

Comparing the theoretical values of the longitudinal (normal) stresses  $\sigma_i(x, s)$  ( $i=1, \dots, n$ ) with the numerical values of the stresses  $\hat{\sigma}_i$  derived as the results of numerical experiment when minimization of sum of squared deviations we have obtained the following:

$$\mathbf{E}^\sigma = \sum_{i=1}^n (e_i^\sigma(x, s))^2 \rightarrow \min,$$

$$\mathbf{E}^\sigma = \sum_{i=1}^n \left( \frac{N(x)}{A} + \frac{M_y(x)}{I_y} z_i(s) + \frac{M_z(x)}{I_z} y_i(s) + \frac{B(x)}{I_\omega} \omega_i(s) - \hat{\sigma}_i \right)^2 \rightarrow \min. \tag{7}$$

On the basis of indispensable conditions for the minimum we have obtained the system of linear algebraic equations relative to the unknowns of the longitudinal stresses equation (5) at the cross-sectional points of the thin-walled bar:

$$\begin{cases} \frac{\partial \mathbf{E}^\sigma}{\partial \left( \frac{N(x)}{A} \right)} = n \frac{N}{A} + \frac{M_z}{I_z} \sum_{i=1}^n y_i + \frac{M_y}{I_y} \sum_{i=1}^n z_i + \frac{B}{I_\omega} \sum_{i=1}^n \omega_i - \sum_{i=1}^n \hat{\sigma}_i = 0, \\ \frac{\partial \mathbf{E}^\sigma}{\partial \left( \frac{M_z(x)}{I_z} \right)} = \frac{N}{A} \sum_{i=1}^n y_i + \frac{M_z}{I_z} \sum_{i=1}^n (y_i)^2 + \frac{M_y}{I_y} \sum_{i=1}^n y_i z_i + \frac{B}{I_\omega} \sum_{i=1}^n y_i \omega_i - \sum_{i=1}^n y_i \hat{\sigma}_i = 0, \\ \frac{\partial \mathbf{E}^\sigma}{\partial \left( \frac{M_y(x)}{I_y} \right)} = \frac{N}{A} \sum_{i=1}^n z_i + \frac{M_z}{I_z} \sum_{i=1}^n z_i y_i + \frac{M_y}{I_y} \sum_{i=1}^n (z_i)^2 + \frac{B}{I_\omega} \sum_{i=1}^n z_i \omega_i - \sum_{i=1}^n z_i \hat{\sigma}_i = 0, \\ \frac{\partial \mathbf{E}^\sigma}{\partial \left( \frac{B(x)}{I_\omega} \right)} = \frac{N}{A} \sum_{i=1}^n \omega_i + \frac{M_z}{I_z} \sum_{i=1}^n \omega_i y_i + \frac{M_y}{I_y} \sum_{i=1}^n \omega_i z_i + \frac{B}{I_\omega} \sum_{i=1}^n (\omega_i)^2 - \sum_{i=1}^n \omega_i \hat{\sigma}_i = 0, \end{cases} \tag{8}$$

here the indication on dependency from axial coordinate  $x$  or angular position  $s$  has been omitted and notations  $\eta, \zeta$  and  $y_i, z_i$  have been only used for the purpose of simplification.

## HYPOTHESIS VERIFICATION

The ordinary design models of the thin-walled bar systems have been examined by implementing the numerical experiment. Only structures with the rigid member-to-member joints have been subjected to the structural analysis, where flanges of the one structural member were connected to the flanges or stiffeners of another structural member in order to omit the section contour distortion. Just that very structural decision of the rigid joints ensures the clear transmitting of the bending moments and bimoments from one thin-walled structural member to another.

### Numerical experiment 1

Steel frame structure made of three thin-walled bars of I-section (see Fig. 4) with flange section 600 x 10 mm and web section 800 x 10 mm have been examined. The axis (geometrical locus) of the shear centers of the I-cross-sections coincides with the axis (geometrical locus) of the centers of mass.

Numerical calculation (structural analysis) of the plate finite-element models has been performed using software package SCAD. Figure 4, *b* presents deformed scheme of the structure, where those cross-sections of the thin-walled structural members are also indicated, for which warping values have been calculated.

Comparing the results of the numerical calculation for three end cross-sections (see Table 1) adjacent to the considered joint, we can see that its warping values practically coincide with each other only for the end cross-sections of the rafters located at the one and the same horizontal plane, besides the warping values for the rafters end cross-sections differ markedly from the warping value for the column end cross-section.

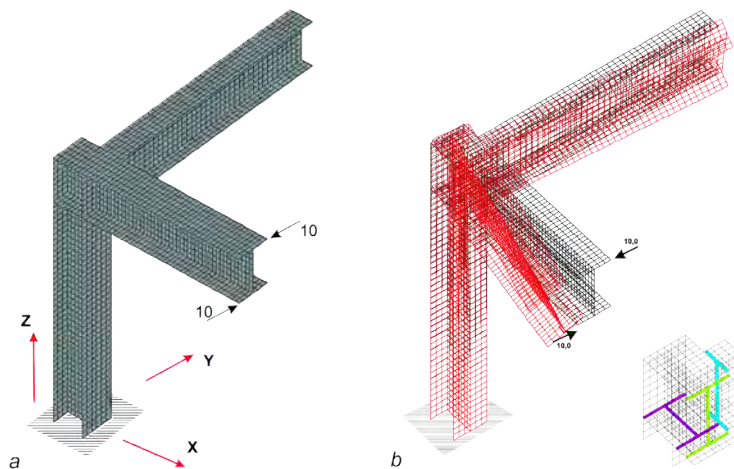


Figure 4. Plate finite-element model of the structure to the Numerical Experiment 1: a – initial; b – deformed

Table 1. Results of the numerical experiment (Numerical Experiment 1)

Characteristic, $\text{mm}^{-1}$	Rafter along axis $y-y$	Rafter along axis $x-x'$	Column
Warping $\theta'(x), \times 10^{-5}$	-11,0397	+ 11,16	+ 9,6751

### Numerical Experiment 2

A knee frame has been examined (see Fig. 5). The lower end of the frame column was rigid supported; the end of the rafter was free, where external torque moment 1 kNm was applied. Frame column had I-section with web section and flange section 300 x 10 mm. Frame rafter had I-section with web section 400 x 10 mm and flange section 300 x 10 mm.

Two structural decisions of the rigid rafter-to-column joint have been considered: (1) with one skewed stiffener and (2) with two transversal stiffeners. Additionally, frame design model, where the column web was oriented perpendicularly to the rafter web (see Fig. 5), has been also examined.

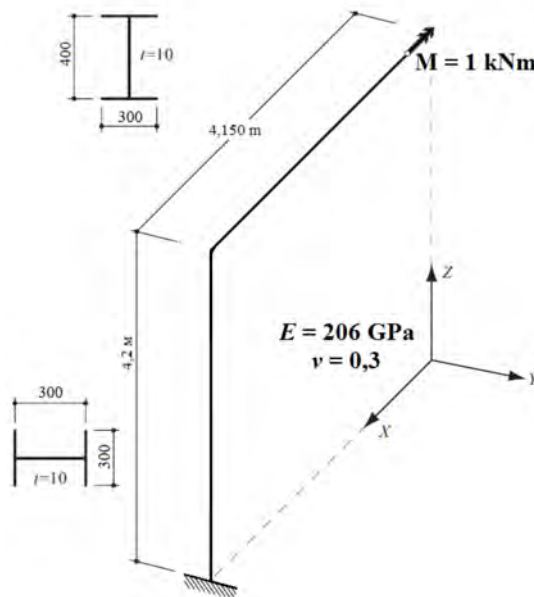


Figure 5. Design model of the structure (Numerical Experiment 2)

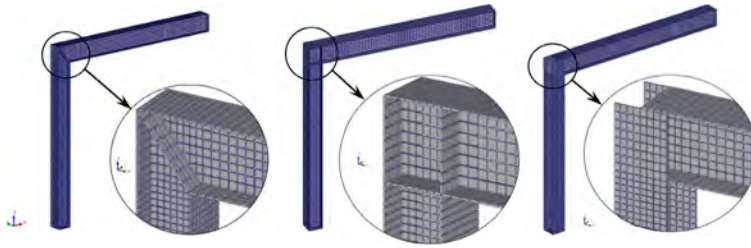


Figure 6. Plate finite-element models of the rafter-to-column joints (Numerical Experiment 2)

The results of the numerical experiment have been compared in order to detect the dependence of the warping value from the load type. The warping values at the rafter and column end cross-sections sided to the joint as well as its ratio have been estimated depending on different conditions of external torque moment application: (1) at the rafter free end, (2) at the middle of the rafter span, (3) at the middle of the column height too.

Table 2 presents the results of the numerical experiment. As a result of implemented numerical experiment it has been detected that changing the design scheme of the load application on the structure causes significant changing not only the warping values, but also the ratios of the warping values at the rafter and column end cross-section sided with joint under consideration.

Table 2. Warping values at the end cross-sections of the rafter and column, 10-2 m-1, as well as its ratio by the different conditions of the external torque moment application

Joint structural decision	The location of the external torque moment application					
	At the end of the rafter		At the middle of the rafter span		At the middle of the column height	
	$\frac{\text{Rafter warping}}{\text{Column warping}}$	Ratio	$\frac{\text{Rafter warping}}{\text{Column warping}}$	Ratio	$\frac{\text{Rafter warping}}{\text{Column warping}}$	Ratio
Joint 1	$\frac{1,6428}{1,1995}$	1,36957	$\frac{0,844576}{0,60955}$	1,38557	$\frac{1,78992}{2,4204}$	0,7395
Joint 2	$\frac{1,61008}{-1,3974}$	-1,1522	$\frac{0,805494}{-0,6968}$	-1,15599	$\frac{-2,0744}{2,40584}$	0,86224
Joint 3	$\frac{1,38199}{-1,2153}$	1,13716	$\frac{0,696314}{-0,60951}$	-1,14242	$\frac{-1,8117}{2,10829}$	0,85932

### Numerical Experiment 3

A knee rectangular frame with rigid supports at the ends of the column and rafter has been considered. External torque moment has been applied at the middle of the rafter span. The frame structural members had I-section with web section 300 x 10 mm and flange section 200 x 10 mm. Four structural



decisions for the rigid rafter-to-column joint have been examined: (1) without stiffeners or stiffening diaphragms, (2) with one skewed stiffener, (3) with two transversal stiffeners and (4) with two transversal and one skewed stiffeners (see Fig. 7).

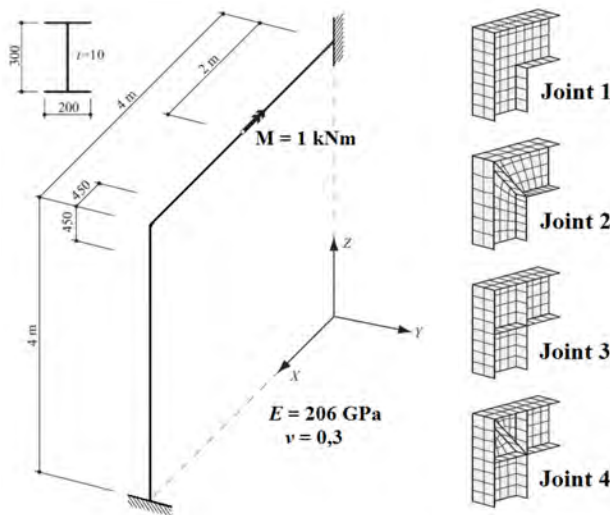

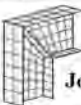




Figure 7. Design model of the structure (Numerical Experiment 3)

Table 3. The results of numerical experiment 3

Plate finite element model of the joint	Characteristic	Rafter	Column
 <b>Joint 1</b>	Warping value, $\times 10^{-3} \text{ mm}^{-1}$	+ 0,00512	+ 0,0006
	Bimoment, $\text{Nm}^2$	- 52,0886	+7,781292
 <b>Joint 2</b>	Warping value, $\times 10^{-3} \text{ mm}^{-1}$	+ 0,00541333	+ 0,00010667
	Bimoment, $\text{Nm}^2$	- 52,9171	- 10,5611
 <b>Joint 3</b>	Warping value, $\times 10^{-3} \text{ mm}^{-1}$	+ 0,00362667	- 0,00198
	Bimoment, $\text{Nm}^2$	+118,1281	- 60,2334
 <b>Joint 4</b>	Warping value, $\times 10^{-3} \text{ mm}^{-1}$	+ 0,0020933	- 0,00044
	Bimoment, $\text{Nm}^2$	+246,8	-50,0292

The results of the numerical experiment show that the structural decision of the rigid rafter-to-column joint has significant influence on the warping and bimoment distribution in the structural system (see Table 3). The values of the warping and bimoment at the end cross-sections of the rafter and column sided with rafter-to-column joint were different for all design cases.

Therefore, the results of the performed investigation have pointed that the suggestion concerning to «joint warping» existence or, in other words, the equal warping for the each end member cross-section sided to joint under consideration often is not true even for those design cases, where plane design models with spatial application of the structural loading are considered.

In a general case we have no possibility to indicate so called joint center, i. e. the point, where axes pass through the shear centers of the end member cross-sections sided to the joint under consideration are intersected. This structural joint doesn't meet certain conditions of theory of plane thin-walled frames. Only the spatial finite-element model of the thin-walled bar system can describe correctly the actual interaction of the thin-walled bars at the structural joint.

In the paper (Cichoń and Koczubiej 2008) polish scientist S. Koczubiej has proposed an approach to solve the described problem. As the full finite-element modeling of all thin-walled bars of the structural system leads to the cumbersome design models, he proposed to use shell finite elements in the joint region only and thin-walled bar finite elements in other structural regions (see Fig. 8 and Fig. 9). Proposed approach reduces significantly initial data volume and, in this way, design model of the structure. At the same time, structural design model reflects truly its behavior as for the bar structure under the loading.

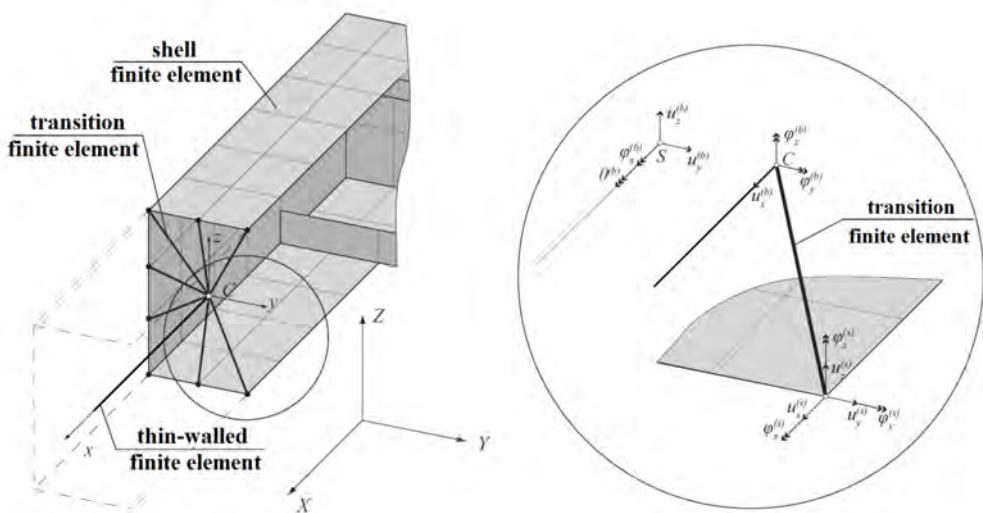


Figure 8. Structural modeling using shell and thin-walled finite elements (Cichoń and Koczubiej 2008)

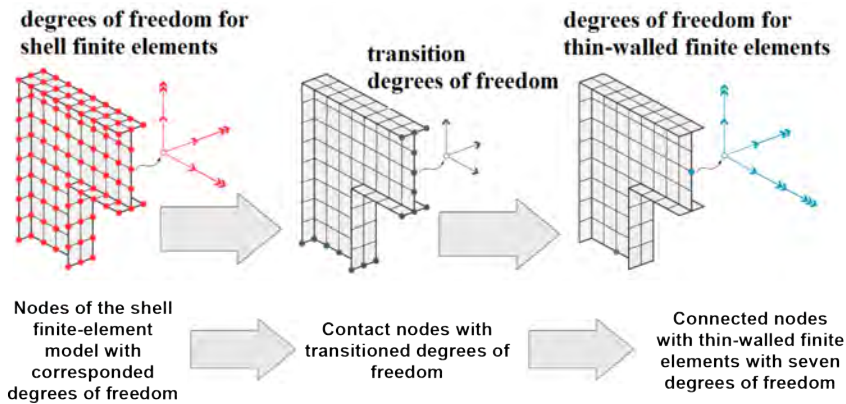


Figure 9. Transformation of variables of the finite-element method when structural modeling using shell and thin-walled finite elements (Cichoń and Koczubiej 2008)

## CONCLUSION

In this paper a working hypothesis relating to the structural analysis of the space structures from thin-walled open profiled bars using seven degree of freedoms has been undertaken. The verification has been reduced to the analysis of the results of calculation of the certain bar systems; their behavior under the loading has been simulated using thin plate finite element models. The results of the performed investigation have pointed that the suggestion concerning «joint warping» existence or, in other words, the equal warping for the each end member cross-section sided to joint under consideration often is not true even for those design cases, where plane design models with spatial application of the structural loading are considered. Only the spatial finite-element model of the thin-walled bar system can describe the actual interaction of the thin-walled bars at the structural joint correctly.

## REFERENCES

1. Bychkov, D. V. Structural mechanics of bar thin-walled structures [Текст] / D. V. Bychkov. – М.: Gosstroyizdat, 1962. – 476 p. (in Russian)
2. Vlasov V. Z. Thin-walled elastic bars [Текст] / V. Z. Vlasov. – М.: Goshortehizdat, 1940. – 256 p. (in Russian)
3. Horbunov, B. N. Theory of frames from thin-walled bars [Текст] / B. N. Horbunov, A. I. Strelbitckaja. – М.: Gostehizdat, 1948. – 198 p. (in Russian)

4. Horodetckyj, A. S. FEM application to analysis of thin-walled bar systems [Текст] / A. S. Horodetckyj, V. S. Zdorenko, V. S. Karpilovskij // Strength of materials and structural theory. – Issue 28. – K.: Publisher “Budivel’nyk”, 1976. – p. 134–140. (in Russian)
5. Postnov, V. A. Finite element method for analysis of shipboard structures [Текст] / V. A. Postnov, I. Ya. Kharhurim. – M.: Sudostroenije, 1974. – 344 p. (in Russian)
6. Tusnin, A. R. Numerical calculation of structures from thin-walled bars with open profiles [Текст] / A. R. Tusnin. – M.: Publisher “ASV”, 2009. – 144 p. (in Russian)
7. Tchernov, S. A. Relating to the analysis of space thin-walled bar system [Текст] / S. A. Tchernov, I. F. Diyakov // Automatization and modern technologies. – 2008. – № 2. – p. 3–7. (in Russian)
8. Tchernyj, A. N. Relating to the question of joint connections simulation of thin-walled bar system [Текст] / A. N. Tchernyj // Mechanics and control processes. – Ulianovsk: USTU, 1996. – p. 54–58. (in Russian)
9. Bazant, P. Large-deflection spatial buckling of thin-walled beams and frame [Текст] / P. Bazant, M. E. Nimeiri // Journal of Structural Engineering. – ACSE, 1973. – №99. – P. 1259–1281.
10. Cichoń, C. Consistent FEM model for thin-walled space frames [Текст] / C. Cichoń, S. Koczubiej // Czasopismo Techniczne, 21, Budownictwo 1-B. – 2008. – Vol. 21. – p. 3–20.
11. Gluck, G. Computer method for analysis of multi-storey structures [Текст] / G. Gluck, J. Kalev // Computer and Structures. – 1972. – Vol. 2. – № 5–6. – p. 25–32.

# RESOURCE-WISE SOLUTIONS – A KEY TO SUCCESSFUL FUTURE BUSINESS

**Tarja Meristö, Jukka Laitinen**

FuturesLabs CoFi, Laurea University of Applied Sciences  
tarja.meristo@laurea.fi, jukka.laitinen@laurea.fi

## INTRODUCTION

Sustainable business models usually cover economic, social and ecological aspects of the development (UN 1987). However, the significant dimensions of the sustainable growth are also the use of time and capital, which added to the aspects of the sustainable development will form the concept of lean resource management (Kettunen 1995). Lean-resource management will lead to resource-wise solutions including all these aspects throughout the whole business process and ecosystem consisting of core-businesses, related businesses and enablers (Meristö & Laitinen 2014).

The companies themselves are aware of the impact of resource-wise solutions on the future business. Totally 99 companies were interviewed between 9/2013 and 10/2014 in Western Uusimaa, Finland, in the project concerning sustainable business which was carried out by Novago Business Development and Laurea University of Applied Sciences. The interviewed companies covered several different branches and business areas including retail, tourism and catering business, wellbeing, technology industry, construction and marketing and communication. Currently, the majority of the companies thought that sustainability is basic business but in the future (5 – 10 years from now on) its role as a competitiveness factor will increase. In the near future, the companies will focus on economic sustainability, which is quite understandable in these economically challenging times. Quite many of the respondents were also going on to put emphasis on ecological issues (e.g. products and services, materials, debris) or concentrate on social sustainability (e.g. work wellbeing, product responsibility, norms and standards). When discussing the main sources for the sustainability pressure, the customers (54 answers) were seen to be the most important motivator. Also, the personnel of the company (51) seem to be also in an active role when rising the awareness for sustainability issues. Education (28), authorities (25), subcontracting network (25), competitors (22) and media (18) received also were also mentioned relatively often. Finance (4) received only few mentions (Meristö & Laitinen 2014).

The views collected at Metnet Luleå in 2013 show an increasing importance of sustainability in education sector as well. 21 seminar participants from education sector and 2 company representatives answered a questionnaire in Metnet seminar in 2013. Regarding resource-wise solutions it was

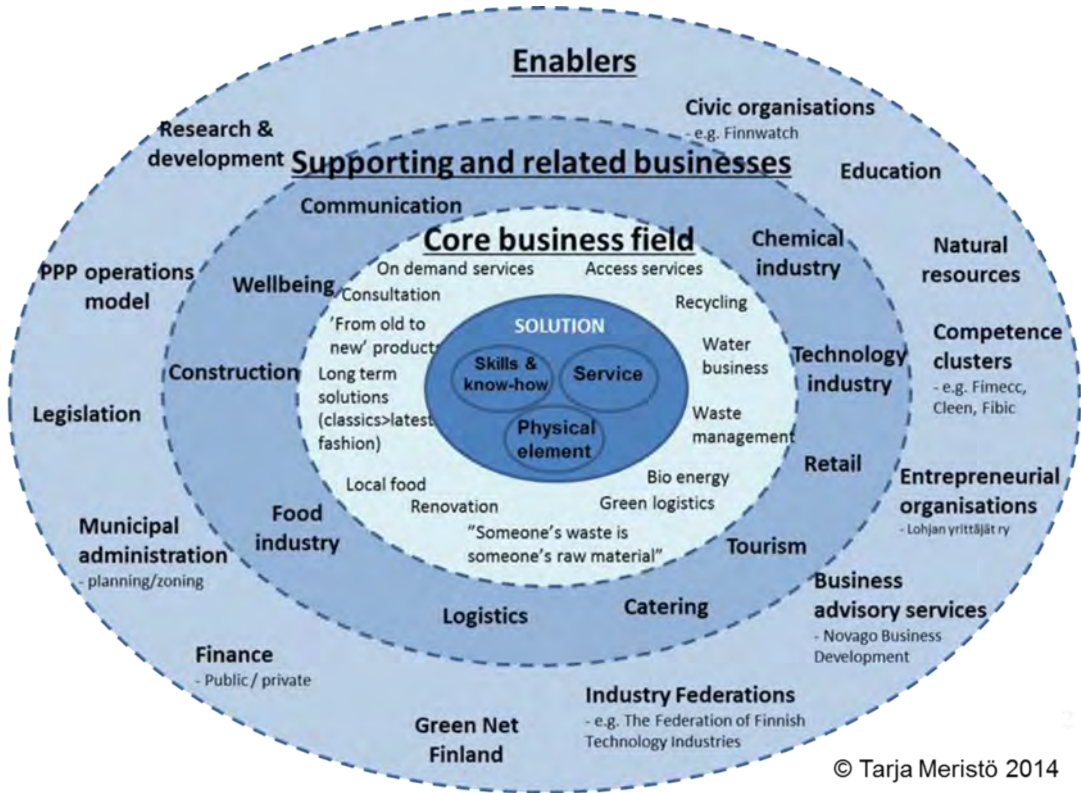
remarkable that materials and energy were seen as the most important issue in the sustainable business. According to the respondents, the importance of the sustainability will increase in future and it will be seen more like an opportunity and competitiveness factor, not only empty words.

In this paper we will focus on resource-wise solutions as a starting point to successful business models for the future. Especially Environment, Health and Safety (EHS) drivers for the future will form a complex set of enabling and constraining factors. The attitude towards these forthcoming trends is a key to successful business models. Offensive, proactive attitude will open new opportunities whereas defensive reactive mindset will highlight more threats coming up from the changes (Meristö 1991, Meristö et al 2000). As a framework for the paper we use the sustainable business cluster developed in western Uusimaa (Meristö & Laitinen 2014), which we will develop further with water related business cluster as well as with case studies concerning climate change as a driver for resource-wise solutions (Berninger 2012).

Methodological approaches in this paper will consist of the multidisciplinary futures research field including e.g. multiple scenario methodology (Meristö 1989), visionary concept design (Kokkonen et al 2004) and minitrend concept (Vanston & Vanston 2011).

## FRAMEWORK

As a framework, we apply the sustainable business cluster which illustrates the ecosystem of sustainable business in the Western Uusimaa (Meristö et. al 2014). The cluster of sustainable business in Western Uusimaa includes not only cleantech companies, but companies throughout all business clusters, e.g. construction industry, retail companies and wellbeing companies, which all have the sustainable eco-system their own. According to Porter's (1990) cluster definition we have divided the actors of the eco-system in three different positions: core business field, supporting & related businesses and enablers (Figure 1). We have develop Porter's model further and e.g. in the core business field we define the businesses through three elements of the competitive advantage: services, physical elements and skills & know-how. The more the focus is on service and know-how, the more sustainable is the solution. Also, the more eco-efficient the product or the physical element is and using renewable/recycled materials during its production process, the more sustainable is the whole solution (Meristö et. al 2014). Of course, the business relying on the utilization of skills and know-how belongs to the sustainable eco-system as well.



© Tarja Meristö 2014

Figure 1. Sustainable business cluster in Western Uusimaa (Meristö et. al 2014).

Balanced Triple Helix (Figure 2) model will summarize the elements of sustainability, i.e. the economic, social and ecological dimensions to the elements of regional development, i.e. government, industry and university actors and their roles in the region (Meristö & Laitinen 2013). Resource-wise solutions in industry side need support from government and university. Unique research work can lead to business innovations, even to radical innovations only in the networked environment where all the actors have a broader shared vision but also the goals of their own with high ambition level.



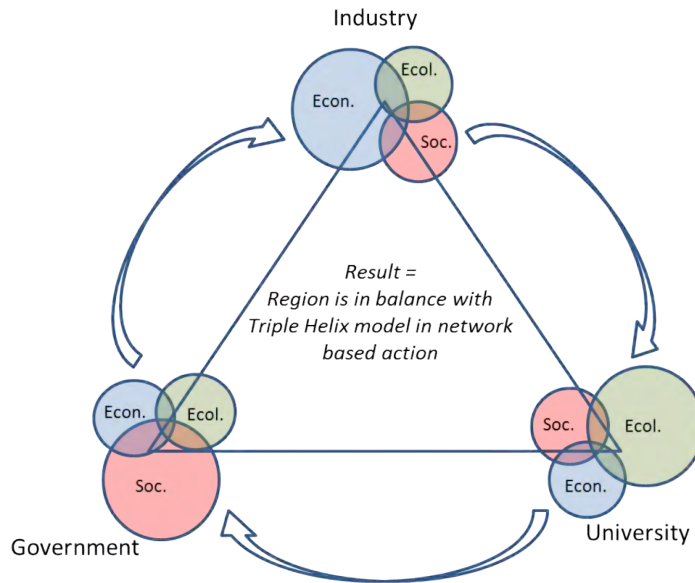


Figure 2. Balanced Triple Helix Model combines Triple Helix actors to the sustainability concept (Meristö & Laitinen 2013).

## METHODS

Methodological approaches in this paper will consist of the futures research (e.g. Masini 1993; Bell 1997) field including e.g. multiple scenario methodology (Meristö 1989), visionary concept design (Kokkonen et al 2004) and minitrend concept (Vanston & Vanston 2011). Futures studies are a multidisciplinary scientific research field focusing on possible, desirable and probable futures in long run (Amara 1981).

According to Ossip Flechtheim (1943) the main task of futures research is to avoid the threatening consequences from the human behavior, rather to promote solutions to improve the living conditions on the earth and to avoid unsustainable elements in every case. The value basis of futures research forms a strong starting point for the sustainable business models and it will also promote resource-wise solutions to fulfill the principle "to save the world is a profitable business" (Meristö 1991).

Multiple scenario approach is a supporting tool especially for strategic planning process in order to open up the opportunities and threats as well as totally new perspectives in longer run to the future. Scenarios are not predictions, rather they are possible outcomes, which will form a basis for strategy work and will

give an estimate for flexibility needs integrated to the strategy in the case the basic line will not be realized as expected. Scenarios will help companies to deal with uncertainty and make decisions under uncertainty. In the field of sustainable business this follows the proverb, where “the early bird finds the worm” (Meristö 1989).

Practical tools to develop futures research further and implement its results in everyday business life e.g. are visionary concept design (Kokkonen et al 2004) and minitrend concept (Vanston & Vanston 2011). Visionary concept design will produce with the help of alternative scenarios for different thematic purposes systematically scenario-specific products, services, business models as well as new values and needs not yet recognized. Scenarios also will help in timing in the form of scenario specific navigation marks (Meristö 1999). Minitrends on the other hand will open megatrends to the pragmatic level by recognizing the direct and indirect influences and by categorizing them e.g. into the groups where you can follow the money, follow the leaders, examine limits, consider human nature or take notes of demographics as well as analyze frustrations and search convergences, as described in minitrend book (Vanston & Vanston 2011). Minitrends will shorten the time perspective to the next 2-4 years and bring the future opportunities closer to exploit in everyday business work. Visionary concept design combined to minitrends in the context of sustainable development will produce innovations, which are by definition resource wise solutions to the market.

## RESULTS

Scarcity of clean water is one of the important megatrends influencing world-widely. Drink water for people, process water for industry, natural water for leisure and tourism as well as wastewater for recycling are all in the core of sustainable water business ecosystem (Kettunen 2010). According Kettunen’s research report, marketing and brand promotion have been the main pitfalls in this field, as well as the lack of co-operation. Water related business ecosystem is slowly growing up and its relations between different actors and hubs are strengthening. Also the research activities around water issues will be resourced and their role according triple helix model is crucial by offering new information and insights to the future opportunities for companies, but also for governments both at local and global levels. Still, environmental issues are political by background, and that can form barriers for developing new business models in the market, if the legislative and administrative enablers are not in time. Water seems to be like oil business in old days, where oil crisis and even oil wars established every now and then.

- water-wise
- resource-wise
- climate-wise

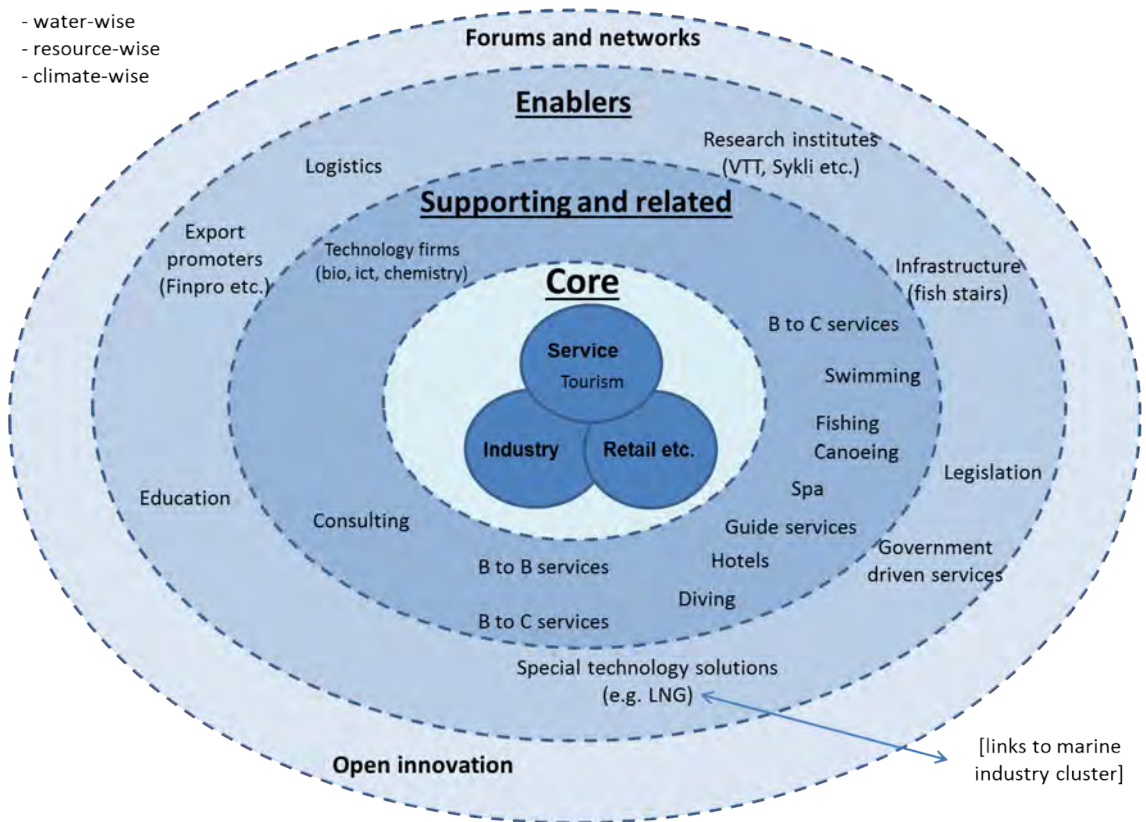


Figure 3. Water related business cluster in Western Uusimaa.

Minitrend method was piloted in the foresight seminar arranged in Tampere Subcontracting Fair in September 2015. Potential minitrends related to climate change from the logistics theme were explored by applying the Impact Wheel tool (Vanston & Vanston 2011). At first, direct and indirect implications related to climate change were considered and then the results were analyzed to find potential minitrends (Figure 4). The pilot group found four potential minitrends which were: 1) Regional pipe network for waste management, 2) Transforming waste to energy and to new products, 3) Raw material logistics for 3D printing and 4) Knowledge management utilizing the internet of things.

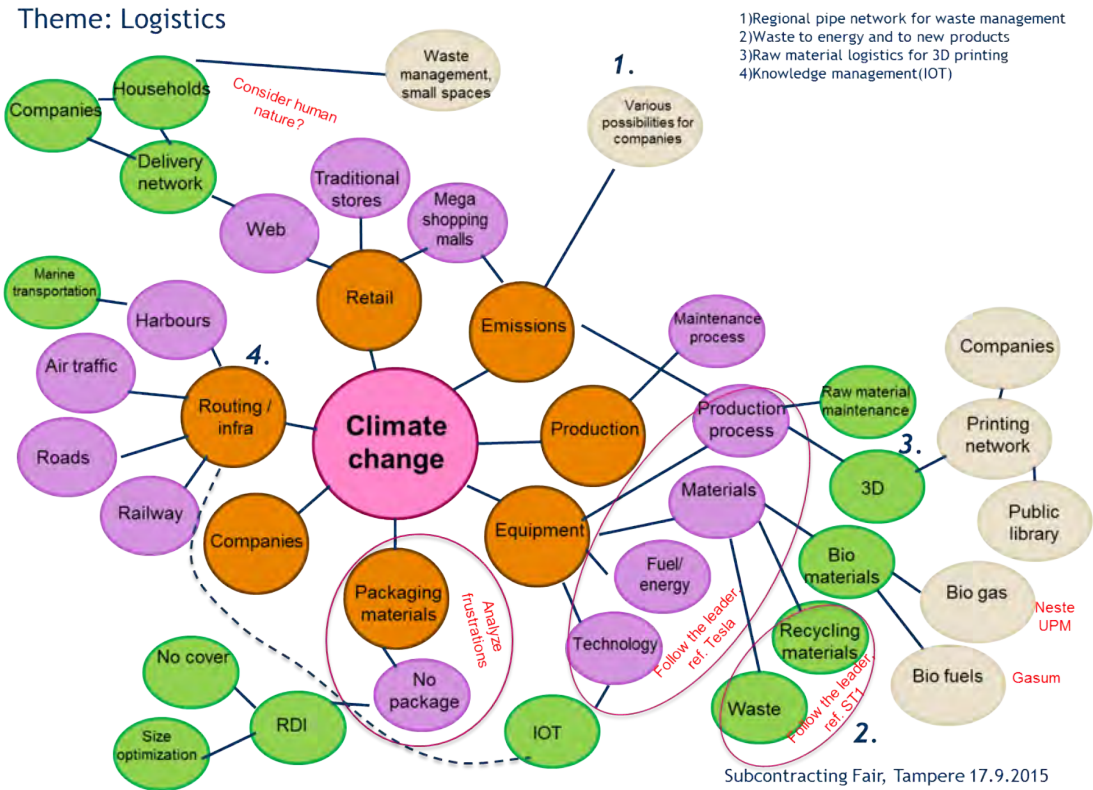


Figure 4. Impact wheel results: minitrends related to climate change (Subcontracting Fair, Tampere 17<sup>th</sup> September 2015).

## CONCLUSION

Resource-wise solutions based on visionary concept design and mega- and mini trends were developed in future workshop with participants from all triple helix groups i.e. from industry, university and government. The preliminary results show that the lean resource management as well as eco-efficiency issues are well established but more attention should be focus on consumer-driven businesses, on future generations with new values and on rapid prototyping and experimental work, where research and development vary with practical applications in real life context. In this way the resource-wise solutions will reach the planning process, too (Figure 5).

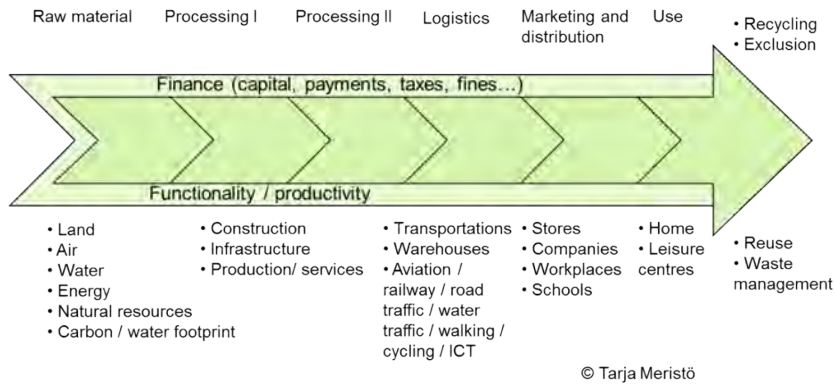


Figure 5. Sustainable business as a value chain.

## REFERENCES

- Amara, R. (1981) Searching for Definitions and Boundaries. *The Futurist*, February 1981. pp. 25-29.
- Bell, W. (1997) *Foundations of Futures Studies I: History, Purposes, Knowledge*. New Brunswick, NJ: Transaction Publishers, 1997.
- Berninger K. (2012) *Hiilineutraali Suomi. Gaudeamus (a book in Finnish on Coal-Neutral Finland)*.
- UN (1987) *Our Common Future – Report of the World Commission on Environment and Development*.
- Kettunen, J. (1996) *Suomen ekoviennin mahdollisuudet. KTM (a report in Finnish on Opportunities for Finnish Eco Export. A report to the Ministry of Trade and Industry)*.
- Kettunen, J. (2010) *Veteen liittyviä mahdollisuuksia Länsi-Uudellamaalla. Helmi-ohjelma. (Opportunities related to water. Helmi Programme). (In Finnish)*.
- Kokkonen et al (2004) *Visioiva tuotekonseptointi. Teknova (a book in Finnish on Visionary Concept Design)*.
- Masini, E. (1993) *Why Futures Studies?* Grey Seal, London.
- Meristö, T. (1989) Not Forecasts but multiple scenarios when coping with uncertainties in the competitive environment. *European Journal of Operational Research* Vol 38, pp. 350-357, 1989.

Meristö, T. (1991) Skenaariotyöskentely yrityksen johtamisessa. (Scenario Working in Company Management). Acta Futura Fennica No 3, VAPK-kustannus, Helsinki, Finland (in Finnish).

Meristö, T. & Laitinen, J. (2013) Sustainability as a Business Opportunity Today and Tomorrow: Triple Helix Perspective, in Proceedings of The METNET Seminar 2013 in Luleå: HAMKin julkaisuja 1/2014. HAMK University of Applied Sciences, Hämeenlinna, Finland.

Meristö, T. & Laitinen, J. (2014) Kestävän liiketoiminnan mahdollisuudet Länsi-Uudellamaalla – nykytila ja tulevaisuuden näkymiä (a report in Finnish on Opportunities for Sustainable Business in Western Uusimaa – a Present Situation and Alternative Future Views).

Meristö, T., Laitinen, J. & Ahola, A. (2014) Future Sustainable Innovations – a Competitive Advantage or a Must? In proceedings of The XXV ISPIM Conference – Innovation for Sustainable Economy & Society, Dublin, Ireland on 8-11 June 2014.

Porter, M. E. (1990), *The Competitive Advantage of Nations*, Macmillan, London.

Vanston, J. & Vanston, C. (2011) *Minitrends: How Innovators & Entrepreneurs Discover & Profit From Business & Technology Trends*.

# ADHESIVE BONDED STEEL STRUCTURES UNDER CYCLIC LOADING

**Lukáš Ledecký, Yvonne Ciupack, Hartmut Pasternak**

Chair of Steel and Timber Structures, Brandenburg University of Technology,  
Cottbus, Germany

**Christoph Mette, Elisabeth Stammen, Klaus Dilger**

Institute of Joining and Welding, University Braunschweig, Germany

## ABSTRACT

Adhesive bonding has the potential to advance the productivity, efficiency and quality of steel construction. It can be seen as an alternative to classical bonding methods, because fundamental problems such as residual stresses and the reduction of the cross section can be prevented. Steel construction is ideally suited for the application of bonding technology, due to the high grade of pre-manufacturing. Under workshop conditions, durable bonded joints with a sufficient load carrying capacity and serviceability can be realized, but it is not yet possible to design adhesive bonded steel structures based on the current level of standardisation. Instead, costly and time-consuming approvals are necessary, inhibiting innovation for small and medium-sized companies. The establishment of adhesive bonded steel structures in the standardisation process could provide a remedy. In an earlier research project the basis for the design of two application examples for the steel façade construction was developed, thus completing the first step for the development of Eurocode-based design of adhesive bonded steel joints. However, the results of this research refer only to quasi-static, short time loads, so there is still a lack of knowledge regarding the mechanical behaviour of bonded joints under cyclic loading. This is the central aspect of this article. The object of investigation is an adhesively bonded façade connection, of which potential and viability was investigated in an earlier research project. In addition, cyclic small sized specimen tests are carried out, to develop general rules and examine their transferability for specimen components.

## INTRODUCTION

The applicability of bonding technology for steel structures has been validated in a variety of investigations. For example, the pedestrian and pipeline bridge in Marl over the canal Lippe (see Figure 1) demonstrates the durability of bonded joints. The bridge was built in 1956, with a span of 56 m. The bar-shaped elements are bonded to the gussets. For easy mounting and in case of a bondline failure additional bolts are used, but even in the latest official report (Trittler 1963), all bondlines were described as being in working order. The potential of bonding technology has been demonstrated in previous research



projects. In the first project (Dilger and Pasternak 2008) the load carrying capacity and serviceability of different application of bonding were evaluated experimentally. A subsequent research project (Dilger and Pasternak 2012) regards the development of Eurocode-based design rules for adhesive bonded joints in steel façades. Within the scope of these investigations three different adhesives were analysed, while the studies were limited to quasi-static loads. Thus, it was shown that adhesive bonding is an innovative joining technique for steel structures and has the potential to increase the innovation ability of small and medium sized companies. The achieved knowledge is an essential basis for the development of design rules based on the currently used semi-probabilistic safety concept. Despite this, there is still a lack of confidence and a low level of acceptance in civil engineering regarding bonded steel joints. One reason is the lack of available knowledge on the lifespan of bonded steel connections. Because a façade is loaded by permanent loads, wind and temperature change, quasi-static loading cannot be assumed. In general and specifically for steel construction, there is insufficient knowledge about fatigue behaviour of bonded joints. To increase the acceptance of this innovative joining technology the investigation of bonded joints under cyclic loading is necessary.



Figure 1. First bonded steel bridge

## ADHESIVE BONDED FAÇADE CONNECTION

All studies focus on a specific application of bonding technology in steel structures. Figure 2 shows a bonded connection of a trapezoidal sheet to the supporting structure of a typical mullion and transom façade.

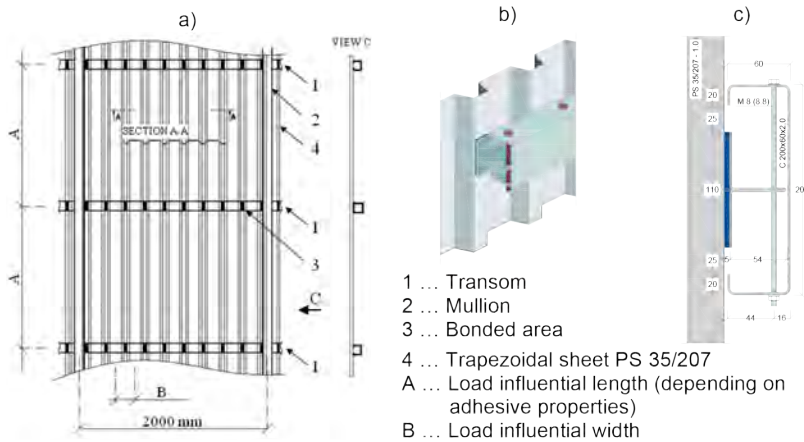


Figure 2. Façade with adhesively bonded connections a) technical view; b) schematic figure; c) cross section normal to the longitudinal axis

The connection is realized by a special T-shaped connection profile. The function of the bonded joint is to transfer the wind loads from the trapezoidal sheet to the transom profile. The transfer of permanent loads is realized by the transom profile with closed cross-section positioned in the centre and connected directly, without bonded connection. By constructing the fastening this way, restraints can be avoided. The bonding procedure is realized under workshop conditions and the prefabricated joint can be connected to the façade structure by a simple plug and screw method. Thus, compliance with high manufacturing requirements can be guaranteed and reproducible bondlines can be realized. Due to the relinquishment of visible fastener heads, manufacturing errors and tolerances can be compensated, and the self-cleaning effect of the façade is assured. Figure 2 shows the result of an optimization procedure regarding the geometrical relations of the bonded joint. The objective of optimization, which was the scope of a previous research project (Meinz 2010), was to minimize stress concentrations as well as achieve the maximum load capacity. Through the applied bondline geometry shown in Figure 2, a nearly uniform normal stress distribution in the bondline can be achieved.

## DETERMINATION OF CYCLIC TEST PROCEDURES

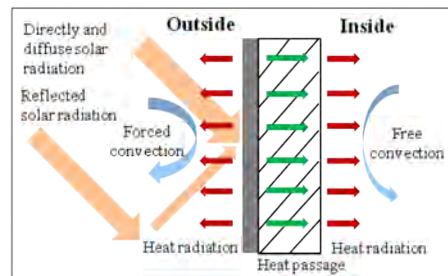
### General Remarks

In comparison with classical steel connections, the performance of adhesive bonds must be regarded as time and environment dependent. Specifically, the load bearing and deformation behaviour of a bondline is characterised by creep and relaxation processes, affected by temperature effects and permanently altered by ageing processes. These polymer specific properties

must be considered. Because the studied façade connection is mainly stressed by temperature and wind loads, the first aim is to derive a representative experimental process based on actual measured environmental data.

City	Maximum [°C]	Minimum [°C]
Berlin	77.91	-18.52
Bremen	76.32	-16.12
Dresden	78.46	-18.33
Düsseldorf	76.48	-15.43
<b>Erfurt</b>	<b>78.25</b>	<b>-19.52</b>
Hamburg	76.00	-16.45
Hannover	76.82	-16.77
<b>Karlsruhe</b>	<b>80.34</b>	-16.56
Kiel	73.52	-16.67
Magdeburg	78.35	-17.48
Mainz	78.41	-14.98
München	79.13	-18.73
Potsdam	78.03	-17.10
Saarbrücken	78.16	-16.02
Stuttgart	79.33	-17.21
Wiesbaden	78.01	-16.15

a)



b)

Figure 3. Temperature values and influencing parameters: a) temperature values obtained by simulation; b) the façade temperature influencing parameters

## TEMPERATURE IMPACTS

Based on temperature measurements of different weather stations in Germany, the extreme temperatures for a specific period and the variation of temperature load over time are determined by statistical means. Different thermo-physical effects such as radiation and convection are considered for this calculation. The influencing parameters are summarized in Figure 3. The obtained values of the simulation are given in Figure 3a) and confirm a temperature range from  $-20^{\circ}\text{C}$  to  $80^{\circ}\text{C}$ . These results are in agreement with Eurocode 1 (DIN EN 1991 1 5 2010) and the definition of the German Code for external walls (DIN 18516 1 2010).

Based on an hourly approach, a suitable loading cycle was determined statistically, which is shown in Figure 4. The dashed line in Figure 4 characterizes the code requirements (DIN EN 1991 1 5 2010), where the minimum temperature of the coldest month is assumed to be  $-20^{\circ}\text{C}$ . For every month a “model day” is developed based on the smallest and highest façade temperatures in each month. This procedure results in the curve, shown in Figure 4, which defines the temperature variation during a model day. During the experimental investigations a model day will be repeated the number of times equal to the number of days in a month.

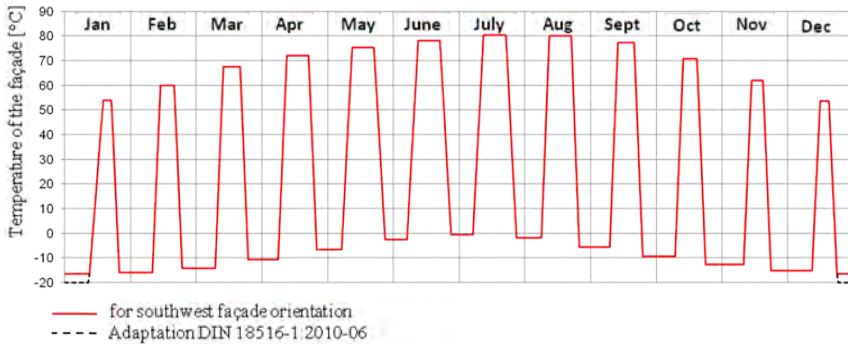


Figure 4. Statistically determined temperature load cycle (Germany)

## Wind loads

In a following step a test procedure for wind loading based on actual measured wind data is developed. To determine the wind load history the energy spectrum of the free wind flow is assumed by the frequencies of the gusts that give a substantial contribution to the energy spectrum. According to (Zuranski 1979) this scale ends at 0.2 Hz. To take into account the vortex shedding effect, the unsteady flow is analysed by the Strouhals-number. In the framework of the project a 10 m wide quadratic building, located in wind zone II according to Eurocode (DIN EN 1991-1-4 2010) is examined. Thus an average wind speed of 25 m/s and vortex frequency of 0.3 Hz is assumed. As a conservative approach the sampling frequency of the wind speed measurement is assumed to be 1 Hz.

As a preparative step the natural frequency of the façade system is determined by considering different adhesive strengths and transom spacing. Because this frequency is higher than 15 Hz for every analysed case, the façade motion induced load can be neglected due to the minimal dynamic response (according to (Nakagami 2003)). Based on the recommendations of Eurocode (DIN EN 1991-1-4 2010), the transition of wind speed at the local wind pressure on surfaces is done strictly.

The wind data processing is described as a four step procedure in Figure 5. The basis is characterized by actual measured wind speed data, which is analysed for a specific period (source of data for 1 Hz sampling rate: (KIT 2015), source of data for 10 minutes sampling rate: (DWD 2015)).

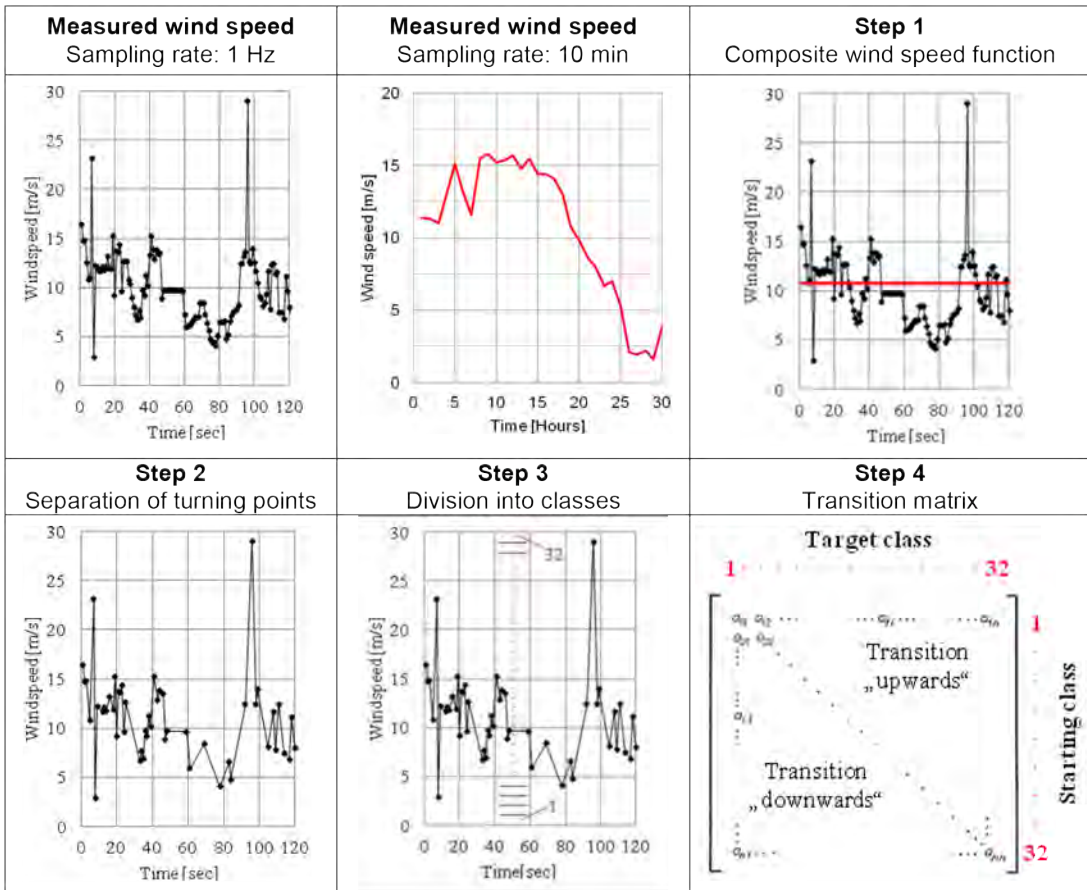


Figure 5. Wind data processing

In the first step the speed function is determined by composition of the measured wind speed data for different sampling rates and in the second step the turning points of wind speed measurements are separated. These reduced values are divided into classes based on an assumed range of wind speed variation (step 3). For example, the measured wind speed data in 2014 for the German city Karlsruhe was divided into 32 classes. Based on the Markov-Matrix method, the transition of various classes is counted in step 4. The temporary results of the mentioned procedure are summarized in Figure 6. From the representation in form of amplitude spectrum the stress range of cycles can be seen. The mean values of cycles are considered by the Haigh diagram (Haibach 2006).

The described method allows a description of the load history. For the implementation of the determined sequence in tests, it is necessary to simulate time dependent effects by equivalent temperature impacts. These facts are of particular importance for the subsequent proposal of the design concept.

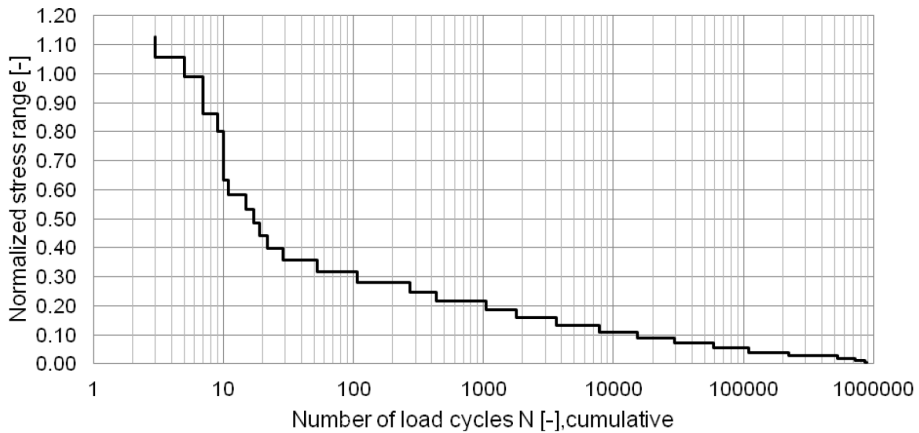


Figure 6. Amplitude collective for wind loads

## EXPERIMENTAL INVESTIGATIONS

### General remarks

Cyclic as well as quasi-static small scale and model component tests allow a comprehensive consideration of the effects mentioned. Three different adhesive systems are examined, which are well suited for cyclic loading. The aim of the experiments is to understand the load bearing and deformation behaviour dependent on the different adhesives under constant and varying load amplitudes.

### Small scale specimens

To describe the behaviour of the bondline under cyclic loading, it is of particular importance to understand the carrying behaviour at static loading. Thus quasi-static tests created the basis for the determination of bondline properties. Since the bondline of the presented façade connection is loaded purely by normal stress, adhesive properties are determined based on butt joint tests according to (DIN EN 15870 2009). The test setup is shown in Figure 7.

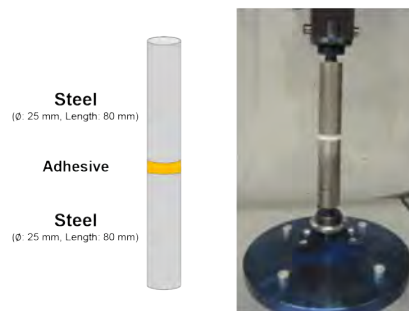


Figure 7. Test setup for small sized specimen tests

The experiments were carried out with a test expansion rate of  $0.001 \text{ s}^{-1}$  and were conducted with four different bondline thicknesses as well as two different temperature conditions. The selection of the adhesives is based on the suitable properties for the application example in cooperation with the adhesive manufacturer. Table 1 summarizes the properties of the chosen adhesive systems as a result of the butt joint tests at room temperature. Herein  $\sigma_{d,A}$  is the characteristic value of the tensile strength (5%-fractile) according to Eurocode (DIN EN 1990 2010). In order to predict the mechanical behaviour of a bondline with an analytical model, it is desirable to avoid adhesive failure of the bonded joint. This can be achieved by an adequate selection of the adhesive and the adhesion property of the adherent surface. All failure modes observed in the butt joint tests occurred with a cohesive failure or a special cohesive failure (cohesive failure close to the substrate) according to (EN ISO 10365 1995).

Table 1. Results of small scale sample tests at room temperature

Adhesive basis	Parameter [MPa]	Adhesive layer thickness [mm]			
		0,3	1,0	3,0	5,0
Acrylate	$\sigma_{d,A}$	25,44	24,57	20,05	20,29
Polyurethane	$\sigma_{d,A}$	11,94	11,72	7,26	4,09
Epoxy	$\sigma_{d,A}$	35,91	36,62	31,25	23,63

The influence of a cyclic loading on the mechanical behaviour of the bondline is investigated at the polyurethane adhesive by applying a sinusoidal load. The structures of the specimen are the same to the static investigations as shown in Figure 7. The setup of the fatigue test is shown in Figure 8.



### Fatigue Test Setup

- Stress ratio:  $R=0.1$
- Frequency: 5 Hz
- Temperature: Roomtemperature
- Maximum cycles:  $2 \cdot 10^6$

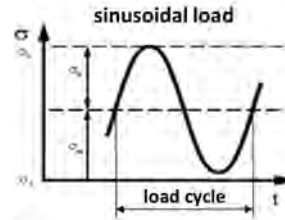


Figure 8. Test setup for the fatigue test

The stress ratio  $R$  is chosen with a value of 0.1 which means that the specimen is exposed to a varying but permanent tensile force. To prevent heating of the adhesive due to mechanical load the test is carried out at a frequency of 5 Hz. If  $2 \cdot 10^6$  load cycles are carried out and no damage is detected the value of the load is assigned within the fatigue strength range. The result of the fatigue test with specimen bonded by the polyurethane adhesive is shown in Figure 9 (blue line).

The preparation of the results is based on the maximum likelihood estimation. The failure criterion is the complete failure of the adhesive joint. All specimens show a cohesive failure mode. The notch sensitivity ( $k$ ) is calculated with a value of 15.34. The fatigue strength is reached when  $2 \cdot 10^6$  cycles are exceeded. The threshold of the load which the joint can withstand permanently (fatigue limit  $S_k$ ) is evaluated with a value of 1.2 kN.

Material: Kőrapor 842  
 Substrat: Steel  
 Load: axial sinusoidal  
 Enviroment: Air, RT  
 Frequency:  $f=5$  Hz  
 Probability of survival: 50%

$\Delta$   $R = 0,1$  - specimen  
 $\square$   $R = 0,1$  - component  
 $\blacktriangleright$  without fracture  
 $S_k$  Fatigue limit [kN]

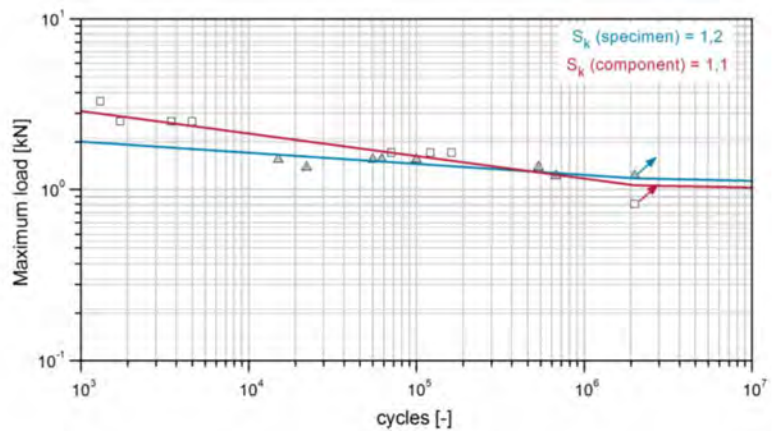


Figure 9. Comparison of results of cyclic tests

### Specimen Components

To investigate the principles of the mechanical behaviour of the bonded façade connection, pre-examinations on specimen components under quasi-static conditions were carried out (Figure 10a)). A strip coated trapezoidal profile was used with a length of 500 mm, a profile thickness of 1.0 mm and a connection profile thickness of 2.5 mm. The joint length was chosen to be 100 mm and the width to be 40 mm. Because the wind load acts perpendicular to the connection, it leads to normal stresses in the bondline.

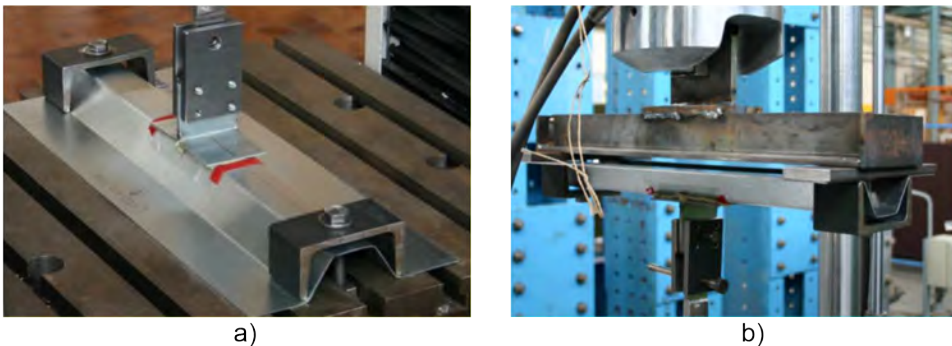


Figure 10. Test setup for specimen component tests: a) quasi-static test; b) cyclic test

The rib ends of the trapezoidal sheet are braced against the table of the testing machine. The conduction is realized by a specific pendulum rod to avoid constrains through horizontal effects. This construction allows deformations to develop freely. With the mentioned test setup the actual conditions in the mounted state are well represented. Table 2 shows the result of this quasi-static investigation for 3 adhesive systems.

Based on experiments with cyclic impacts on specimen components, the fatigue strength of the bonded façade connection can be deduced. Figure 10b) shows the test setup for investigations on specimen components with constant amplitudes. The test conditions follow the investigations on small sized specimens. Thus a frequency of 5 Hz as well as a stress ratio of 0.1 is realized. The failure criterion is defined to be a cohesive failure of the bondline. The obtained results of small sized specimen and specimen component tests for the polyurethane based adhesive are summarized in Figure 9 (red line).

Table 2. Results of specimen component tests at room temperature

Ultimate load [kN]	Adhesive basis		
	Acrylate	Polyurethane	Epoxy
	5.66	4.84	6.31

## CONCLUSIONS AND FUTURE WORK

As mentioned previously, the paper relates to the current state of the ongoing research project.

The geometry of the application example is defined based on the adhesive properties as well as the predicted loading by temperature and wind. The adhesives are chosen in accordance to the requirements of the façade connection and the adhesion properties of the steel adherents. Based on statistic calculations temperature-time function as well as scientific-based concept of wind-stress function are defined.

The future work focuses on experimental investigations on small sized specimens and specimen components under cyclic loading with constant and variable amplitudes. A further objective is to create a scientifically based guideline for the use in application-oriented design situations. For direct utilization of the research results, recommendations for design and quality requirements should be integrated.

Essential foundations for the design of fatigue strength and estimation of the lifetime of bonded joints in steel construction should be created. General rules for the investigations of structural behaviour of bonded steel joints under cyclic loading as well as an analytical model should be determined, thus making the results accessible to small and medium-sized companies.

## ACKNOWLEDGMENTS

The IGF research project (IGF-No. 18161 BG) of the Research Association for Steel Application (FOSTA), Sohnstraße 65, 40237 Düsseldorf, has been funded by the AiF within the programme for sponsorship by Industrial Joint Research (IGF) of the German Federal Ministry of Economic Affairs and Energy, based on an enactment of the German Parliament.

## REFERENCES

Dilger K., Pasternak H., et al. (2008), AiF Project No. 169 ZBG, Neue Konstruktionen durch Einsatz von Klebverbindungen im Stahlbau, Forschungsbericht für die Praxis P654, Forschungsvereinigung Stahlanwendung e. V., FOSTA, Verlags- und Vertriebsgesellschaft, Düsseldorf, Germany.

Dilger K., Pasternak H., et al. (2012), IGF Project No. 16494 BG, Entwicklung eines Eurocode-basierten Bemessungskonzepts für Klebverbindungen im Stahlbau (in Anlehnung an DIN 1990), Germany.

DIN 18516-1 (2010), Cladding for external walls, ventilated at rear –Part 1: Requirements, principles of testing.

DIN EN 15870 (2009), Adhesives – Determination of tensile strength of butt joints, German version EN 15870:2009.

DIN EN 1990 (2010), Eurocode 0: Basis of structural design; German version EN 1990:2002 + A1:2005 + A1:2005/AC:2010.

DIN EN 1991-1-4 (2010), Eurocode 1: Actions on structures – Part 1-4: General actions – Wind actions; German version EN 1991-1-4:2005 + A1:2010 + AC:2010.

DIN EN 1991-1-5 (2010): Eurocode 1: Actions on structures – Part 1-5: General actions – Thermal actions; German version EN 1991-1-5:2003 + AC:2009.

DWD (2015), Archiv des Deutschen Wetterdienst, <http://www.dwd.de/>.

EN ISO 10365 (1995), Adhesives – Designation of main failure patterns (ISO 10365:1992); German version EN ISO 10365:1995.

Haibach, E. (2006), Betriebsfestigkeit, 3., korrigierte und ergänzte Auflage. Springer Verlag, Germany.

KIT (2015), KIT, Institut für Meteorologie und Klimaforschung: <http://imkbemu.physik.uni-karlsruhe.de/~fzkmast/>.

Meinz, J. (2010), Kleben im Stahlbau – Betrachtungen zum Trag- und Verformungsverhalten und zum Nachweis geklebter Trapezprofilanschlüsse und verstärkter Hohlprofile in Pfosten-Riegel-Fassaden, Dissertation, Brandenburgische Technische Universität Cottbus, Germany.

Nakagami, Y. (2003), Probabilistic Dynamics of Wind Excitation on Glass Façade, Dissertation, TU Darmstadt, Germany.

Trittler, G. (1963), Neue Entwicklungen der Verbindungstechnik im Stahlbau, VDI Zeitschrift 105 (8), pp. 325-364.

Zuranski, J. A. (1979), Windeinflüsse auf Baukonstruktionen, Verlagsgesellschaft Rudolf Müller, Köln-Braunsfeld, Germany.

# NEW T-BEND TESTING METHOD TO EXAMINE FORMABILITY OF COLOR COATED STEEL SHEET IN DIFFERENT TEMPERATURES

**Mikko Långvik, Kauko Jyrkäs**

Häme University of Applied Sciences

**Antti Markkula, Meri Rosenberg**

SSAB Europe Oy

## ABSTRACT

A new testing procedure to measure the formability of a colour-coated steel sheet was developed. Modified T-bend tests were conducted using two different paint coating systems (polyester and polyurethane). Bending was done in two stages at different temperatures using a tensile test machine and temperature chamber. Pre-bending was done inside the temperature chamber, while the actual T-bend was rapidly done outside the chamber using the Erichsen impact tester Model 471. Forming was performed in temperatures of -20 °C, -10 °C, 0 °C, +10 °C, +20 °C, +30 °C, +40 °C and +50 °C. After forming, the specimens were exposed for 1000 h in a condensation humidity test at +60 °C.

The testing procedure proved suitable for evaluating the formability of different colour-coating systems. The objective was to find a method for creating OT tight bends, but the study was limited to 2T bends because of the nature of the testing procedure. The established method can be used to ascertain the optimal forming temperature and the limiting forming temperature range for demanding bending operations. With minor adjustments, even OT tight bends can be created.

It was discovered that formability at elevated temperatures of +40 °C or +50 °C yielded much better results than when the forming occurred in a colder environment. It was also discovered that forming at less than +20 °C easily leads to cracking for tight bends (2T-3T). As expected, polyurethane coating proved to have better formability properties than polyester coating. The difference between coatings is the most significant between the forming temperatures of +10 °C and +30 °C.

## INTRODUCTION

A colour-coated steel sheet is a complex multilayer structure, which consists of steel, a zinc layer, primer and one or multiple top paint layers. Because many different types of materials exist in the coating structure, a variety of different failure types can be identified during forming. This is due to the fact that

the different layers and layer boundaries have different forming properties. The formability of a thin sheet is determined by the weakest coating layer. When observing how thin colour-coated sheets form, failure can be defined as cracking that can be observed visually and that alters the appearance and corrosion resistance of the complete product. The best situation with respect to forming would be a situation in which the coating layers have at least the same forming properties as the steel itself. Unfortunately, this is seldom the case. [1, 2, 3, 4, 5, 6, 7, 8, 9, 10]

Colour coatings are polymer based. Two important temperature-dependent features exist in polymeric materials, both of which affect the coating flexibility. This means that colour coating may depend strongly on the forming temperature and its behaviour when forming. Polymeric materials normally have a specific glass transition temperature ( $T_g$ ) or temperature range. In many cases, the  $T_g$  correlates with the material's performance when forming. The brittle-ductile transition temperature ( $T_b$ ), which is lower than  $T_g$ , is also important. When the temperature is below the  $T_b$ , the coating becomes brittle and cannot be formed. When the temperature is above the  $T_b$ , the coating becomes hard and ductile. When the temperature is above the  $T_g$ , the coating becomes soft. In other words, forming should be performed above a certain temperature range to ensure faultless results. Temperature dependence can be quite steep. Just a few degrees difference in the forming temperature can thus be the difference between a faultless product and a faulty product. [1, 11, 12, 15]

The glass transition temperature is dependent upon the polymer material. Each coating's glass transition temperature ( $T_g$ ) is a net result of the effects of its constituents and the compositions and ratios of its polymeric building blocks. The binder resin in the coating governs this behaviour. [11, 15, 16]

Additionally, colour-coated steel sheets are normally zinc coated. Paint forms a corrosion-resistant barrier only when it is intact. The zinc coating ensures that minor flaws, like scratches in the paint, do not give corrosion straight starting points. Zinc is a less noble metal than steel and therefore it protects the exposed steel surface from corrosion. Scratches would be filled quite rapidly by corrosion products of zinc, i.e. white rust (zinc oxides), which reduces corrosion rates to low levels again [1, 2, 3, 5, 9, 13, 14]

The formability of a zinc coating is affected by the grain size, crystallographic orientation, thickness, phase composition of the intermetallic layer and temperature. The ductile-brittle behaviour of zinc coatings are strongly dependent on temperature. Pure zinc becomes brittle at temperatures of around +10 °C because the low temperature prohibits some deformation mechanisms from occurring in the coating. [1, 4, 5, 9, 10] Because the zinc layer is between the paint and steel, it is crucial that zinc can withstand forming operations. If zinc fails between the steel and paint layers, high stress peaks will occur locally, which can result in the whole coating system cracking. Still, it is typical that zinc is the first layer to crack during forming. The cracking of the zinc coating can lead to cracking in the colour coating,

which in turn leads to the formation of white rust in these areas. Zinc coating has a tendency to crack beneath the paint in tight bends. Such cracks cannot be observed visually if the colour coating has a formability that is high enough to cover these particular cracks. [1, 2, 4, 5, 7, 9, 10, 13, 14]

Pre-painted steels normally have quite low strength and have good formability. Thickness is also limited to somewhat low values for both the steel sheet and zinc coating. Normally, the formability of a pre-painted steel sheet depends on the severity of the bend radii, the paint system and the ductility of the zinc coating. Other factors that affect bendability are the thickness of the sheet and coating and the strength level of the steel. Tension-bend cracking has traditionally been minimised by carefully selecting the material and coating system. In addition to these traditional bendability criteria, there have been claims that the forming temperature could have a serious effect on the forming results. [1, 2, 3, 5, 9, 13]

Pre-heating temperatures of between +50 °C and +75 °C have been used by a few companies in roll-forming lines to ensure that the colour and metallic coatings remain intact. Several investigations have found that pre-heating above +50 °C significantly reduces cracking in both zinc and colour coating by improving the ductility of the coatings. The undamaged coating increases the service life of the pre-painted steel sheet substantially. Normally, manufacturers have provided handling instructions for customers regarding the minimum allowed forming temperature for pre-painted sheets. This begs the question of whether or not they should also provide optimal forming temperatures for their customers. [1]

## OBJECTIVE

In this study, the formability of pre-painted and zinc-coated steel sheets have been investigated at different temperatures. Formability has been tested using a modified T-bend test. The idea has been to examine how a particular forming temperature affects the formability of the coating layers. The focus has been on the cracking behaviour of the paint coating. The aim was to discover the lowest possible forming temperature for two different paint coating systems. A secondary goal was to ascertain the optimal forming temperature range for coating systems.

## MATERIALS

Test material consisted of pre-painted DX53D+Z275 steel at a nominal thickness of 0.57 mm. The paint coatings were polyester and polyurethane based. Polyester coating has a considerably weaker forming capability than polyurethane coating. These coating types were chosen so that common paint coating alternatives with a clear difference in the forming properties could be used. Both of these coatings are used for, e.g. corrosion protection in outdoor applications. The nominal thickness, including the primer, of the



polyurethane coating was 40  $\mu\text{m}$ , whereas it was 25  $\mu\text{m}$  for the polyester coating. The thickness of the primer used for the polyurethane coating was 10  $\mu\text{m}$ , whereas it was 6  $\mu\text{m}$  for the polyester coating.

## EXPERIMENT

Testing was done using a Zwick ZO50 tensile test machine. The test procedure was basically modified from the standard EN 13523-7 T-bend test. Specimens were pre-formed inside a heat chamber to obtain a loose V-shape at a particular test temperature. The pre-forming tools were designed by the researchers at the Sheet Metal Centre. Picture 1 shows the test tooling and assembly. After pre-forming, the specimens were removed from the chamber and the desired T-bend was rapidly done with an Erichsen bend and impact tester Model 471. The hammer used for the impact machines had a mass of  $2300 \pm 200$  g, while the drop height was 650 mm. To ensure sufficient closure of T-bends, the hammer was dropped five times for each specimen. Certain T-bends were formed using the necessary number of steel strips for the test material in the pre-formed test specimen during closing via a series of impacts. These particular steel strips were also placed in a heat chamber so that they would not affect the temperature of the specimen. The desired forming temperature was secured using 4 mm thick plates that were either heated up or cooled down at the test temperature both on top of the test specimen and also underneath it. The test temperature was confirmed using two thermometers, one integrated with the heat chamber and the other one being an external thermometer.



Figure 1. Pre-bending tooling assembly and the temperature chamber.

The test specimens consisted of steel sheets, and their dimensions were approximately 40 mm x 300 mm. The test temperatures were -20 °C, -10 °C, 0 °C, +10 °C, +20 °C, +30 °C, +40 °C and +50 °C. The target T-bends for the polyester coating were 0T, 0.5T, 1T, 2T and 3T. The target T-bends for the polyurethane coating were 0T, 0.5T, 1T, 1.5T and 2T. The radii were actually larger (about 2T) than what they are in standard T-bend testing because of the thick steel plate above the specimen during the impact bend. In other words, the 0T bend made by the impact machine is equal to the 2T bend made by a standard T-bending machine. So the actual size of the bends for the polyester coating were 2T, 2.5T, 3T, 4T and 5T, whereas they were 2T, 2.5T, 3T, 3.5T and 4T for the polyurethane coating. Three parallel samples were tested with a particular T-bend at each test temperature. The graphs and tables show the actual T-bend values.

The bended specimen was checked for cracking after the bend was made. Then, the specimens were exposed to a +60 °C condensation humidity test (QCT) for 1000 h. The test machine was made by the research team according to standard SFS-EN ISO 6270-1 Paints and varnishes – Determination of resistance to humidity – Part 1: Continuous condensation. The climate inside the chamber was kept at a constant state during testing. The specimens were placed in the centre of the chamber so that the bends pointed upwards. The specimens were examined and photographed after 24 h, 50 h, 100 h, 150 h, 250 h, 500 h, 750 h and 1000 h.

The specimens were evaluated using a rating scale of 0–3 points, which corresponded to the cracks that could be visually observed on the bent area. A score of 3 points meant no cracks at all, whereas 0 points indicated that the bent area had cracked entirely. One point was given for a specimen that had a few cracks, and 2 points was given for a specimen with slight cracking throughout the specimen area. In this paper, the results are presented as an average rating for the three specimens.

## RESULTS

We concluded that most of the specimens cracked already during bending if they cracked at all. We were able to easily see these cracks during visual inspection. When the specimens were exposed to the condensation humidity test, we only observed minor changes in the cracking. The polyester-coated samples formed in the range of +20 °C to +30 °C showed some increase in the extent of cracking in 2T, 2.5T and 3T bends during the condensation humidity test, but the overall changes were minor. The condensation humidity test proved quite useful for evaluating the degradation interface because it showed clearly the cracks that penetrated the whole paint layer. For cracks penetrating the paint layer, moisture reacted with the zinc coating and white rust clearly formed, which we easily detected during visual inspection.

The polyester-coated specimen experienced cracking much more than the polyurethane-coated specimen. Cracking was much more evident in bends

with a small radius than in bends with a higher radius. The polyester-coated specimens with 2T bends cracked before they were exposed to the condensation humidity test if they had formed at +30 °C or less. The forming temperature was clearly linked to the cracking tendency. Forming at temperatures of +20 °C and +30 °C led to cracking for polyester-coated specimens with 2T, 2.5T and 3T bends. Forming at temperatures of +40 °C and +50 °C showed that the polyester coating was able to avoid cracking behaviour even with 2T bended specimens. The 4T and 5T bended specimens did not show any tendency to crack at any forming temperature above +20 °C degrees. The 5T bends did not crack at all even at temperatures as low as 0 °C. It is notable that polyester-coated specimens with a very loose 5T bend cracked when formed at -20 °C before the condensation humidity test. The results are presented in Tables 1 and 2. Picture 2 shows polyester-coated samples formed at different temperatures with a 2T bend, whereas Picture 3 shows polyurethane-coated samples at different temperatures with a 2T bend.

Table 1. Rating based on the cracking of the polyester-coated specimens formed at different temperatures before and after 1000 h in the QCT chamber. The first value is the mean rating of the parallel samples before QCT, while second value is the rating after 1000 h in the QCT chamber.

PES	-20°C	-10°C	0°C	+10°C	+20°C	+30°C	+40°C	+50°C
2T	0/0	0/0	0/0	0/0	0/0	1/0	3/2	3/2
2.5T	0/0	0/0	0/0	0/0	0/0	1/0	3/3	3/3
3T	0/0	0/0	0/0	0/0	2/1	2/1	3/3	3/3
4T	0/0	0/0	1/0	1/0	3	3/3	3/3	3/3
5T	0/0	3/2	3/3	3/3	3	3/3	3/3	3/3

Table 2. Rating based on the cracking of the polyurethane-coated specimens formed at different temperatures before and after 1000 h in the QCT chamber. The first value is the mean rating of the parallel samples before QCT, while the second value is the rating after 1000 h in the QCT chamber.

PUR	-20°C	-10°C	0°C	+10°C	+20°C	+30°C	+40°C	+50°C
2T	0/0	0/0	0/0	0/0	3/2	3/3	3/3	3/3
2.5T	0/0	0/0	0/0	0/0	3/3	3/3	3/3	3/3
3T	0/0	0/0	0/0	2/1	3/3	3/3	3/3	3/3
3.5T	0/0	0/0	0/0	2/1	3/3	3/3	3/3	3/3
4T	0/0	0/0	0/0	3/2	3/3	3/3	3/3	3/3

The polyurethane-coated specimens did not crack when using 2T bends at forming temperatures of +20 °C and above. The condensation humidity test for 2T bends only revealed minor changes at a temperature of +20 °C. On the other hand, the polyurethane coating lost its formability properties at temperatures below +20 °C. This change occurred quite rapidly and clearly compared to the polyester coating, which exhibited more of a step-by-step decrease in formability properties depending on the temperature. When the

temperature dropped to +10 °C, the polyurethane coating clearly cracked at 2T, 2.5T and 3T bends even before we had a chance to begin the condensation humidity test. At 0 °C and below, every sample cracked at all bend radii before we had a chance to begin the condensation humidity test. The level of cracking depended on the temperature. The worst cracking took place at temperatures of below zero for both polyester and polyurethane coatings.

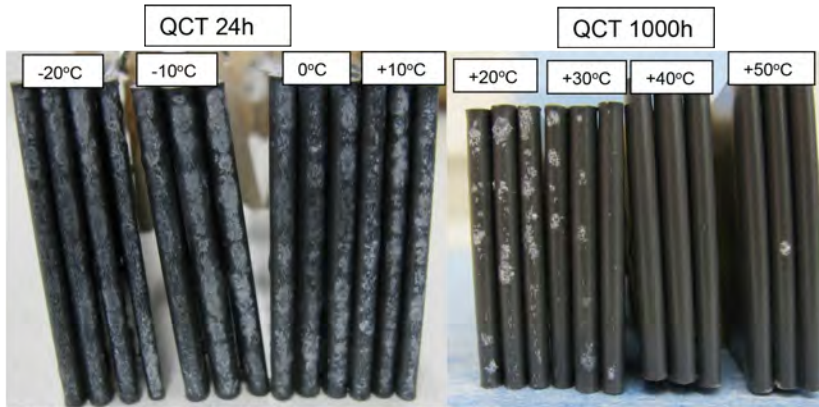


Figure 2. Polyester-coated samples after QCT with a 2T bend radius.

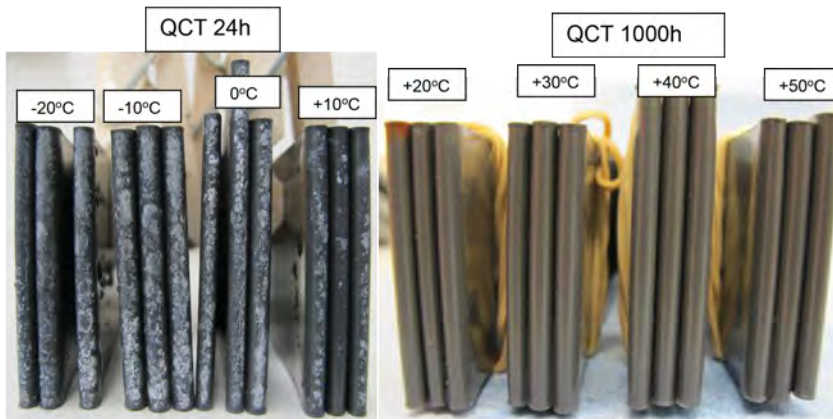


Figure 3. Polyurethane-coated samples after QCT with a 2T bend radius.

## CONCLUSIONS

We confirmed that the testing procedure is suitable for testing the formability of different kinds of colour-coated steel sheets. Adjustments should be made in the future so that tighter bends than 2T can be produced.

The forming temperature is clearly connected to the formability of colour-coated steel sheets. Specimens that formed at temperatures of +40 °C and +50 °C showed only minor tendencies or no tendency at all to crack before and during the condensation humidity test at a +60 °C temperature treatment.

It is evident that higher forming temperatures are much more important when the coating material has lower formability properties, such as for polyester types of coil paint compared to polyurethane types of coil paint. We demonstrated that the formability properties of polyester-coated specimens improved dramatically when the forming temperature increased to +40 °C. At the same time, the polyurethane-coated samples showed no tendency to crack when formed at +20 °C.

A time of 1000 h for the condensation humidity test proved to be too long. Basically, only a 24 h test is needed to show how cracking of the paint coat increases in a specimen due to the effect of elevated heat and humidity.

## **FURTHER WORK**

In test procedure there was used thick plate above formed specimen. This was done in temperature control of view. It was noted that this practise was not the best solution because part of the impact energy was 'lost' during the impact and it made the T-bends 'looser' than the T-bends typically prepared according to the EN 13523-7 standard. By eliminating the thick plate from the testing procedure, it would be possible to achieve even OT bends, which would enable more accurate results.

The extent to which the formability of different kinds of metallic coatings depend on temperature should be examined based on samples without paint. The aim would be to discover the optimal forming temperature for different metallic coatings and the temperature at which cracking limits formability.

The optimal forming temperature for different kinds of paint coatings should be studied. Another important issue is to find the lowest possible forming temperature for each coating.

More metallographic analyses of the cracked samples are needed in the future to establish what caused the cracking. Another interesting issue would be to study how cross sections of non-cracked specimens that form at higher temperatures differ from cross sections of cracked specimens. More research is also needed on how the cracking of zinc coatings affects the colour coating of steel sheets.

## **Acknowledgments**

The Authors wish to thank FIMECC HYBRIDS for funding of this study and the management of SSAB Europe Oy, R&D facility, in Hämeenlinna, Finland, for helping us to publish this article.

## REFERENCES

- [1] Warm Roll-Forming of Pre-Painted Sheet Steel, U. S. Steel Technical Bulletin-Construction, United States Steel Corporation, TBP 2005.12
- [2] Understanding Tension Bend Cracks, <http://www.colourroof.com/pdf/>, 2.6.2015
- [3] Roll-Forming Steel Strip, Technical Bulletin FTB-5, 3.10.2010, BlueScope Steel
- [4] Deformation and Damage Mechanisms of Zinc Coatings on Hot-Dip Galvanized Steel Sheets: Part II. Damage Modes, R. Parisot, S. Forest, A. Pineau, F.Nguyen, X. Demonet and J-M. Mategne, Metallurgical and Materials Transactions A, Volume 35A, March 2004–813
- [5] Deformation and Damage Mechanisms of Zinc Coatings on Hot-Dip Galvanized Steel Sheets: Part II. Deformation Modes, R. Parisot, S. Forest, A. Pineau, F.Nguyen, X. Demonet and J-M. Mategne, Metallurgical and Materials Transactions A, Volume 35A, March 2004–797
- [6] Self-Healing Effect by Zinc Phosphate and Calcium Silicate Included in Organic-Inorganic Composite Coating on 55%Al-Zn Coated Steel Sheet, A. Matsuzaki, M. Nagoshi, H.Noro, M. Yamashita; and N. Hara, Materials Transactions, Vol. 52, No. 6 (2011) pp. 1244 to 1251
- [7] Fracture mechanics analysis of coating/substrate systems Part II: Experiments in bending, Sung-Ryong Kim, John A. Nairn, Engineering Fracture Mechanics 00 (2000) 1-25
- [8] Fracture mechanics analysis of coating/substrate systems Part I: Analysis of Tensile and Bending Experiments, Sung-Ryong Kim, John A. Nairn, Engineering Fracture Mechanics, Volume 65, Issue 5, 1 March 2000, Pages 573–593
- [9] The Metallurgy of Zinc Coated Steel, A. R. Marder, Progress in Materials Science, Volume 45, Issue 3, June 2000, Pages 191–271
- [10] K.M. Goggins, A.R. Marder, Crack Initiation and Propagation in Hot-Dip Galvanneal Steel Sheet during Bending, 3rd International Conference on Zinc Coated Sheet, Barcelona, S4I (1991), pp. 1–11
- [11] Viscoelastic Properties of Paint Films and Formability in Deep Drawing of Pre-Painted Steel Sheets, K. Ueda, H. Kanai, T. Amari, Progress in Organic Coatings, Volume 45, Issue 1, September 2002, Pages 15–21
- [12] Effects of Mechanical Properties of Paint Film on the Forming of Pre-Painted Steel Sheets, K. Ueda, H. Kanai, T. Suzuki, T. Amari, Progress in Organic Coatings, Volume 43, Issue 4, December 2001, Pages 233–242

- [13] Corrosion Resistance of Painted Zinc Alloy Coated Steels, R. P. Edavan, R. Kopinski, *Corrosion Science*, Volume 51, Issue 10, October 2009, Pages 2429–2442
- [14] Performance of Coated Steel Systems Exposed to Different Media: Part 1. Paint Coated Galvanized Steel, B. del Amo, L Véleva, A. R. Di Sarli, C. I. Elsner, *Progress in Organic Coatings*, Volume 50, Issue 3, August 2004, Pages 179–192
- [15] Formability-Related Studies of Color Coated Steel, M. Lagus, Bachelor's Thesis, Åbo Akademi University, 2015
- [16] [The World of Surface Coatings Is Centered Around the Glass Transition Temperature, Part 1, G. Curtzwiler, D. Gottschalk, C. Konecki, R. Peterson, S. Wand, J. W. Rawlin-s, *Coatingstech*, August 2014, Pages 28-38



# BUCKLING BEHAVIOR OF PERFORATED COLD-FORMED COLUMNS

**Marsel Garifullin, Alexey Sinelnikov, Maria Bronzova, Nikolai Vatin**

Peter the Great St.Petersburg Polytechnic University

## ABSTRACT

Housing question is one of the most important issues on a national scale. To provide citizens with cheap, energy-efficient, comfortable and eco-friendly housing, a special type of construction should be developed. Studies have shown that the optimal structural scheme for low-rise buildings that meets all regulatory requirements is a frame system. In this connection, thin-walled cold-formed steel (CFS) structures seem to be the best material for constructing the cladding panels. The framework of the cladding panels is usually constructed from CFS C-shaped profiles. To increase the thermal effectiveness of the cladding panels, CFS profiles are perforated on their webs and thus are called thermoprofiles. However, these perforations have a negative impact on bearing capacity of profiles and require accurate evaluation. In this article a relatively new type of thermoprofiles with reticular-stretched perforations is considered. The key feature of this profile is completely different geometry of perforations and the presence of the intermediate longitudinal stiffener. The article deals with the buckling analysis of perforated CFS C-sections subjected to compression.

## INTRODUCTION

Thin-walled cold-formed steel sections are widely used in various fields of industrial and civil engineering, bridges, storage racks, car bodies, railway coaches, transmission towers and poles, various types of equipment (Veljkovic & Johansson 2008; Vatin & Sinelnikov 2012; Heinisuo et al. 2014). Over the last decade cold-formed constructions have been actively used in the construction of cladding panels in residential housing (Zhmarin 2012). To increase the thermal effectiveness of these panels cold-formed steel profiles are perforated on webs and thus are called thermoprofiles (Figure 1). Traditionally, thermoprofiles with longitudinal perforations are mostly used in construction.

In this article a new type of thermoprofile with reticular-stretched perforations (hereinafter – RST-profiles) is considered. The key features of this profile are completely different geometry of perforations and the presence of the intermediate longitudinal stiffener.

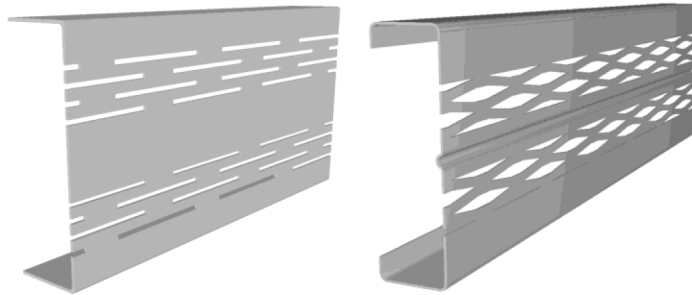


Figure 1. Thermoprofiles: traditional (left) and reticular-stretched (right).

Due to the fact that RST-profile has been designed recently, very little research has been devoted to the investigation of its mechanical properties.

Sinelnikov (Vatin, Havula, et al. 2014b; Vatin et al. 2015; Vatin, Havula, et al. 2014a) and Nazmeeva (Vatin, Nazmeeva, et al. 2014) investigated the buckling behavior of compressed cold-formed columns made of RST-profiles. Trubina (Trubina, Abdulaev, Pichugin & Garifullin 2014; Vatin, Sinelnikov, et al. 2014; Trubina, Abdulaev, Pichugin & Rybakov 2014a; Trubina et al. 2015; Garifullin et al. 2015; Trubina, Abdulaev, Pichugin & Rybakov 2014b) analyzed the problem of local and global buckling of RST-profiles in bending. Rybakov (Lalin et al. 2014; Rybakov & Sergey 2015) presented four types of finite elements to analyze cold-formed members with various boundary conditions on the ends. Belyy (Belyy & Serov 2013) introduced a new method for the approximate estimation of steel structures service life in buildings. Al Ali (Al Ali 2014; Al Ali et al. 2015; Al Ali et al. 2012) presented investigated thin-walled cold-formed steel members with closed cross-sections. Tusnin (Tusnin 2009; Tusnin 2010; Tusnin 2014; Tusnin & Prokic 2015) introduced thin-walled finite elements to analyze spatial cold-formed structures with open cross sections. Tusnina (Tusnina 2014a; Tusnina 2014b; Danilov & Tusnina 2014) presented a finite element analysis of cold-formed Z-purlins supported by sandwich panels. Prokic (Tusnin & Prokic 2014a; Tusnin & Prokic 2014b) analyzed the behavior of thin-walled open section I-beams under torsion and bending. Björk (Björk & Saastamoinen 2012; Heinilä et al. 2009; Nykänen et al. 2014) studied the influence of residual stresses on the fatigue strength of cold-formed rectangular hollow sections.

Despite the growing interest in RST-profiles, the influence of perforations on the resistance of profiles remains an open issue. Buckling behavior of these sections has also not been investigated extensively.

This article deals with buckling performance of cold-formed C-sections made of RST-profile. Firstly, the experimental results of the compressed columns are provided. The second part contains the nonlinear FE analysis of these columns.

## EXPERIMENTAL INVESTIGATIONS

Laboratory tests were carried out for two types of specimens:

- RST-profiled columns without nodal connections at the ends, Sn (n - number of the sample);
- RST-profiled columns as part of the nodal connection, Cn (n - sample number).

Experimental study of the profile was conducted in the laboratory of Häme University, InnoSteel Sheet Metal Development Centre, Finland. The test specimens were produced by OOO Arsenal ST, Russia.

The steel used for the production of the profile had the following characteristics:

- Design strength: 350 N/mm<sup>2</sup>;
- Zinc coating: 350 g/m<sup>2</sup>;
- Zinc coating thickness: 25 microns.

The characteristics of the samples are shown in Table 1.

Table 1. Characteristics of the samples tested

Type	S1, S2, S3	C1, C2, C3
Profile	TCc 200-45-2.0	
Length, mm	1000	350
Boundary conditions	Top – pinned, bottom - fixed	

The ends of Sn specimens (Figure 2a) were cut using a circular metal saw (not machined). Support wooden blocks (thickness 40 mm; edge is positioned 3 mm from the end of the profile) were placed inside the ends of the columns. The lower ends of the specimen were placed on a hinged steel support. The load of a hydraulic cylinder was applied through a thick steel plate to the upper ends of the specimens. All the specimens were loaded using the displacement control until the failure. The loading rate was 3 mm/min.

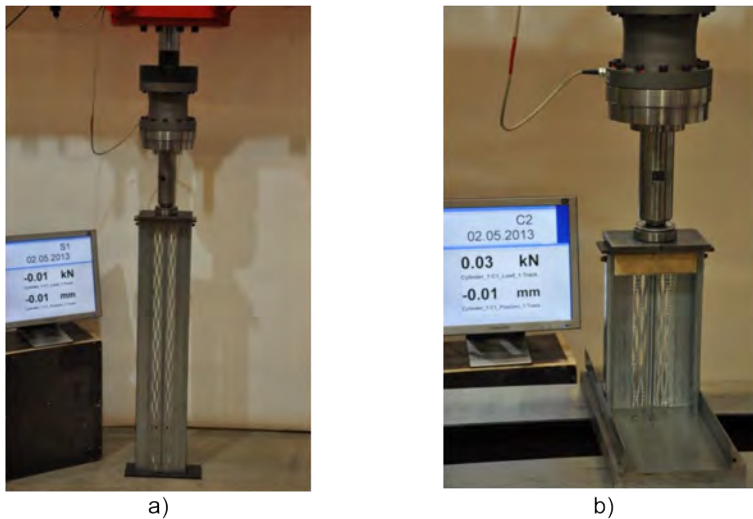


Figure 2. Overall view of test setup: a) S1, b) C2.

Every Cn specimen (Figure 2b) was constructed from a vertical column (hereinafter – stud) and a horizontal element (hereinafter – rack). The 350 mm long studs were made of the same profile as Sn specimens. The racks represented U-shaped cold-formed profile without any perforations on webs. The flanges of every stud were fixed with 4+4 self-drilling screws on the flanges of the racks. The studs were fixed to the head of the hydraulic cylinder. The racks were fixed rigidly to the test frame. The specimens were loaded using the displacement control until the failure. The loading rate was 1.5 mm/min.

During the experiments every tested specimen experienced local buckling with subsequent global (flexural) buckling. A summary of the buckling test results is given in Table 2.

Table 2. Experimental test results

Specimen	Length, mm	Force, kN
S1	1000	84.4
S2		68.9
S3		83.4
mean		<b>78.9</b>
C1	350	90.8
C2		91.0
C3		99.9
mean		<b>93.9</b>

The observed failure mechanisms of the Sn and Cn columns are shown in Figure 3 and Figure 5 respectively. Figure 4 and Figure 6 illustrate the load-displacement curves for the tested columns.

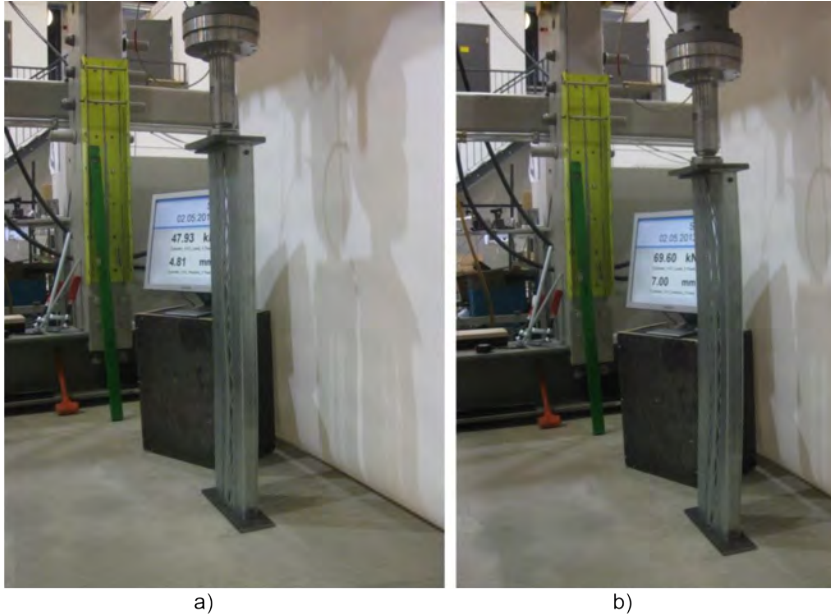


Figure 3. Observed failure mechanisms for tests on S2: a) local buckling, b) global (flexural) buckling.

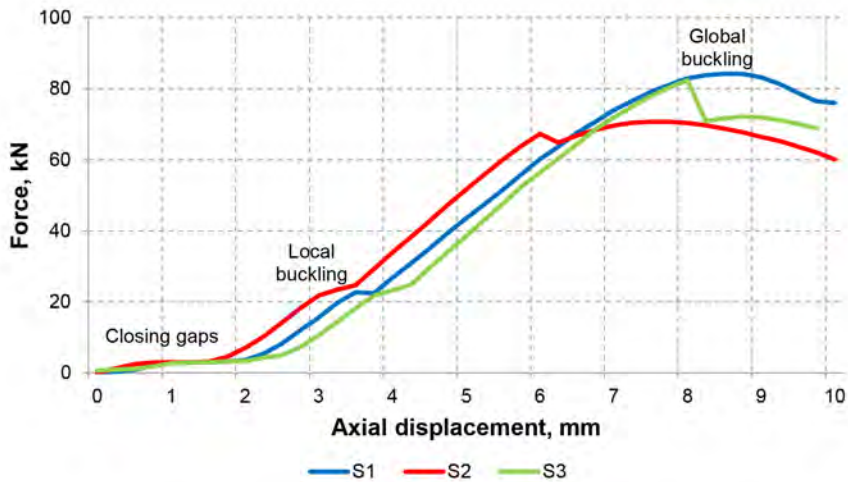


Figure 4. Force-displacement response for Sn specimens.

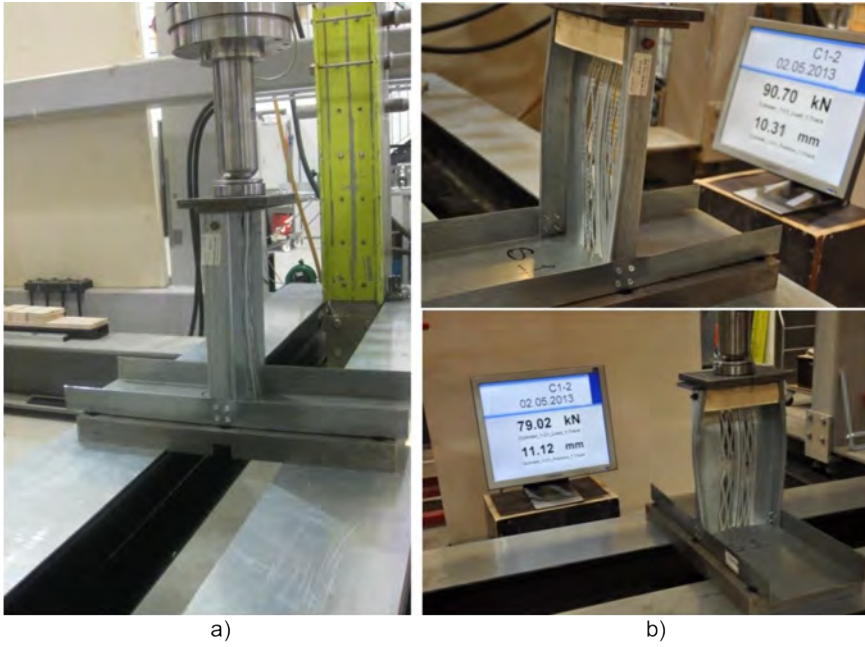


Figure 5. Observed failure mechanisms for tests on C1: a) local buckling, b) global (flexural) buckling.

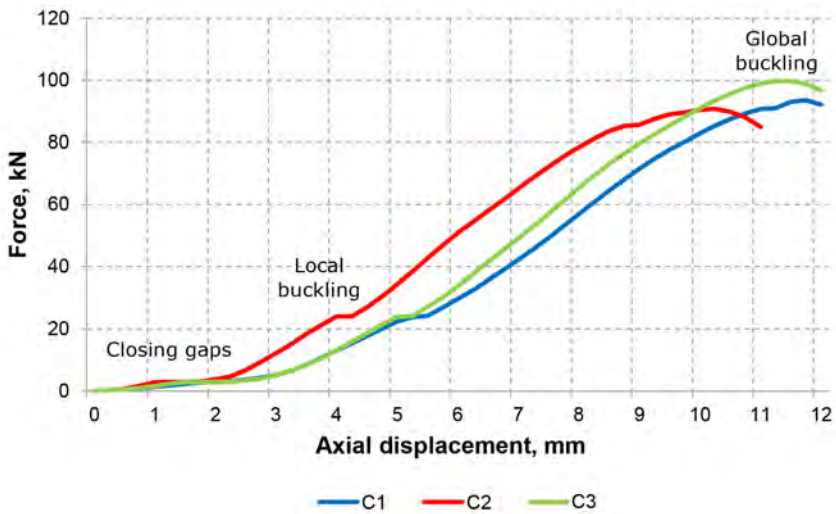


Figure 6. Force-displacement response for Cn specimens.

## FINITE ELEMENT ANALYSIS OF COMPRESSED COLUMNS

To validate the experimental data FE buckling analysis of these profiles was conducted. The simulation was arranged in such a way to repeat the tests: 1000 mm and 350 mm columns made of RST-profile were loaded by compressive loads. Geometrical properties of the RST-profile used for tests and modeling are presented in Figure 7.

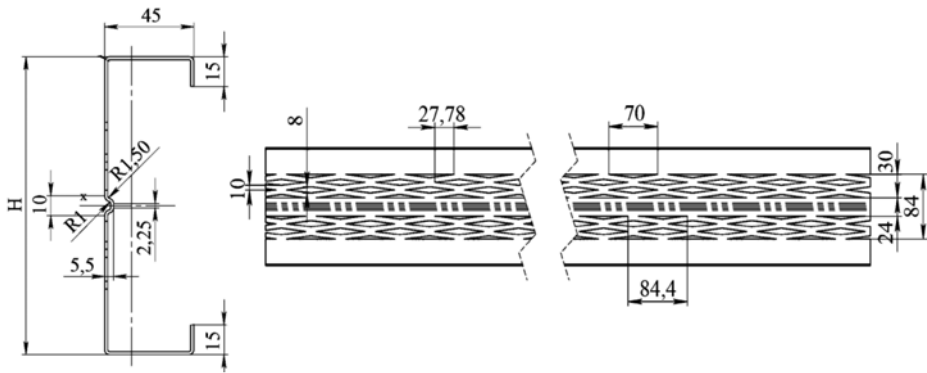


Figure 7. Geometrical dimensions of RST-profile.

The mesh of the models was created using 4-node, quadrilateral, shell elements (S4R). The boundary conditions are shown in Figure 8. All the models were loaded with concentrated compressive forces acting in Z direction through the rigid bodies at the ends of each model.

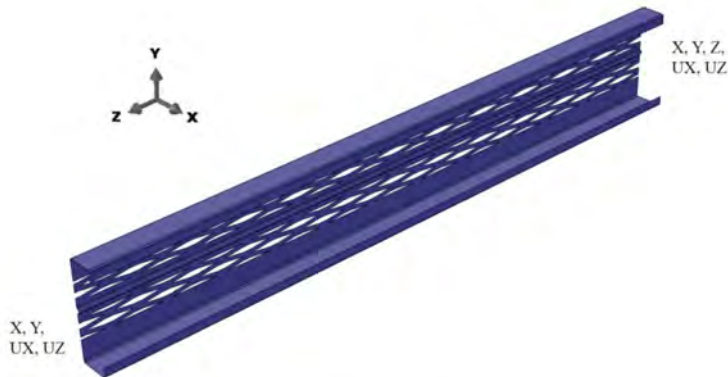


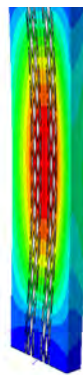
Figure 8. Boundary conditions of the members tested.



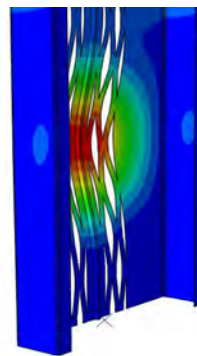
For each column a buckling analysis with physical and geometrical nonlinearity in Abaqus was performed. The results of the FE analysis are presented in Table 3. The table includes the buckling forces determined experimentally, by modeling and analytically by EN 1993-1-3-2009. Figures 9-11 illustrate deformed shapes and the load-displacement curves for the columns tested in comparison with the experimental data.

Table 3. The results of FE analysis.

Specimen	Length, mm	Force, kN		
		Experiments	FEM	EN 1993-1-3-2009
S1	1000	84.4	<b>84.8</b>	<b>49.7</b>
S2		68.9		
S3		83.4		
mean		<b>78.9</b>		
C1	350	90.8	<b>92.1</b>	<b>55.9</b>
C2		91.0		
C3		99.9		
mean		<b>93.9</b>		



a)



b)

Figure 9. Deformed shape of the models: a) S1, b) C1.

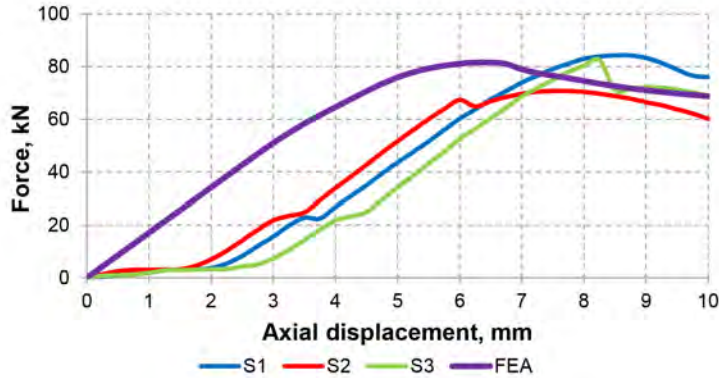


Figure 10. Force-displacement response: S1.

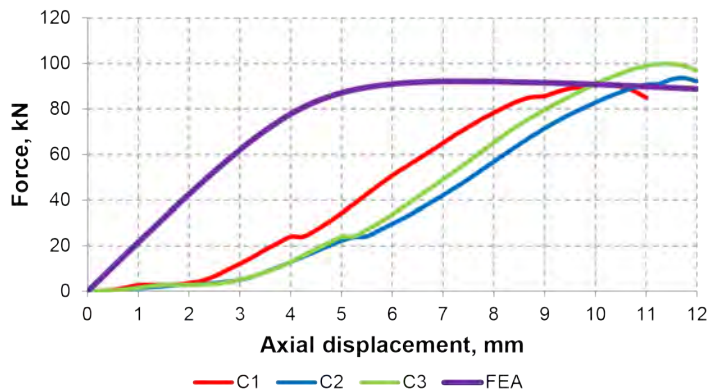


Figure 11. Force-displacement response: C1.

## CONCLUSIONS

Nonlinear FE models were developed and verified against previously conducted compression tests on cold-formed steel C-section columns. Computer simulations showed good agreement with the experimental data. Discrepancy between the results was less than 10%. Despite the close results, the values of buckling forces for the tests and simulations corresponded to the different values of displacements. This might be the result of closing the gaps, which, in their turn, occurred due to the initial geometric imperfections of the columns.

Simulation tests for short columns (350 mm) showed very close results, however, the deformed shape obtained from modeling was completely opposite to the one from the experimental tests. This demonstrates the need for a more detailed modeling with the particular attention paid to nodal connections and wooden plates in the top of the models.

Analytical calculations made in accordance with EN 1993-1-3-2009 showed considerably lower results. This probably means that the building codes provide more reliable values of buckling forces for this type of profile. Anyway, RST-profile remains poorly explored and requires more careful and detailed research. It also seems reasonable to provide computer modeling taking into account initial geometrical imperfections of the elements, since the fact that CFS structures with such perforations are very sensitive to any mechanical deformations.

## ACKNOWLEDGEMENTS

The experimental work was conducted with the help of Dr. Arto Ranta-Eskola, Director of Research, Rautaruukki Oyj (Finland). The authors also gratefully acknowledge the helpful comments and suggestions of the reviewers, which have improved the paper.

## REFERENCES

- Al Ali, M. 2014. Compressed Thin-Walled Cold-Formed Steel Members with Closed Cross-Sections. *Advanced Materials Research* 969: 93–96.
- Al Ali, M. et al. 2012. Thin-Walled Cold-Formed Compressed Steel Members and the Problem of Initial Imperfections. *Procedia Engineering* 40: 8–13.
- Al Ali, M., Tomko, M. & Demjan, I. 2015. Experimental Investigation and Theoretical Analysis of Polystyrene Panels with Load Bearing Thin-Walled Cold-Formed Elements. *Applied Mechanics and Materials* In Print.
- Belyy, G. & Serov, E. 2013. Particular Features And Approximate Estimation Of Steel Structures Service Life In Buildings And Facilities. *World Applied Sciences Journal* 23(13): 160–164.
- Björk, T. & Saastamoinen, H. 2012. Capacity of CFRHS X-joints made of double-grade S420 steel. *Tubular Structures XIV - Proceedings of the 14th International Symposium on Tubular Structures, ISTS 2012*: 167–176.
- Bronzova, M.K., Vatin, N.I. & Garifullin, M.R. 2015. Frame buildings construction using monolithic foamed concrete. *Construction of Unique Buildings and Structures* 1(28): 74–90.
- Danilov, A. & Tushina, O. 2014. The joints of cold-formed purlins. *Journal of Applied Engineering Science* 12(2): 153–158.
- Garifullin, M., Trubina, D. & Vatin, N. 2015. Local buckling of cold-formed steel members with edge stiffened holes. *Applied Mechanics and Materials* 725-726: 697–702.

- Heinilä, S., Björk, T. & Marquis, G. 2009. The influence of residual stresses on the fatigue strength of cold-formed structural tubes. *ASTM Special Technical Publication 1508 STP*: 200–215.
- Heinisuo, M., Lahdenmaa, J. & Jokinen, T. 2014. Experimental research on modular thin-walled steel structures. *Proceedings of the 12th International Conference on Steel, Space and Composite Structures*: 85–97.
- Lalin, V., Rybakov, V. & Sergey, A. 2014. The Finite Elements for Design of Frame of Thin-Walled Beams. *Applied Mechanics and Materials 578-579*: 858–863.
- Nykänen, T. et al. 2014. Residual strength at  $-40^{\circ}\text{C}$  of a precracked cold-formed rectangular hollow section made of ultra-high-strength steel - an engineering approach. *Fatigue & Fracture of Engineering Materials & Structures 37(3)*: 325–334.
- Rybakov, V. & Sergey, A. 2015. Mathematical Analogy Between Non-Uniform Torsion and Transverse Bending of Thin-Walled Open Section Beams. *Applied Mechanics and Materials 725-726*: 746–751.
- Trubina, D. et al. 2015. Comparison Of The Bearing Capacity Of LST-Profile Depending On The Thickness Of Its Elements. *Applied Mechanics and Materials 725-726*: 752–757.
- Trubina, D., Abdulaev, D., Pichugin, E. & Rybakov, V. 2014a. Effect of Constructional Measures on the Total and Local Loss Stability of the Thin-Walled Profile under Transverse Bending. *Applied Mechanics and Materials 633-634*: 982–990.
- Trubina, D., Abdulaev, D., Pichugin, E. & Rybakov, V. 2014b. Geometric Nonlinearity of the Thin-Walled Profile under Transverse Bending. *Applied Mechanics and Materials 633-634*: 1133–1139.
- Trubina, D., Abdulaev, D., Pichugin, E. & Garifullin, M. 2014. The Loss of Local Stability of Thin-Walled Steel Profiles. *Applied Mechanics and Materials 633-634*: 1052–1057.
- Tusnin, A. 2014. The Influence of Cross-Section Shape Changing on Work of Cold Formed Beam. *Advanced Materials Research 1025-1026*: 361–365.
- Tusnin, A.R. 2010. Features of numerical calculation of designs from thin-walled bars of an open profile. *Industrial and Civil Engineering 11*: 60–63.
- Tusnin, A.R. 2009. Finite element for numeric computation of structures of thin-walled open profile bars. *Metal constructions 15(1)*: 73–78.
- Tusnin, A.R. & Prokic, M. 2014a. Bearing capacity of steel I-sections under combined bending and torsion actions taking into account plastic deformations. *Journal of Applied Engineering Science 12(3)*: 179–186.

- Tusnin, A.R. & Prokic, M. 2014b. Behavior of symmetric steel I-sections under combined bending and torsion actions allowing for plastic deformations. *Magazine of Civil Engineering* 5(49): 44–53.
- Tusnin, A.R. & Prokic, M. 2015. Selection of Parameters for I-beam Experimental Model Subjected to Bending and Torsion. *Procedia Engineering* 111: 789–796.
- Tusnina, O. 2014a. A Finite Element Analysis of Cold-Formed Z-Purlins Supported by Sandwich Panels. *Applied Mechanics and Materials* 467: 398–403.
- Tusnina, O. 2014b. An Influence of the Mesh Size on the Results of Finite Element Analysis of Z-Purlins Supported by Sandwich Panels. *Applied Mechanics and Materials* 475-476: 1483–1486.
- Vatin, N., Havula, J., et al. 2014a. Buckling force of the thin-walled cross-sections and shear resistance of their joints: tests and FEM-modelling. *Proceedings of the International Conference „Innovative Materials, Structures and Technologies“*: 187.
- Vatin, N. et al. 2015. Reticular-Stretched Thermo-Profile: Buckling of the Perforated Web as a Single Plate. *Applied Mechanics and Materials* 725-726: 722–727.
- Vatin, N., Sinelnikov, A., et al. 2014. Simulation of Cold-Formed Steel Beams in Global and Distortional Buckling. *Applied Mechanics and Materials* 633-634: 1037–1041.
- Vatin, N., Havula, J., et al. 2014b. Thin-Walled Cross-Sections and their Joints: Tests and FEM-Modelling. *Advanced Materials Research* 945-949: 1211–1215.
- Vatin, N., Nazmeeva, T. & Guslinsky, R. 2014. Problems of Cold-Bent Notched C-Shaped Profile Members. *Advanced Materials Research* 941-944: 1871–1875.
- Vatin, N.I. & Sinelnikov, A.S. 2012. Long span footway bridges: coldformed steel cross-section. *Construction of Unique Buildings and Structures* 1: 47–53.
- Veljkovic, M. & Johansson, B. 2008. Thin-walled steel columns with partially closed cross-section: Tests and computer simulations. *Journal of Constructional Steel Research* 64(7-8): 816–821.
- Zhmarin, E.N. 2012. International association of light-gauge steel construction. *Construction of Unique Buildings and Structures* 2: 27–30.

# THE EFFECT OF RIVETS APPLICATION ON THERMAL CHARACTERISTICS OF SANDWICH PANEL ROOFINGS

**Alexander Danilov**

Professor, PhD, Moscow State University of Civil Engineering (MGSU)

**Olga Tusnina**

PhD Student, Moscow State University of Civil Engineering (MGSU)

## INTRODUCTION

Thin-walled cold-formed structures are attractive and economically advisable type of designs. Thin-walled members have some features, which do not permit use of classical methods of analysis of steel structures. Small thickness and non-symmetrical shape of thin-walled profiles cause local buckling of their flanges and webs, restrained torsion [1] accompanied by warping and distortion of member cross-section [2, 3].

Many researchers have studied their stress-strain state under different load conditions and on the development of new types of structures and engineering methods of analysis [4, 5].

Thin-walled cold-formed purlins are typically used as load bearing elements in the roofing of modular buildings [6]. Sandwich panels or layered roofs made of trapezoidal sheeting make up the building envelope. Sandwich panels are usually fastened to purlins by self-drilling screws. Screws permeate an insulation layer of sandwich panels and conduct heat through the sandwich panel, so the screws may be considered as “cold bridges”. Besides application of screws complicates water-proofing measures of roofing because of through holes in sandwich panel.

From the viewpoint of estimating the load-bearing capacity of connection between sandwich panel and purlins with screws, such a solution has also some negative features. Roofing structures experience alternating loads such as negative wind pressure and temperature load. Load of variable direction loosens impermeability of connection and its deformability increases. Then sandwich panels cannot be taken into account in analysis of purlin load bearing capacity directly as it is recommended in Eurocode 3 [7]. Some reduction factors need to be introduced in currently applied design methods to take above mentioned adverse factors into consideration.

Besides, moisture penetrates through the gaps in panel sheeting around screws, in winter it freezes and reduces the thermal and mechanical characteristics of roofing. Certain difficulties take place as well in the course of roof structure installation. As the screws are inserted from the outside and permeate through the thickness of sandwich panel, they can deviate from the

set final position on the top flange of purlin. This factor also affects the load bearing capacity of connection and of purlin itself.

The mentioned negative factors make it necessary to develop some new constructive solutions to avoid them. The application of blind rivets may be one of possible solutions [8]. The blind rivets are well-known kind of fasteners used on a level with screws in the connections of cold-formed elements [9]. In the considered application the blind rivets connect the inner sheet of sandwich panel to the top flange of purlin. Fastening of sandwich panels by rivets is carried out from within the building and rivets can be installed strictly in design position. Blind rivets do not destroy insulation layer of panel and improve its thermal characteristics.

But the blind rivets application has also several negative aspects. In case of wind uplift action the adhesion between the insulation layer and inner sheeting of the panel nearby connection can be broken and the bearing capacity of connection at this moment nearly exhausts. So this type of connection may be allowable only for sandwich panels with polyurethane core, as it has a high level of adhesion to sheeting of panel. Another negative factor in application of rivets lies in the inability to check the quality of the formation of rivet head and so the quality of connection. However, despite the mentioned shortcomings rivet connections are worthy of consideration and will be discussed in this paper.

## METHODS

Two similar roofing structures with self-drilling screws and blind rivets as fasteners were considered. Sandwich panel SPC120/80PU with polyurethane core of thickness 120 mm (coefficient of thermal conductivity  $\lambda=0.05$  W/( $m^2 \cdot ^\circ C$ )) with sizes 600x1000 mm was fastened to Ruukki Z-purlin 200x2 (height 200 mm, thickness 2 mm).

In the first case, self-drilling screws ( $\lambda=58$  W/( $m^2 \cdot ^\circ C$ )) fasten sandwich panel to purlin in each corrugation (Figure 1). In the second case 5 rivets installed with equal pitch along sandwich panel were used (Figure 2).

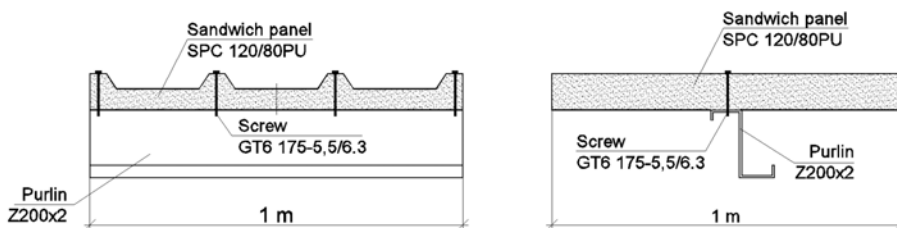


Figure 1. Considered system with screw fasteners



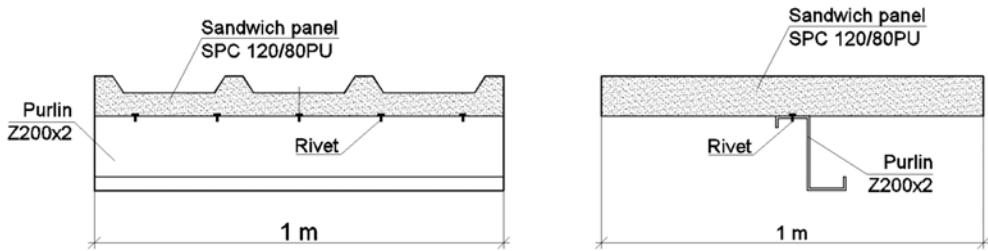


Figure 2. Considered system with rivet fasteners

Numerical thermal analysis of considered systems was performed with the use of the computer programs MSC.NASTRAN and TEPL. Both programs allow carrying out the analysis of three-dimensional temperature fields in structure.

The algorithm implemented in program TEPL is based on the methods given in [10]. Beside the temperature distribution in structure the value of thermal resistance is received in result of numerical analysis performed with TEPL. MSC.NASTRAN does not allow obtaining automatically the value of thermal resistance.

Finite-element model of roofing system created in MSC.NASTRAN is shown on Figure 3.

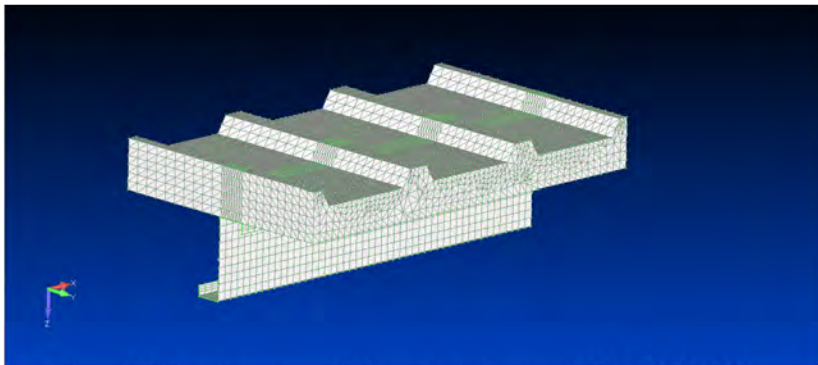


Figure 3. Finite-element model of investigated system in MSC. NASTRAN

The temperature of indoor air assumed was  $+18\text{ }^{\circ}\text{C}$  and of outdoor air  $-30\text{ }^{\circ}\text{C}$ . Heat exchange on boundary surfaces of air was taken into account by setting convection coefficients on these surfaces. Heat transfer factor on the surfaces bordering indoor air (surface of purlin and inner face of sandwich panel) was set  $\alpha_{in}=8.7\text{ W}/(\text{m}^2\cdot^{\circ}\text{C})$  and on the surfaces bordering outdoor air (corrugate face of panel) it was set  $\alpha_{out}=23\text{ W}/(\text{m}^2\cdot^{\circ}\text{C})$ .

## RESULTS

The values of thermal resistance of two investigated systems are represented in Table 1. It shows that the thermal resistance of roof made with the use of self-drilling screws was about 9% lower than the one with the use of rivets.

Table 1. Comparison of thermal resistance values of structures made with the use of screws and rivet

$R_o, (m^2 \cdot ^\circ C) / W$		The relative difference
Self-drilling screws	Blind rivets	
1,6734	1,8188	8,7%

The contour plots of temperature distribution in the structure obtained from the numerical analysis with the use of MSC.NASTRAN and TEPL are represented below (Figures 4 and 5). Heat flow is going out of building through the screws. It is clearly seen in Figure 4. The temperature of inner face of sandwich panel (Figure 5) is lower when screws are used.

The value of thermal resistance was calculated also manually based on the recommendations of Russian building standards and rules SNiP "Thermal performance of the buildings".

Cold bridges such as screws cannot be taken into account in manual analysis based on SNiP recommendations. There exists a procedure for obtaining the value of thermal resistance taking into account point inhomogeneity of insulation layer but this procedure requires the results of analysis of three-dimensional temperature field. This procedure was automated in program TEPL.

So manually the analysis was carried out without taking into account cold bridges in sandwich panel insulation layer. In the Table 2 the comparison of the thermal resistance values of structures made with the use of screws obtained in program TEPL and manually by methods of SNiP "Thermal performance of buildings".

As show the table data the thermal resistance obtained manually without taking into account screws as cold bridges are higher at about 13% than those based on numerical analysis.

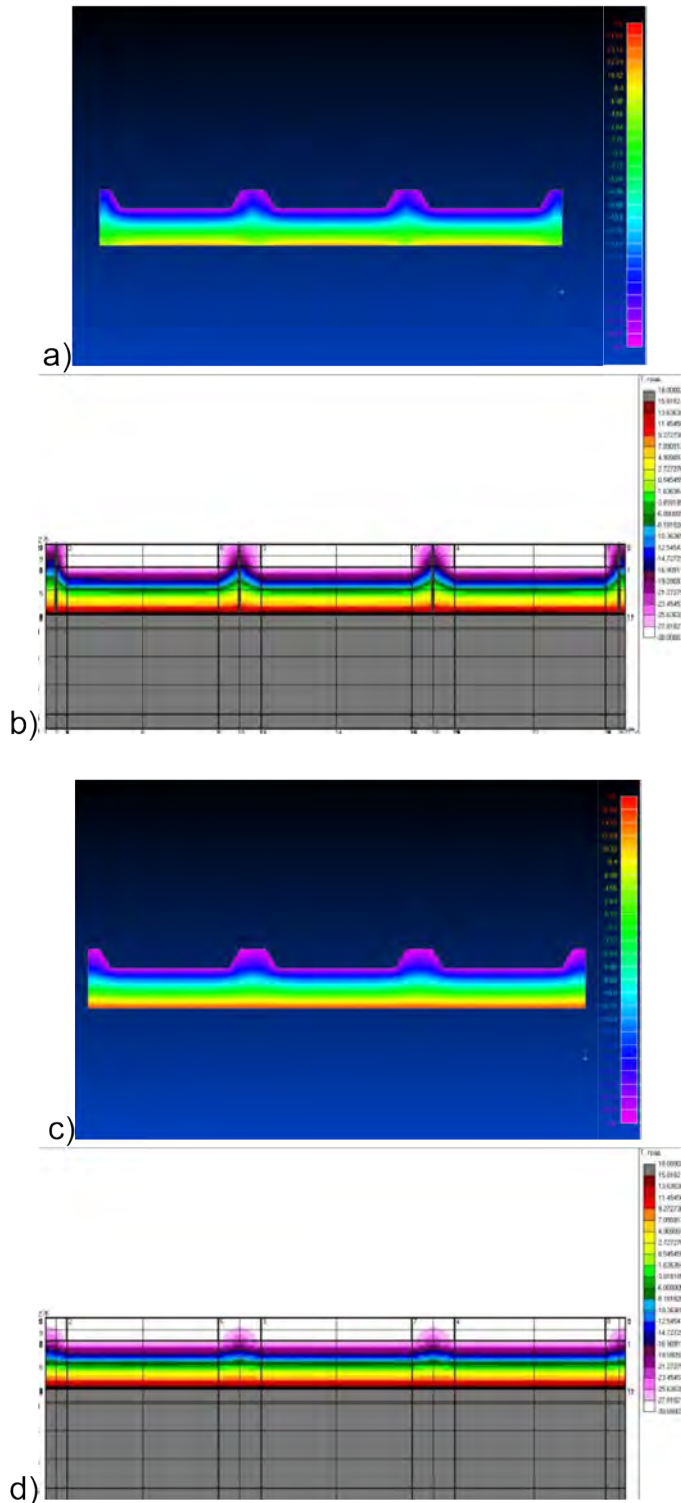


Figure 4. Comparative contour plots of temperature distribution in cross-section of sandwich-panel fastened to purlin with the use of: a, b – screws (a-MSC.NASTRAN; b-TEPL); c, d – rivets (c-MSC.NASTRAN; d-TEPL)

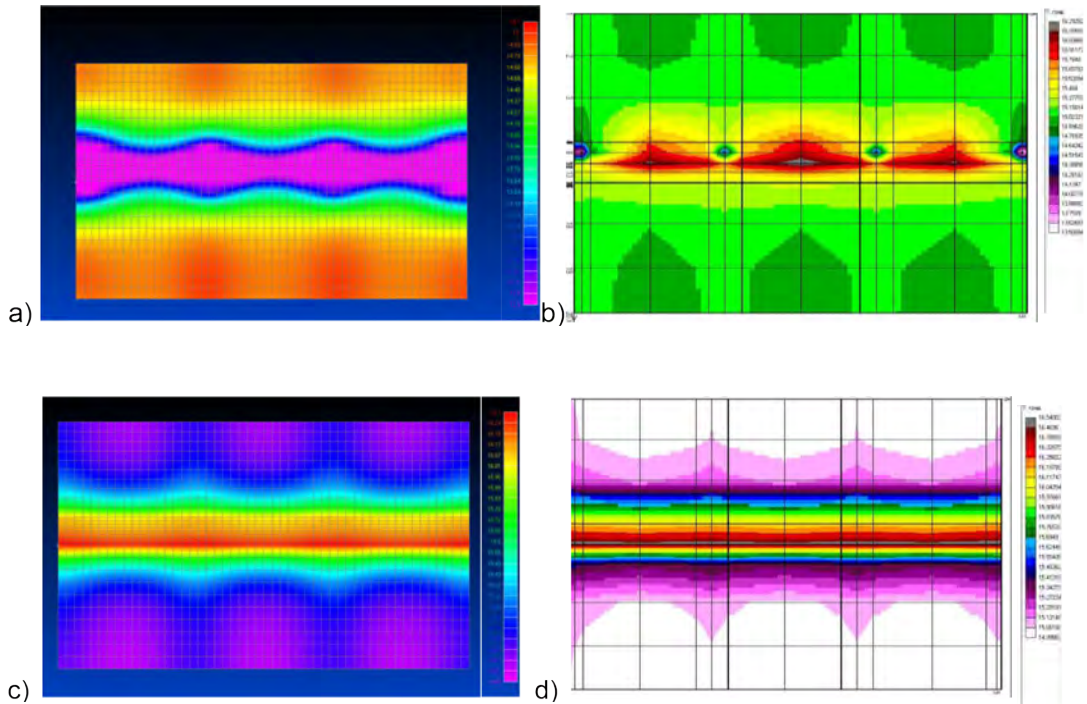


Figure 5. Comparative contour plots of temperature distribution on the inner face of sandwich-panel fastened to purlin with the use of: a, b – rivets (a-MSC.NASTRAN; b-TEPL); c, d – screws (c-MSC.NASTRAN; d-TEPL)

Table 2. Comparison of the thermal resistance values of structures made using screws obtained in program TEPL and manually by methods of SNiP "Thermal performance of buildings"

$R_o, (m^2 \cdot ^\circ C) / W$		The relative difference
Numerical analysis	Manual analysis	
1,6734	1,8877	12.8%

## CONCLUSIONS

As a result of carried out analysis the following conclusions can be drawn:

1. Self-drilling screws as cold bridges decrease considerably the thermal resistance of roofing and should be taken into account in thermal analysis.
2. The rivets allow achieving higher values of thermal resistance.
3. Though the overall replacement of penetrating fasteners by rivets does not seem to be likely it is still possible to reduce the proportion of them in panel to purlin connections thus reducing the heat losses.

## REFERENCES

1. Vlasov V. Z. (1959) Thin-walled elastic beams. - M.: Fizmatgiz, 574 p.
2. Heinisuo M., Liukkonen V.-P., Tuomala M. (1995) New beam element including distortion // Nordic Steel Construction Conference, pp.65-72.
3. Vatin N.I., Rybakov V.A. (2007) An analysis of metal structures - the seventh degree of freedom // StroyPROFIL. No. 2(56), pp. 60-63.
4. Ayrumyan E.L. (2008) The features of the analysis of thin-walled cold-formed steel structures // Montazhnyye i spetsialnyye raboty v stroitelste. No. 3, pp. 2 7.
5. Belyy G.I. (2014) Some methods of calculating rod elements of constructions from thin-walled cold-bent profiles // Bulletin of Civil Engineers. No. 4 (45), pp. 32-37
6. Mezentseva Ye.A., Lushnikov S.D. (2009) Prefabricated buildings of light steel structures // Vestnik MGSU. Spetsvypusk No. 1, pp. 62-64.
7. EN 1993-1-3:2004 Eurocode 3: Design of steel structures. Part 1-3: General rules - Supplementary rules for cold-formed members and sheeting.
8. Tusnina O. (2013) Design of thin-walled Z-purlins connections with sandwich panels in roof made by rivets // Design, Fabrication and Economy of Metal Structures, International Conference Proceedings, Miskolc, Hungary, pp. 157-163.
9. Ayrumyan E. L. (2009) Blind rivets or self-frilling screws? (Recommendations on application in light steel thin-walled structures) // Montazhnyye I spetsialnyye raboty v stoitelstve. No. 3, pp. 2-8.
10. Patankar S. (1984) Numerical heat transfer and fluid flow. - M.: Energoatomizdat, 150 p.
11. Svod pravil SP 50.13330.2012 Thermal performance of the buildings/ Minregion Rossii. Moscow, 2012. 95 p.

# COLUMN BUCKLING CURVES FOR HIGH STRENGTH STEEL

**Kuldeep S. Virdi**

Emeritus Professor of Structural Engineering, City University London

## INTRODUCTION

Steel manufacturers worldwide are producing steel of higher and higher grades. One perceived drawback of higher grade steels is a reduction in ductility. Current building standards adopt ultimate strength as one of the limit states of design. Calculation of ultimate strength on the basis of sufficient plasticity in the cross-section has been shown to be logical and has led to economical designs of steel structures. To ensure this level of plasticity is realised in building structures, Eurocode 3 (EN 1993-1-1, 2010) specifies certain criteria for ductility of structural steels. While grades of steel up to S460 are deemed to satisfy the ductility criteria in Eurocode 3, the current rules prevent higher grades of steel being used in buildings. Earlier studies, notably (Može, Beg and Lopatič 2007), showed that structural elements made of these higher grades of steels do exhibit sufficient ductility. A project with the acronym ROUSTE was initiated, funded by EU's Research Fund for Coal and Steel, to investigate thoroughly the structural behaviour of beams, columns and connections to demonstrate that higher grades of steel up to S960 do indeed display sufficient plasticity before failure. One of the aims of the project is to propose alternative ductility criteria which would permit the use of grades of steel up to S960 without compromising safety. As part of this investigation, it was necessary to examine the required buckling curves for the design of axially loaded columns made of this grade of steel.

## PREVIOUS STUDIES

Since grades of steel above S460 are of relatively recent development by the steel manufacturers, published literature is rather limited.

## COMPUTATIONAL APPROACH

In this approach, theoretical failure loads are obtained using the finite difference method. A key feature of the method is that it is extremely fast when compared with finite element computations and yet provides similar level of accuracy. The output is the ultimate load rather than a critical load based on eigenvalues.

The method is based on calculating the equilibrium deflected shape of the column, in the form of deflections at a discrete number of points, for increasing

values of the applied loading. With increasing amount of inelastic stresses developing within the column, the stiffness of the column progressively reduces until, just before collapse, it completely vanishes. The load corresponding to the final deflected shape so obtained is taken as the ultimate load. This is very similar to the procedure usually taken in experimental evaluation of ultimate load.

The calculation of the deflected shape of the column in equilibrium with some applied loading requires two basic algorithms. The first relates to the calculation of the stress resultants within the section for an assumed strain distribution over the cross-section. This phase is often referred to as the calculation of the moment-thrust-curvature relationship. The second algorithm deals with improving the values of the assumed deflections, so that internal stress resultants approach equilibrium with the external forces and moments at convergence. For this phase, a variety of iteration methods can be adopted. In this work a rapidly converging Newton-Raphson procedure has been described.

The evaluation of internal stress-resultants at points along the length of the column is carried out using two-dimensional Gauss quadrature together with mapping of the quadrilaterals using the so-called natural coordinates (Viridi 1981). Calculation of the equilibrium deflected shape for a given axial load is based on finite differences, sub-dividing the column length into equal segments and satisfying equilibrium at the nodal points. Generalised Newton-Raphson iterative procedure has been used. Having obtained an improved approximation to the true solution, the process is repeated until satisfactory convergence has been obtained (Viridi 1981). The ultimate strength of a column (stability analysis) can be found by using the above procedure for first finding the equilibrium deflected shape for a small value of the applied load. The load is then increased and the procedure is repeated. The highest value of the load for which an equilibrium deflected shape can be obtained is accepted as the ultimate load of the column as shown in Figure 1.

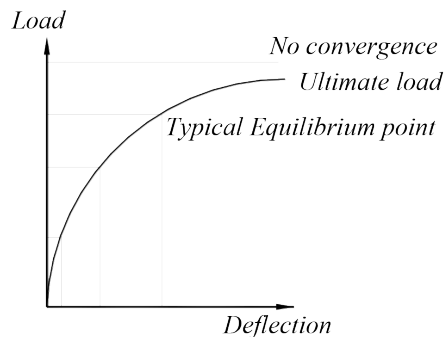


Figure 1. Load-deflection graph for stability analysis



The above method has been validated against tests on composite columns [3] and circular and rectangular hollow section columns (Viridi 1981). Parametric studies using the above method have led to a design method (Viridi and Dowling 1976), which formed the basis for current design rules for axially loaded composite columns in Eurocode 4 (EN 1994-1-1 2009). A computer program, labelled COMPSEF, based on the above method has been used in the present study. The computer program gives the graphical interpretation of the cross-section idealisation, a fully annotated printout of results including deflected shape of the column at each stage of loading and a load-deflection plot which gives confidence in the ultimate load obtained. The printed data can be used to examine the state of stress at any of the finite difference points along the length of the column.

## **PARAMETRIC STUDY**

To build the buckling curve, a parametric study was undertaken. A range of cross-sections used in practice was chosen. Material properties adopted were based on test done by one of the partners in the project Ruoste. Columns were analysed for several lengths covering the range of slenderness parameter  $\lambda$  specified in the Eurocode 3 (EN 1993-1-1, 2010). The loading on the columns was perfectly axial force, that is, with zero end-eccentricity. Instability was introduced using a sinusoidal lack of slenderness of the column length divided by 1000. This value has been adopted in several studies aimed at defining the column buckling curve, for example, that for composite columns (Viridi and Dowling 1976). In the present study, residual stresses were not considered.

## **STRESS-STRAIN CURVE**

Stress-strain curve obtained by one of the partners in the project Ruoste, has been adopted. The raw data has imperfections, as shown in Figure 2 below with the strain axis stretched horizontally. This arises inevitably from the measurement system used.

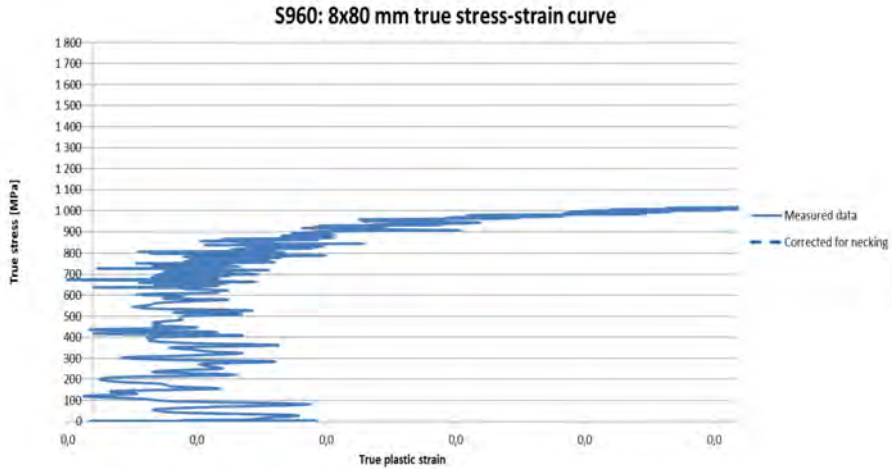


Figure 2. Stress-strain curve from manufacturer

To obtain smooth stress-strain curves, 7 cubic splines (zzz) were used fit the raw data. The purpose-made program automates processing of test data and produces output in graphical form. Figure 3 below shows the excellent fit obtained.

The graph in Figure 3 also shows that the proof stress (0.002 strain) is 957 MPa. This value can be rounded to 960 MPa. The tangent modulus at the first Cubic Spline Point is 223800 MPa. For practical purposes, the standard Young's Modulus of 200GPa can be safely used. The coefficient of correlation of the errors is: 0.001328, which reflects a very good fit.

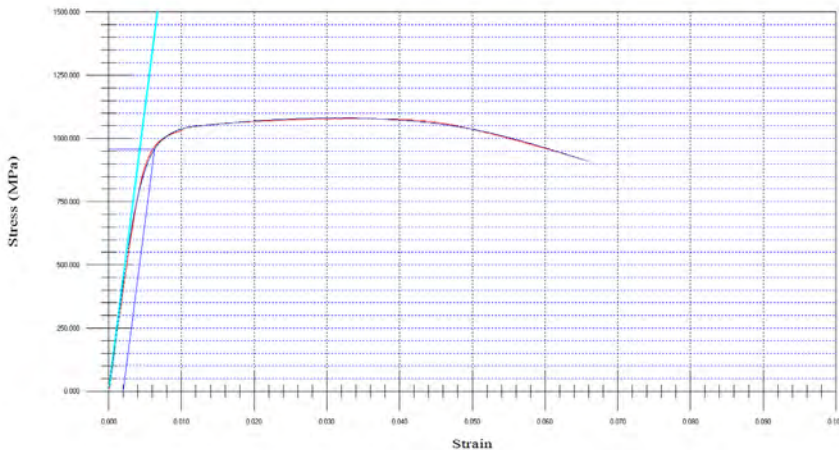


Figure 3. Cubic spline fit to the raw stress-strain data.

## RANGE OF SECTIONS

Five sections were selected from the HEA range. These include the smallest section and the largest section in the range together a few others making an even spread. Both Major axis and Minor axis bending have been covered.

HEA 100    HEA 200    HEA 300    HEA 500    HEA 1000

## RANGE OF COLUMN LENGTHS

Column lengths adopted were in the range 1m to 30m. For a given section, the upper limit was governed by the maximum value of the slenderness parameter as defined in EN 1993-1-1: 2005(E), Fig 6.4 (typically 3.0).

For example, Column HEA 300 was analysed for lengths (in mm) of:

2000	3000	4000	5000	6000
7000	8000	9000	10000	14000

## RESULTS OF PARAMETRIC STUDY

In each case, the computer program generates a plot of the load deflection response. The reducing stiffness of the column as the maximum load is approached gives confidence in the stability analysis. Such curves have been obtained for all the columns analysed in the study. For brevity, only one such graph is presented in Figure 4 below. Results from approximately 60 cases of major axis bending of HEA sections are shown in Figure 5.

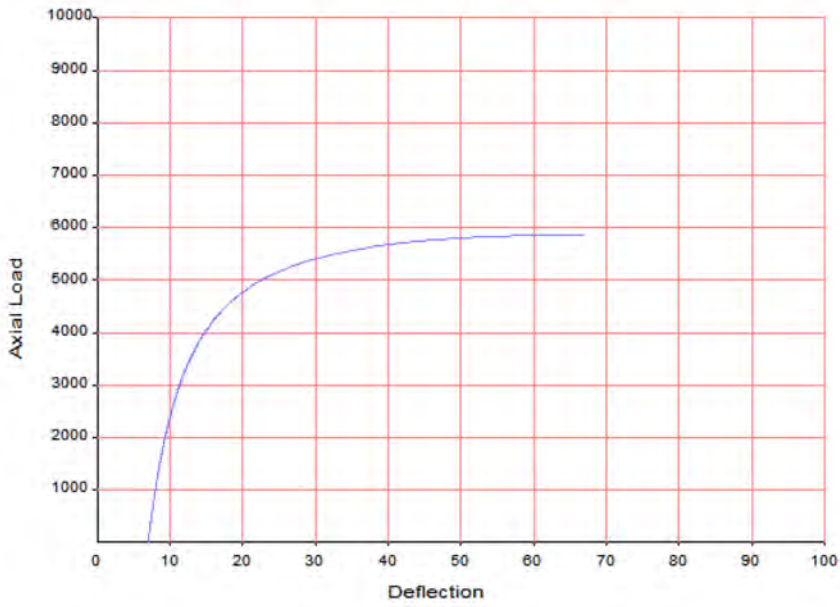


Figure 4. Typical load-deflection response obtained (HEA 300, Length = 7000mm)

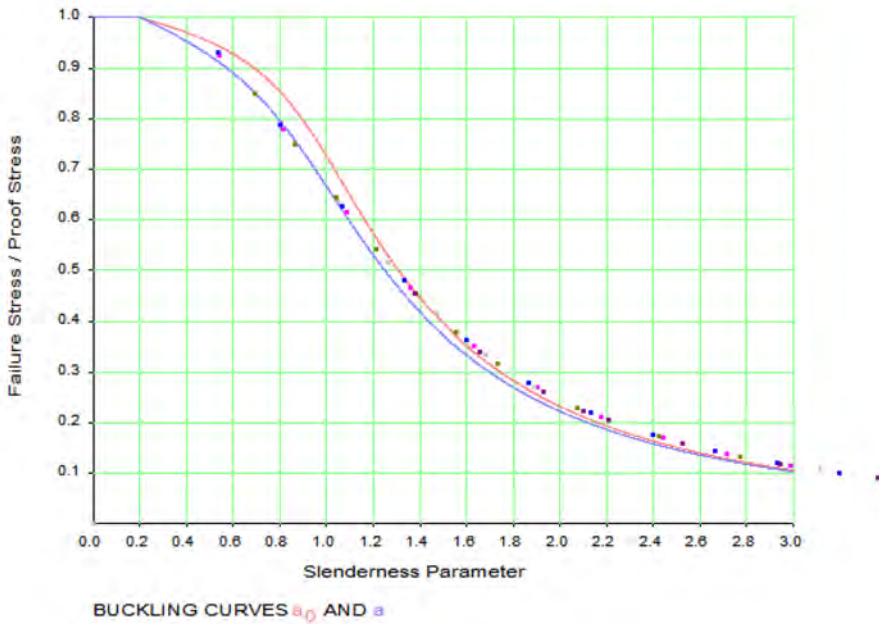


Figure 5. Computed results (Major Axis) compared with EC3 Curves a and a0

Results from approximately 40 cases of minor axis bending of HEA sections are shown in the next slide. There are fewer cases than for Major axis bending because sections larger than HEA300 all have the flange width around 300mm. Thus, the behaviour of sections larger than HEA300 should not differ significantly from that of HEA300. This is borne out by the results obtained.

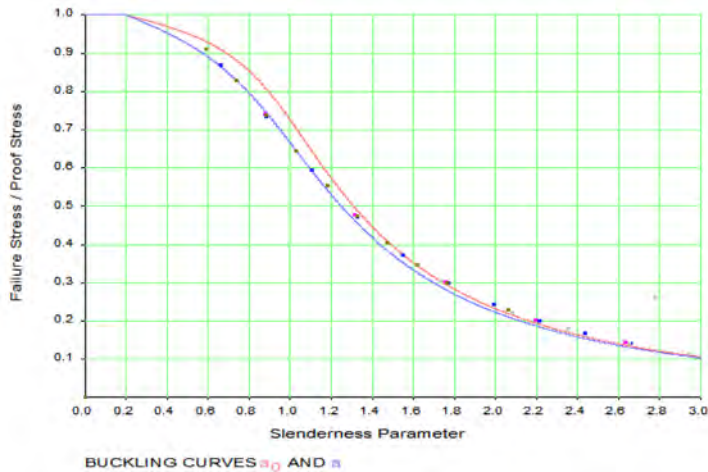


Figure 6. Computed results (Minor Axis) compared with EC3 Curves a and a0

## CONCLUSION

For both the major axis and minor axis bending, Eurocode 3 Curve a is shown to be satisfactory for adoption as the design curve for Grade S960 steel in the short to medium slenderness range.

For very slender columns the data obtained fits Eurocode 3 Curve a0 better than Curve a.

## FURTHER WORK

With the availability of test results, for global buckling as well as residual stress measurements conducted in Ruoste project, these will be used for additional validation of the finite difference method used in the study. Also, the residual stresses will be included in the parametric study to assess if the above conclusion needs to be modified in any form.

## ACKNOWLEDGMENTS

The work described in this paper has been carried out under the Ruoste (Rules On High Strength Steel) project funded by the Research Fund for Coal and Steel, RFSR-CT-2012-00036, 01/07/12 to 30/06/15. The financial support is gratefully acknowledged.

## REFERENCES

- EN 1993-1-1:2005 (2010). Eurocode 3: Design of steel structures – Part 1-1: General rules and rules for buildings, British Standards Institution, London.
- EN 1994-1-1:2004 (2009). Eurocode 4: Design of steel and composite structures – Part 1 1: General rules and rules for buildings, British Standards Institution, London.
- Može, P., Beg, D, and Lopatič, J (2007). Net cross-section design resistance and local ductility of elements made of high strength steel. *Journal of Constructional Steel Research*. Vol. 63, No 11. September, pp.1431-1441.
- Virdi, K S (1981). Design of circular and rectangular hollow section columns. *Journal of Constructional Steel Research*, Vol. 1, No 4. September, pp. 35-45.
- Virdi, K S and Dowling, P J (1976). The Ultimate Strength of Biaxially Restrained Columns. *Proceedings. The Institution of Civil Engineers, London*, Vol. 61, March, pp. 41-58.
- Virdi, KS and Dowling, P J (1976). A unified design method for composite columns. *IABSE Publications*. Vol.36, pp 165-184.

# STABILIZATION OF STEEL STRUCTURES BY SANDWICH PANELS

Olli Ilveskoski

Häme University of Applied Sciences

## INTRODUCTION

In the previous METNET paper in Luleå 2013 bracing systems, connection forces and stiffnesses were discussed. The basic theory of a dual strength and stiffness criterion for the design of bracing used to control the instability was studied. Eurocode was surveyed from the bracing point of view. Despite the Eurocodes' many rules the designers have to master the theory and the statics in the background to make the right choices. The more exact information about e.g. product properties, connection forces, stiffnesses and the fastenings' properties was needed to master the global bracing.

The possibility to use sandwich panels as stabilizing elements reduces the weight and costs of the frame and creates even the method to design frameless buildings. Especially the use of self-supporting sandwich panels as stabilizing elements for single steel members such as beams or columns has been recently researched by EASIE project and the Recommendations on the Stabilization of Steel Structures by Sandwich Panels 2014 is published.

EASIE project included a vast number of tests and theoretical calculations to verify the European standard EN 14509 and to extend the application area outside the scope of EN 14509. It produced information about e.g. the capacity of the sandwich panels, the capacity of fastenings, stabilizing of single steel members and guidelines for frameless buildings. The guidelines deal only with the stabilization of single steel members such as beams and columns but not the stabilization of the whole building. The sandwich panels shall be used as stiffening elements only in cases, in which the load predominantly consists of quasi-static loads, such as self-weight, snow and wind load. Repeated loads, e.g. loads caused by earthquake, are not covered by the Recommendations.

The objective is to study the global stabilization of the whole building with sandwich panels. The hypothesis is that Sandwich panel diaphragms could replace partially or totally traditional bracing solutions e.g. roof and wall bracing trusses. The diaphragm solutions can be very cost efficient compared with the present practise.

## FRAMES AND BRACING STRUCTURAL COMPONENTS

The most elementary system used for an industrial building consists of two columns and a beam. This configuration can be modified in numerous ways



using various types of connections between the beams and columns and for the column base. The types of structures most commonly used in industrial buildings are portal frames with hinged column bases. Portal frames provide sufficient in-plane stability, and thus only require bracings for out-of-plane stability. Fixed column bases may be considered when heavy cranes are used, as they deflect less under horizontal forces. Hinged column bases have smaller foundations and simple base connections. /14/



Figure 1. Example of a column and beam frame stiffened by sheeting and a diaphragm frame /14/ /17/

The bracing of typical steel portal frame structure with its secondary components is generally achieved by bracing usually with circular members in the plane of the roof or wall. Purlins and side rails support the roof and wall cladding, and stabilise the steel framework against lateral buckling. Alternatively, panels providing shear stiffness or steel profiled sheeting used in diaphragm action can be used to provide sufficient out-of-plane stability.

Purlins transfer the forces from the roof cladding to the primary structural elements, i.e. rafters. Furthermore, they can act as compression members as part of the bracing system and provide limited restraint against lateral torsional buckling of the rafter. For frame spacings up to 7 m, it can be economic to span the profiled sheeting between the rafters without the use of purlins. Larger frame spacings reduce the number of primary structural elements and foundations, but require the use of heavier purlins. In industrial buildings, hot-rolled I.sections as well as cold-formed profiles with Z-, C-, U- or custom-made shapes are used. When cold-formed purlins are used, they are usually located at spacings of approximately 1.5 m to 2.5 m. /14/

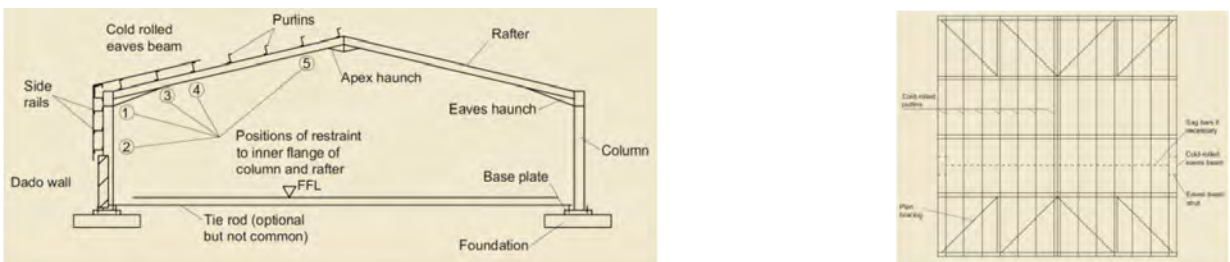


Figure 2. Secondary structural components in a portal frame structure /14/

There are a number types of cladding that may be used in industrial buildings. Single-skin sheeting can generally be used on roof slopes down to as low as  $4^\circ$  provided that the laps and sealants are as recommended by the manufacturers for shallow slopes. The sheeting is fixed directly to the purlins and side rails, and provides positive restraint. Generally steel sheeting is made of galvanised steel grades S280G, S320G or S275G to EN 10326. The steel sheets are usually between 0.50 and 1.50 mm thick including galvanisation.

Sandwich panels are formed by creating a foam insulation layer between the outer and inner layer of sheeting. Composite panels have good spanning capabilities due to composite action in bending. Both standing seam and direct fixing systems are available. These will clearly provide widely different levels of restraint to the purlins. Sandwich elements for roofs generally have a width of 1000 mm with thicknesses between 70 and 200 mm, depending on the required insulation level and structural demands. Component lengths of up to 20 m for roofs and walls permit constructions without or with few joints. The basic material for the outer layers is usually galvanised coated steel sheeting with thicknesses of 0.4 to 1.0 mm.

Fastening techniques include the connections of the sheets to the supporting structure and the connections between sheets. For the fastening of steel sheeting, screws or rivets are used. For profiled sheeting, at least every second rib has to be fixed to the supporting structure. If sheets are used as a stressed skin diaphragm, the number of fixings have to be designed so that they resist the applied shear flow. /14/

## STABILITY DESIGN

The function of lateral bracing is to provide lateral support to a member in order to prevent it from laterally at the bracing position and by so doing increase the buckling strength of the member. The approach used for the design of bracing providing lateral support to single members in compression is to design each bracing member for the force and stiffness required to effectively hold the compression member in position at each bracing member location. Where several members or assemblies (e.g. roof trusses) have to be braced laterally and a bracing system is to be used, the system must be designed to withstand the lateral loading arising from the bracing members. The forces are determined on the assumption that each compression member will deform in a single wave sinusoidal mode. The maximum deformation of the bracing system under this loading together with any other external loading (e.g. wind loading) the system supports must not exceed span /500.

### Bracing of single members subjected to direct compression by local support

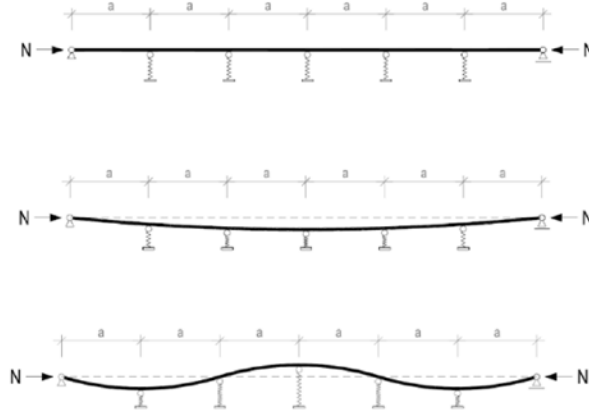


Figure 3. Lateral buckling modes of an elastically supported member

/17/

When determining the buckling strength of the single member its buckling length should be taken to be the distance between adjacent bracing members. Based on classical elastic theory, assuming a perfectly straight member, Timoshenko and Gere have shown the minimum spring stiffness  $C$  to be provided by each bracing member will be:

$$C = k_s \frac{N_d}{a} = 2 \left[ 1 + \cos\left(\frac{\pi}{12}\right) \right] \frac{N_d}{a}$$

/17/

The axial force in the bracing  $F_d$  arising from the design compression force in the member  $N_d$  will be increased due to the initial deviation and from second order linear elastic analyses. A conservative value is  $F_d = N_d / 50$ . /16/

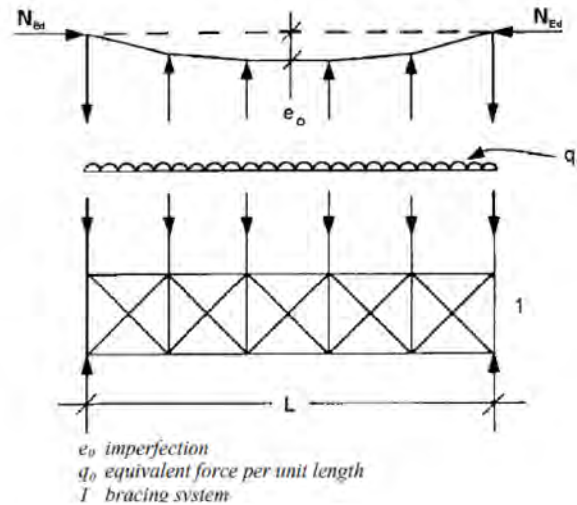


Figure 4. Equivalent stabilising force /6/

Where a bracing system is required to provide lateral stability to a series of compression or bending members (e.g. columns, trusses or beams), this is effectively achieved by providing lateral stiffness using truss or plate action within the plane of the bracing structure. For the general case of a series of similar compression members that require to be braced at positions along their length, the approach is to assume that the deflected shape of each compression member under load will be a sinusoidal form between its supports and will include for the maximum initial out of straightness permitted. Timoshenko and Gere have shown that the problem can be analysed by replacing the initial deviation by an equivalent lateral load acting on the bracing system.

$$q = \sum N_{Ed} \delta \frac{e_0 + \delta_q}{L^2}$$

where  $\delta_q$  is the inplane deflection of the bracing system due to  $q$  plus any external loads calculated from first order analysis. /6/

### Diaphragms

The most economical roof bracing system is achieved by use of a roof diaphragm. A roof diaphragm used in conjunction with a wall cross-bracing or a wall diaphragm system is probably the most economical bracing system. Since design of the diaphragm is essentially that of a deep beam, it is essential to realize that for such a deep beam shear deformations are usually more significant than deformations due to principal stresses in the chord elements.

It is a fact that the framework and cladding will always interact to profoundly affect the behaviour of a complete building. Consequently, frame stresses and deflections calculated on the basis of the bare frame are quite fictitious and are usually quite different from the real values. By taking the cladding into account, the real behaviour of the building can be predicted and worthwhile savings in the cost of the frames can usually be made. /14/

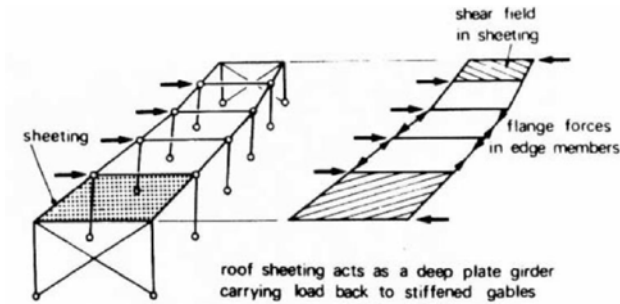


Figure 5. Diaphragm action in a flat roof building /14/

In a flat roofed building subjected to side load each of the roof panels acts as a diaphragm taking load back to the gable ends. If the frames are pin-jointed, then the side loads are resisted entirely by stressd skin action. The structure must be adequately braced during erection. If the frames have rigid joints, then the side loads are shared between the frames and the diaphragms.

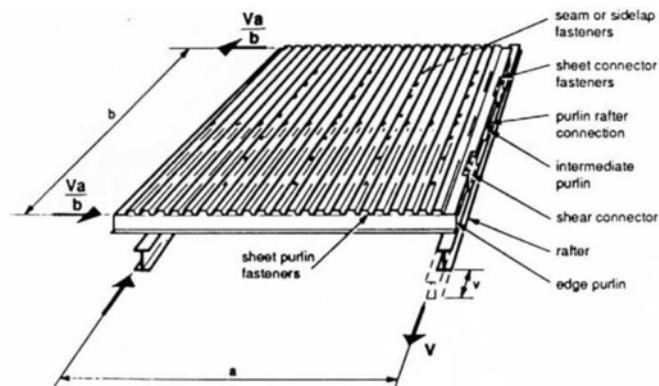


Figure 6. Typical Diaphragm panel /14/

For a typical panel attached on all four sides the strength of the diaphragm depend on a line of seam fastners or line of shear connector fastners. Those two failure modes being ductile, are taken as the design criteria. Any other

failure mode requires to have greater strength than lesser of the above calculated values. Such other modes include e.g. failure at the sheet/ purlin fasteners, shear buckling of the sheeting, failure of the edge members under tension or compression and gross distortion or collapse of the profile at the end of the sheeting.

## SANDWICH PANELS

The European Standard EN 14509 specifies requirements for factory made, self-supporting, double skin metal faced insulating sandwich panels, which are intended for discontinuous laying like roofs and walls. Metal faces can be steel, stainless steel, aluminium or copper. The panel manufacturer shall state the metal grade, thickness and tolerance system of each face. Core materials shall conform to the thermal stability and shrinkage requirements. The adhesion between the core and the faces of the panel has a fundamental role in the satisfactory performance of the panel. The surface preparation of the facing material shall be appropriate for the adhesive or the method of adhesion. The mechanical properties shall be determined according to ISO 12491 and the EN 14509 annexes.

**Table 4 – Test methods, test specimens, type of the test and conditions for ITT**

Characteristic	Test method	Type of test	Min. number of ITT specimens	Compliance criteria and specific conditions
5.1.2 Mechanical properties of a face	EN 10002-1 <sup>a</sup>		3 <sup>a</sup>	
<b>Mechanical properties of a panel and its core material:</b>				
5.2.1.2 Shear strength and modulus	A.3 or A.4 or A.5.6	ITT	3	Statement of declared values
5.2.1.4 Compressive strength and modulus	A.2	ITT	6	
5.2.1.5 Reduced shear strength <sup>c</sup>	A.3.2	ITT	1/10 <sup>d</sup>	
5.2.1.6 Cross panel tensile strength: (and modulus <sup>b</sup> )	A.1	ITT	6	
5.2.1.7 Bending moment capacity and wrinkling stress	A.5	ITT	3	
5.2.1.8 Bending moment capacity over a central support	A.7	ITT	3	
5.2.1.3 Creep coefficient <sup>c</sup>	A.6	ITT	1	[Number]
Cross panel tensile modulus at elevated temperatures <sup>b,f</sup>	A.1.6	ITT	3	
Density	A.8	ITT record		Max, Min, and average densities to be recorded
5.2.2 Thermal transmittance	A.10	ITT	See A.10	Limit value according to A.10
5.2.3 Durability <sup>e</sup>	Annex B	ITT		Pass (see 5.2.3 and Annex B)
5.2.4.2 Reaction to fire	EN ISO 1716, EN ISO 1182	ITT	As specified in EN 13501-1	Classification in accordance with EN 13501-1
	EN 13823 (SBI) EN ISO 11925-2			Specific conditions see C.1
5.2.4.3 Fire resistance <sup>e</sup>	EN 1364-1 or 1364-2	ITT	1	Classification in accordance with EN 13501-2 Specific conditions see C.2
	EN 1365-2 or CEN/TS 13381-1		1	
	EN 14135		1	
5.2.4.4 External fire performance-roofs <sup>b</sup>	ENV 1187	CWFT or ITT	see ENV 1187	Classification in accordance with EN 13501-5 Specific conditions see C.3
5.2.6 Water permeability <sup>e</sup>	EN 12865	ITT	1	EN 12865 and in accordance with A.11
5.2.7 Air permeability <sup>e</sup>	EN 12114	ITT	1	EN 12114 and in accordance with A.12
5.2.9 Airborne sound insulation <sup>e</sup>	EN ISO 140-3	ITT	1	Declaration $R_w(C;C_w)$ (see A.13)
5.2.10 Sound absorption <sup>e</sup>	EN ISO 354	ITT	1	EN ISO 11654 (see A.14)
5.2.5 Dimensional tolerances	Annex D	ITT	1	-

<sup>a</sup> These values are required to adjust test results in accordance with A.5.5.4.  
<sup>b</sup> Required for design purposes only – not declared.  
<sup>c</sup> Roof/ceiling applications only.  
<sup>d</sup> 1/10 = a single test series with 10 specimens.  
<sup>e</sup> Where required.  
<sup>f</sup> Not declared. Required to calculate the wrinkling stress at elevated temperatures.

Figure 7. The mechanical properties test methods



EASIE (Ensuring Advancement in Sandwich Construction through Innovation and Exploitation) European Project presented testing methods as an alternative to design by calculation, which is developed in the EN 14509. EASIE programme carried out 31 examples covering. For each example the strength capacities were solved out; moment in span and on central support, shear on end and central support, reaction to support capacity on end and central support in ULS and SLS and the load span tables.

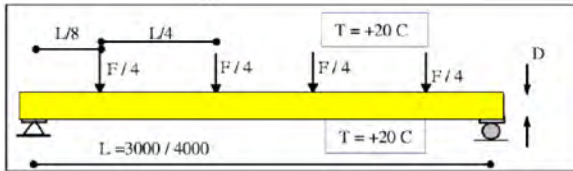


Figure 8. Test arrangement



Figure 9. EASIE test results for rigidities, loads and strength capacities /9/

Extensive parametric studies were carried out to compare the results of the design by testing method with the design by calculation defined in the EN 14509. The design by testing allows to have some benefit by comparison with the design by calculation approach in terms of load/span tables. This is due to the test done in the end use condition and by the use of the rest moment when it's significant.



**Table E.10.1 – Design equations for one-, two- and three-span panels with plane or lightly profiled faces**

	Shear at end support	Shear at internal support	Intermediate support reaction	Bending moment in (end) span	Bending moment at internal support	Maximum deflection in span
Single span of $L$ Uniform load $q$	$\frac{qL}{2}$			$\frac{qL^2}{8}$		$\frac{5qL^4}{384B_s}(1+3,2k)$
Temperature difference $T_1 - T_2$						$\frac{\theta L^2}{8}$
Two equal spans of $L$ Uniform load $q$	$\frac{qL}{2} \left(1 - \frac{1}{4(1+k)}\right)$	$\frac{qL}{2} \left(1 + \frac{1}{4(1+k)}\right)$	$qL \left(1 + \frac{1}{4(1+k)}\right)$	$\frac{qL^2}{8} \left(1 - \frac{1}{4(1+k)}\right)^2$	$-\frac{qL^2}{8} \frac{1}{1+k}$	$\frac{qL^4}{48B_s} \frac{0,26+2,6k+2k^2}{1+k}$
Temperature difference $T_1 - T_2$	$-\frac{3B_s\theta}{2L} \frac{1}{1+k}$	$\frac{3B_s\theta}{2L} \frac{1}{1+k}$	$\frac{3B_s\theta}{L} \frac{1}{1+k}$	$-\frac{3B_s\theta}{4} \frac{1}{1+k}$	$-\frac{3B_s\theta}{2} \frac{1}{1+k}$	$\frac{\theta L^2}{32} \frac{1,1+4k}{1+k}$
Three spans of $L$ Uniform load $q$	$\frac{qL}{2} \left(1 - \frac{1}{5+2k}\right)$	$\frac{qL}{2} \left(1 + \frac{1}{5+2k}\right)$	$qL \left(1 + \frac{1}{2(5+2k)}\right)$	$\frac{qL^2}{8} \left(1 - \frac{1}{5+2k}\right)^2$	$-\frac{qL^2}{10+4k}$	$\frac{qL^4}{24B_s} \frac{0,83+5,6k+2k^2}{5+2k}$
Temperature difference $T_1 - T_2$	$-\frac{6B_s\theta}{L} \frac{1}{5+2k}$	$\frac{6B_s\theta}{L} \frac{1}{5+2k}$	$\frac{6B_s\theta}{L} \frac{1}{5+2k}$	$-3B_s\theta \frac{1}{5+2k}$	$-6B_s\theta \frac{1}{5+2k}$	$\frac{\theta L^2}{4} \frac{1,06+k}{5+2k}$

$$B_s = \frac{E_{F1}A_{F1}E_{F2}A_{F2}e^2}{(E_{F1}A_{F1} + E_{F2}A_{F2})B} \quad k = \frac{3B_s}{E^2G_cA_c} \quad \theta = \frac{\alpha_2T_2 - \alpha_1T_1}{e}$$

$A_c$  = cross-sectional area of the core      ( $G_cA_c = S$  = shear rigidity of the core)

NOTE For geometry and section properties see Figure E.1. For stress systems see Figures E.3 and E.4.

Figure 10. Strength capacities – design by calculation issued EN 14509 /9/

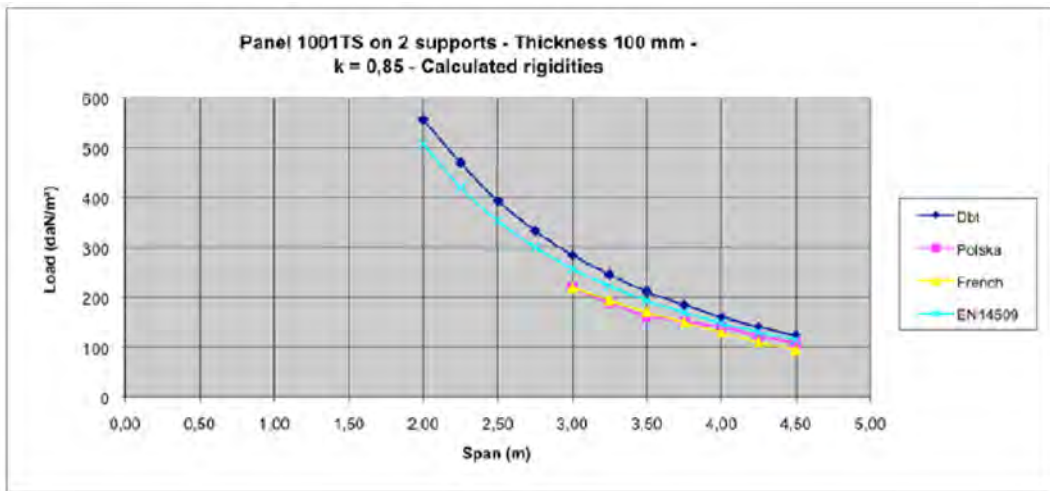


Figure 11. Comparison design by testing and design by calculation /9/

EASIE Programme has produced two guidelines which justify the formula used for the design by testing and that can be also used for the design by calculation. Guideline No 1 deals with flat panels without ribs (cladding panels) and Guideline No 2 deals with ribbed panels with ribs on one face (roof panels).

EASIE project extends the application area outside the scope of EN 14509. It produced information about e.g. the capacity of the sandwich panels, the capacity of fastenings, stabilizing of single steel members and guidelines for frameless buildings. The guidelines deal only with the stabilization of single steel members such as beams and columns but not the whole stabilization of the building. The sandwich panels shall be used as stiffening elements only in cases, in which the load predominantly consists of quasi-static loads, such as self-weight, snow and wind load. Repeated loads, e.g. loads caused by earthquake, are not covered by the Recommendations.

## FASTENINGS FOR SANDWICH PANELS

### Fastening type

Fastenings are typically made at a building site outside the factory. Thus, fastenings are not a subject for a European product standard. The European Recommendations, CIB Publication No. 257 and ECCS Publication No. 115, published in 2000 and 2001, give loading arrangements and procedures with which to determine the tensile and shear resistance of both direct and concealed fastenings.

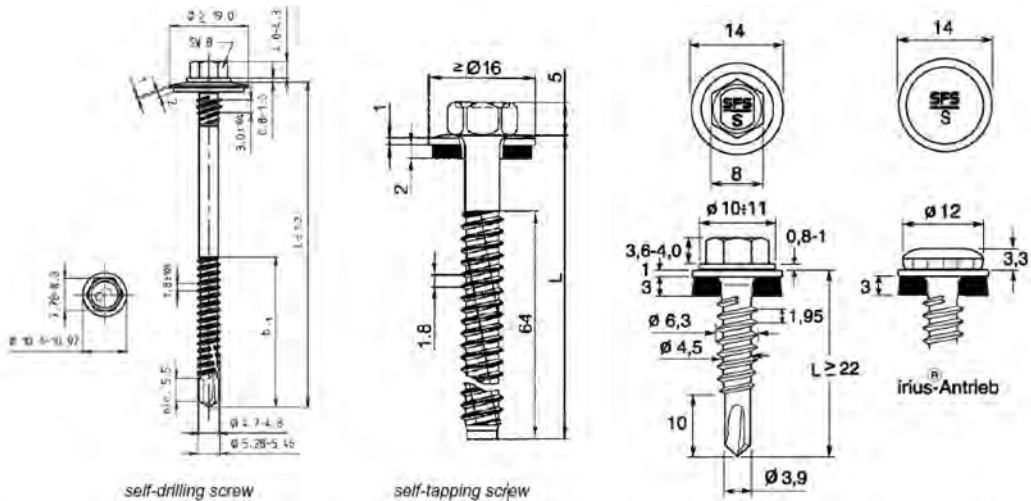


Figure 12. Screw fasteners for fastenings of sandwich panels to substructures and longitudinal joints /13/

Common types of fasteners used to fix sandwich panels to the frames or to the supporting beams are screws drilled through the panels or concealed fastenings placed in the longitudinal or transverse joints of the panels. The screws may have different sizes of washers, different diameters of the screw head and shaft, different geometries and dimensions of the threads in the shaft and finally different structures of the screw ends in order to make it

possible to drill through different materials and material thicknesses of the sub-structure. /12/

Sandwich panels are screwed through the external face sheet to the substructure. The head of the screw and the washer lie on the external face sheet separated from the substructure by the core layer. For the connections of sandwich panels to a steel substructure usually self-drilling or self-tapping screws made of stainless steel are used. The fasteners have a nominal diameter of 5,5 mm to 8,0 mm. The screw fasteners often have an additional support thread, under the head. To get rainproof connections sealing washers with a nominal diameter of approximately 16 mm to 22 mm are used. The sealing washers also increase the resistance against pull-through failure. At the longitudinal joints of roof panels also the external face sheets are connected, whereas this connection mainly contributes to the water tightness and the stabilisation of the large free leg. For determination of the stiffness of shear diaphragms the stiffness of these connections can also be taken into account. Usually for the connection of the external face sheets at longitudinal joints self-drilling screws with nominal diameter 4,8 mm to 6,3 mm are used. To get rainproof and airtight joints sealing washers and often also sealing tapes are used. /13/

The properties and resistance of fastenings have influence on the behaviour of complete sandwich panels. The flexibility of the fastenings changes the deflection of the sandwich panels and has an influence on the bending moment and shear force diagrams of continuous multi-span sandwich panels. The number and location of fastenings at intermediate supports has a direct influence on the bending moment resistance at an intermediate support. /12/

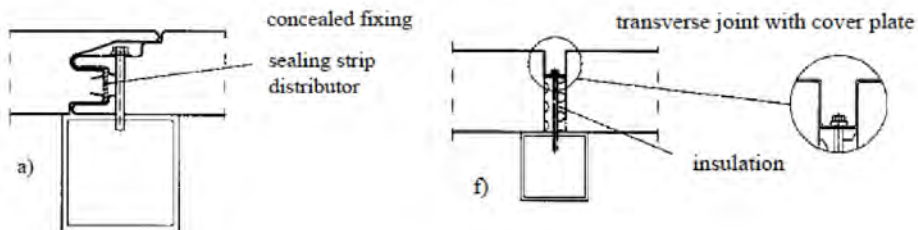


Figure 13. Example of concealed fastenings placed in the longitudinal joints and in the transverse joints of sandwich panels /12/

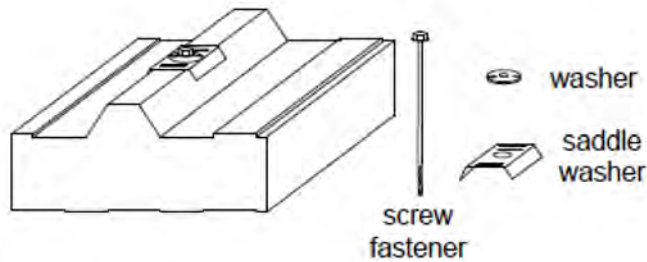


Figure 14. Typical structure of the special strengthening washer plate /12/

Screw fastenings provide supports to the panel which have a certain flexibility. This flexibility has an influence on the deflections of single-span, simply supported wall panels and this may be taken into account by replacing the flexible supports by elastic springs /12/

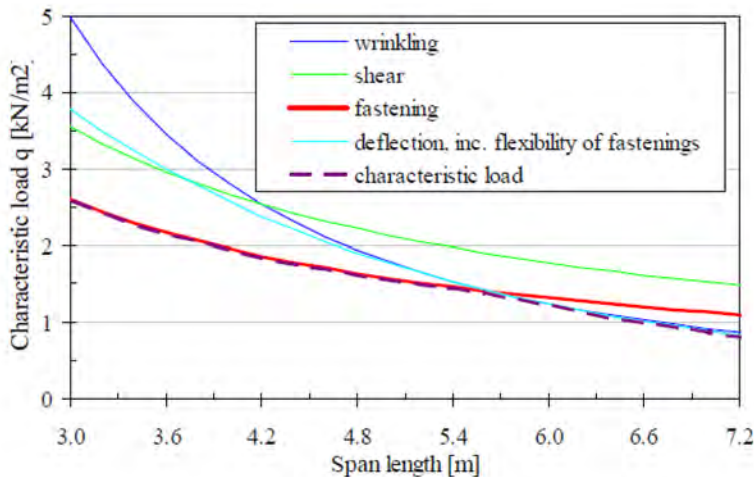


Figure 15. Characteristic wind suction load of a single span and failure criterias/12/

## FASTNING PROPERTIES

For the stiffness of a shear diaphragm the stiffness of the connections is decisive. EASIE Shear Diaphragms Made of Sandwich Panels Project has developed calculation procedures for determination of load bearing capacity and stiffness of fastenings of sandwich panels.

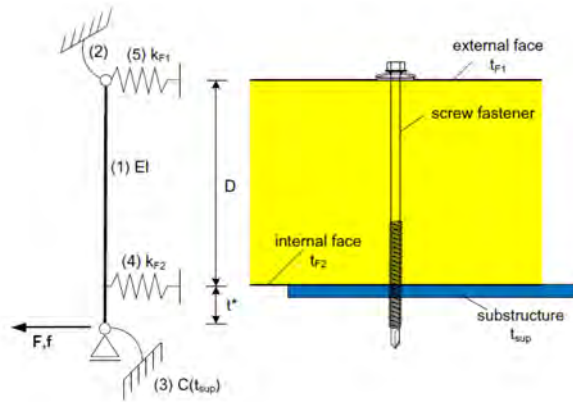


Figure 16. The rotational and longitudinal spring in the model of a fastening /13/

The stiffness of a single component is included as rotational or longitudinal spring in the model of a fastening. If the stiffness of all single components is known, the stiffness of the fastening can be calculated. In addition EASIE Program consists full-scale tests on fastenings to verify the mechanical model and the stiffness determined for the single components. /13/

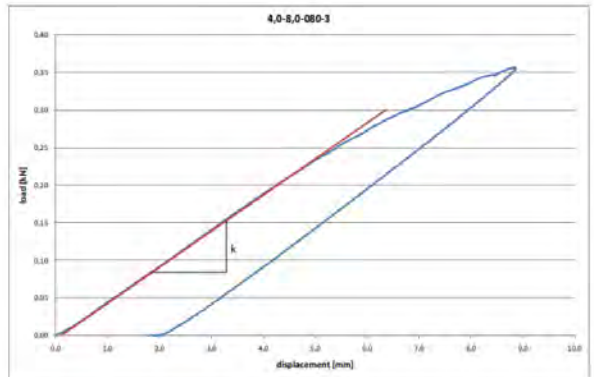
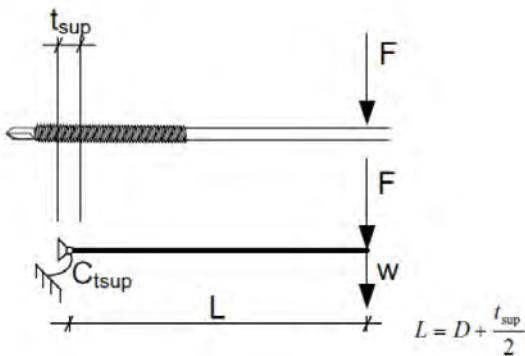


Figure 17. Bending test /13/

The displacement  $w$  at point of load introduction consists of two parts - bending of the fastener and rotation of the fastener at the point of clamping in the substructure. The effect of clamping in the substructure can be considered by a rotational spring with the stiffness  $C$ .

$$w = F \cdot \left[ \frac{L^3}{3 \cdot EI} + \frac{L^2}{C} \right] = \frac{F}{k} \quad C = \frac{L^2}{\frac{1}{k} - \frac{L^3}{3 \cdot EI}}$$

/13/

No.	t <sub>sup</sub> [mm]	D [mm]	L [mm]	d <sub>s</sub> [mm]	EI [N/mm <sup>2</sup> ]	k [N/mm]	C [Nmm]
5,0-5,5-120-1	4,88	120	122,44	4,52	4097827	3,88	138273
5,0-5,5-120-2	4,88	120	122,44	4,52	4097827	4,00	148891
5,0-5,5-120-3	4,88	120	122,44	4,52	4097827	3,79	130885
6,0-6,3-40-1	5,70	40	42,85	5,26	7515240	111,11	333211
6,0-6,3-40-3	5,70	40	42,85	5,26	7515240	114,81	351725
6,0-6,3-80-1	5,70	80	82,85	5,26	7515240	21,56	324419
6,0-6,3-80-2	5,70	80	82,85	5,26	7515240	20,22	283267
6,0-6,3-80-3	5,70	80	82,85	5,26	7515240	22,22	347014
6,0-6,3-120-1	5,70	120	122,85	5,26	7515240	7,04	252336
6,0-6,3-120-2	5,70	121	123,85	5,26	7515240	6,85	248503
6,0-6,3-120-3	5,70	120	122,85	5,26	7515240	7,41	286286
8,0-8,0-40-2	7,80	41	44,90	6,81	21114867	235,29	714623
8,0-8,0-80-1	7,80	80	83,90	6,81	21114867	50,00	659315
8,0-8,0-80-2	7,80	80	83,90	6,81	21114867	51,25	690880
8,0-8,0-110-1	7,80	112	115,90	6,81	21114867	21,43	608208
8,0-8,0-110-3	7,80	110	113,90	6,81	21114867	22,22	598468

Figure 18. Bending test stiffness of fastenings /13/

The stiffness C of the rotational spring representing the clamping of the fastener in the sub-structure can be determined by the following formula:

$$C = 2400 N / mm^2 \cdot \sqrt{t_{sup} \cdot d_1^5}$$

/13/

t<sub>sup</sub> thickness of substructure and d<sub>1</sub> minor diameter of thread

### Hole elongation

The load bearing capacity of an elongated hole depends on the thickness and the tensile strength of the sheet and on the diameter of the fastener or the diameter of the hole. According to EN 1993-1-3 for steel sheets with t < 1,0 mm

the load bearing capacity of a fastening depends linearly on the square root of the diameter of the fastener, linearly on the tensile strength of the steel sheet and linearly on the thickness of the steel sheet in the power of 1,5.

/13/

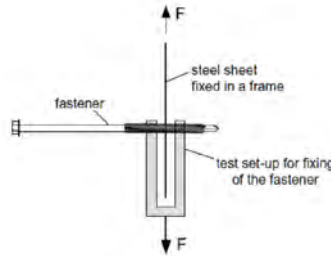


Figure 19. Hole elongation test /13/

### Load bearing capacity of fastenings

The load bearing capacity of a fastening is limited by the load bearing capacity of the elongated hole of the internal face.

$$F_{Rk} \approx F_{F,Rk} = 4,2 \cdot \sqrt{t_{F2}^3 \cdot d_1} \cdot f_{u,F2} \quad F_{Rd} = \frac{F_{Rk}}{\gamma_{M2}}$$

/13/

The stiffness of fastnings  $k_v$  is

$$k_v = k_{vl} \quad k_{vl} = \frac{F_1}{f_1} = \frac{1}{\frac{x_{Fl}}{k_{F2l}} + \frac{t_{sup}^2 + 2 \cdot (1 - x_{Fl}) \cdot D \cdot t_{sup}}{4 \cdot C} + \frac{3 \cdot (1 - x_{Fl}) \cdot D \cdot t_{sup}^2 + 2 \cdot t_{sup}^3}{24 \cdot EI}}$$

/13/

EASIE programm compares the formula results with full –scale tests and values from literature as well. The conclusion is that all the results are well in line.

Being on the safe side, the stiffness  $k_v$  is given in the table. The values apply for thicknesses of the steel supporting structure from 1.5 mm to 4 mm.



Table 1. Stiffness  $k_v$  of fastenings (kN/mm)

<i>nominal thickness of the inner face sheet <math>t_{F2}</math></i>	<i>S220GD</i>	<i>S280GD</i>	<i>S320GD</i>
<i>0.40 mm</i>	<i>1.6</i>	<i>1.9</i>	<i>2.0</i>
<i>0.50 mm</i>	<i>2.0</i>	<i>2.3</i>	<i>2.5</i>
<i>0.63 mm</i>	<i>2.4</i>	<i>2.9</i>	<i>3.1</i>
<i>0.75 mm</i>	<i>2.8</i>	<i>3.3</i>	<i>3.6</i>

In addition to the connection of the panels to the substructure roof panels are also connected at longitudinal joints. As for fastenings of longitudinal joints both steel sheets have the same thickness ( $t = t_{F1}$ ) the formula of the longitudinal fastenings is

$$F_{Rk} = 3,2 \cdot f_{u,F1} \cdot \sqrt{d \cdot t_{F1}^3} \qquad F_{Rd} = \frac{F_{Rk}}{\gamma_{M2}}$$

$t_{F1}$  is the thickness of external face sheet and  $f_{u,F1}$  is the tensile strength of external face sheet

The stiffness of the longitudinal fastenings can be solved with the formula:

$$k_v = k_{v0,5} = 1900 \frac{N}{mm^3} \cdot t_{F1} \cdot d$$

## DIAPHRAGM BRACING OF A STEEL FRAME

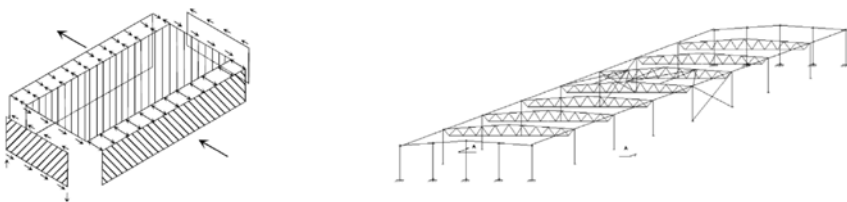


Figure 20. Diaphragm bracing /17/

EASIE project extends the application area outside the scope of EN 14509. It produced information about e.g. the capacity of the sandwich panels, the capacity of fastenings, stabilizing of single steel members and guidelines for frameless buildings. The guidelines deal only with the stabilization of single steel members such as beams and columns but not the whole stabilization of the building. Next challenge will be to develop the use of sandwich panels to

brace whole building frames. Total or partial diaphragm frame bracing with sandwich panels could be a competitive method compared with traditional solutions.

## LOCAL DIAPHRAGM BRACING

Sandwich panels have a high stiffness and strength when loaded in the plane of the panel. This can be used to stabilize the supporting structure of the panels (beams, purlins, columns). The deformation of sandwich panels themselves caused by in-plane shear load may normally be neglected. The flexibility of the fixings usually dominates the shear flexibility. The fixings must be designed for the in-plane shear load. In typical cases, it is not necessary to design the sandwich panels for this additional load, but it is sufficient to design the panels for their primary loading consisting of the distributed snow and wind load and against the forces resulting from the difference of the temperature between the faces. However, this rule resulted from current experiments, which shall not be generalized. The resistance of the individual sandwich panels to in-plane shear load shall be studied in each case. The shear resistance of the individual panels is influenced by imperfections such as incomplete bonding, in addition to material properties and thicknesses. Sandwich panels are normally connected to the supporting structure at the transverse edges only. They usually do not have connections at the longitudinal edges. This is common practice, especially for wall panels. Each panel acts as an individual element. /4/

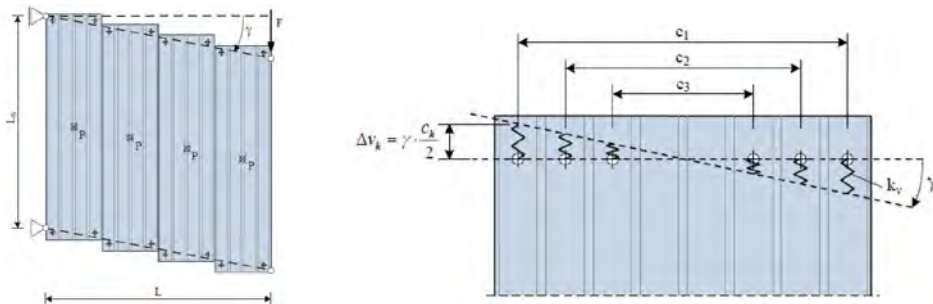


Figure 21. Displacement of shear loaded uni-directionally spanning sandwich panels and fastenings /4/

For stabilization of each beam the shear stiffness available is

$$S_i = \frac{k_v}{2 \cdot B} \cdot \sum_{k=1}^{n_i} c_k^2$$

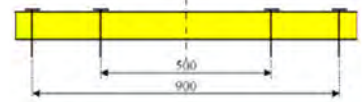
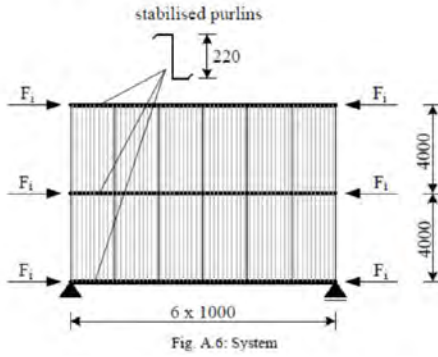


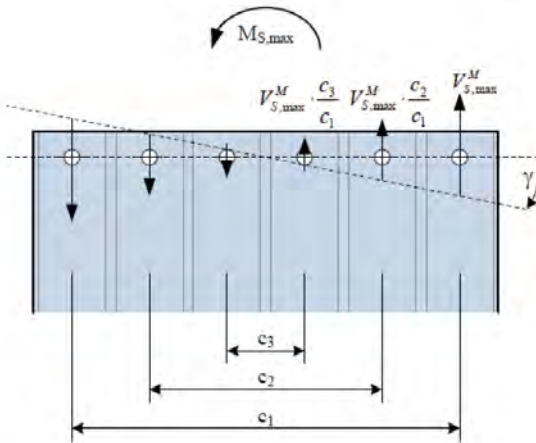
Figure 22. Position of fastenings at the supports of the sandwich panels /4/

For the stabilization of a beam-column with axial force and bending moment

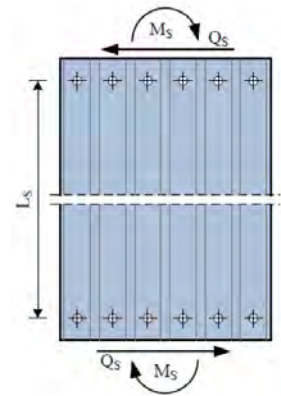
$$F_i = \frac{N_d}{2} + \frac{M_d}{h}$$

For the panels at the ends of the beam-column the moment  $M_S$  is approximately

$$M_{S,max} = m_{i,max} \cdot B = F_i \cdot \left(\frac{\pi}{L}\right) \cdot e_0 \cdot \frac{1}{1 - \frac{F_i}{S_i}} \cdot B$$



Forces resulting in the moment  $M_S$



/4/

The moment  $M_S$  results in the shear forces  $V_{SM}$  in the fastenings. These forces act in longitudinal direction of the panel. The highest forces arise in the outer fastenings of a panel. The force in the highest stressed fastenings is

$$V_{S,max}^M = \frac{M_{S,max}}{\sum \frac{c_k^2}{c_1}} \quad V_{S,max}^Q = \frac{m \cdot M_{S,max}}{L_S \cdot n_f} \quad V_{S,max} = \sqrt{(V_{S,max}^M)^2 + (V_{S,max}^Q)^2}$$

In addition to the design of the fastenings, the displacements resulting from the stabilization should be limited

$$\gamma_{max} = e_0 \cdot \frac{\pi}{L} \cdot \frac{1}{\frac{S_i}{F_i} - 1} \leq \frac{1}{750}$$

/4/

## GLOBAL DIAPHRAGM BRACING PRINCIPLES

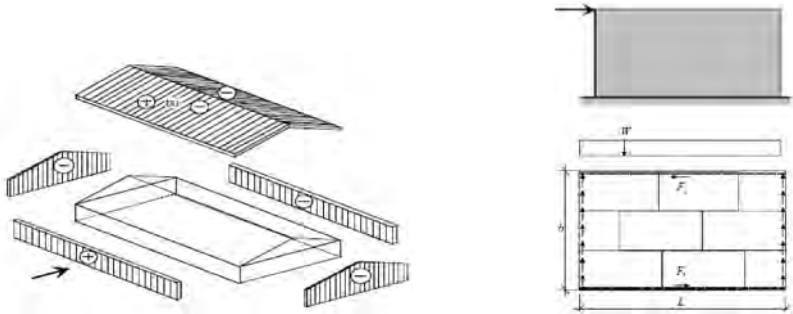


Figure 23. Wind load and Diaphragm bracing /17/

As the whole building frame is braced the horizontal loads are transferred via the structures to the foundation. The design consists of the bracing of the whole frame and single components' internal bracing. Sandwich panels can be used for the single component bracing according to European Recommendations on the Stabilization of Steel Structures by Sandwich Panels /4/. The sandwich panel diaphragms could be used for partial or total stabilization of buildings as the EASIE frameless building studies show. Steel portal frames could use sandwich panels for replacing the roof purling and wall rails braces and sandwich panel diaphragms to replace partially or totally traditional bracing solutions e.g. roof and wall bracing trusses.



Figure 24. Sandwich panel diaphragms / [www.ruukki.com/](http://www.ruukki.com/)

The horizontal wind force of the longitudinal wall and roof slope are transferred to the structures according to the recommendations /17/ as follows:

- half of the longitudinal wall's wind force is transferred to the foundations and the another half to the roof diaphragm
- the roof diaphragm transfers the forces to the end walls' top edge where from the forces move to the foundation via the wall diaphragms and wall bracing

- the roof diaphragm transfers horizontal forces and behaves like a deep beam which height is the frame depth and the length is the roof length
- the wall and roof diaphragm connection has to have capacity to transfer the horizontal forces
- the end walls act like diaphragm walls and must be anchored to the foundation

Steel portal frames and the sandwich panel envelope diaphragms could create a combination structure where the global bracing of the building is arranged with cooperation structures.

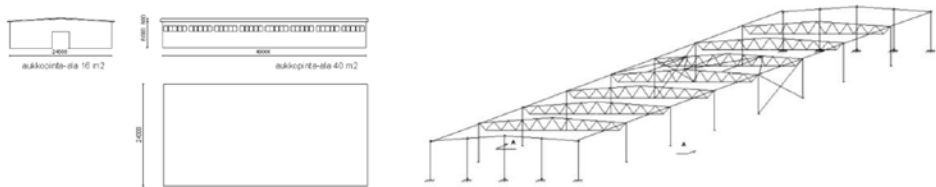


Figure 25. Steel frame and sandwich panel envelope

A typical steel portal frame's bay breath ranges from 15m to 30 m, portal spacing is usually from 5m to 10 m and the heights vary from 4m to 10m. As the building's frame breath is 24m, portal spacing is 6m and the column height 6m the column normal forces can range from 50kN to 300 kN.

If the columns are stabilized to weaker direction with sandwich panels in the longitudinal direction according to the Recommendations /4/ the fastning shear forces range from 223N to 1.7 kN. With the fastning's stiffness value  $k_v = 2340 \text{ N/mm}$  and with the column's normal force value from  $N_d = 250 \text{ kN}$  the maximum displacement of the diaphragm  $\gamma = 1/750 = 0.0013$  is exceeded. As expected the solution's critical member is the fastning's stiffness.

Table 2. Local column member stabilization with sandwich panel diaphragm

$N_d$	$F_i$	$M_{smax}$	$V_{smax}$	$\gamma$
1	51.4	4.712	$4.298 \cdot 10^{-3}$	$3.8 \cdot 10^{-9}$
$5 \cdot 10^4$	$5.005 \cdot 10^4$	$2.455 \cdot 10^5$	223.948	$1.98 \cdot 10^{-4}$
$10 \cdot 10^4$	$1 \cdot 10^5$	$5.126 \cdot 10^5$	467.532	$4.133 \cdot 10^{-4}$
$1.5 \cdot 10^5$	$1.5 \cdot 10^5$	$8.041 \cdot 10^5$	733.458	$6.484 \cdot 10^{-4}$
$2 \cdot 10^5$	$2 \cdot 10^5$	$1.124 \cdot 10^6$	$1.025 \cdot 10^3$	$9.06 \cdot 10^{-4}$
$2.5 \cdot 10^5$	$2.5 \cdot 10^5$	$1.476 \cdot 10^6$	$1.346 \cdot 10^3$	$1.19 \cdot 10^{-3}$
$3 \cdot 10^5$	$3 \cdot 10^5$	$1.865 \cdot 10^6$	$1.701 \cdot 10^3$	$1.504 \cdot 10^{-3}$

If the sandwich panel diaphragm of the longitudinal wall is part of the global bracing system and stabilizes the series of compression steel columns the diaphragm forces must be added the wind forces coming from the end wall of the building. The biggest forces and displacement are on the supports of the longitudinal diaphragm wall.

Table 3. Global frame stabilization with sandwich panel diaphragm

$N_d$	$F_i$	$M_{smax}$	$V_{smax}$	$\gamma$
1	$5.04 \cdot 10^4$	$2.476 \cdot 10^5$	745.966	$1.996 \cdot 10^{-4}$
$5 \cdot 10^4$	$1.004 \cdot 10^5$	$5.148 \cdot 10^5$	985.901	$4.151 \cdot 10^{-4}$
$10 \cdot 10^4$	$1.504 \cdot 10^5$	$8.065 \cdot 10^5$	$1.25 \cdot 10^3$	$6.503 \cdot 10^{-4}$
$1.5 \cdot 10^5$	$2.004 \cdot 10^5$	$1.126 \cdot 10^6$	$1.54 \cdot 10^3$	$9.082 \cdot 10^{-4}$
$2 \cdot 10^5$	$2.504 \cdot 10^5$	$1.478 \cdot 10^6$	$1.859 \cdot 10^3$	$1.192 \cdot 10^{-3}$
$2.5 \cdot 10^5$	$3.004 \cdot 10^5$	$1.868 \cdot 10^6$	$2.214 \cdot 10^3$	$1.506 \cdot 10^{-3}$
$3 \cdot 10^5$	$3.504 \cdot 10^5$	$2.301 \cdot 10^6$	$2.608 \cdot 10^3$	$1.856 \cdot 10^{-3}$

As the sandwich panels are used for both local and global diaphragm bracing the fastening forces range from 745 N to 2.6 kN as the column compression forces range from 50 kN to 300 kN. With the fastening's stiffness value  $k_v = 2340$  N/mm and with the column's normal force value from  $N_d = 200$  kN the maximum displacement of the diaphragm  $\gamma = 1/750 = 0.0013$  is exceeded. The influence of the fastening stiffness growth from the value  $k_v = 2340$  N/mm to 3600 N/mm can be checked from the table 3. In that case the fastening shear forces range from 742 N to 2.35 kN displacements are in order with the normal compression forces up to 300 kN.



Table 4. Global frame stabilization with sandwich panel diaphragm with higher fastning stiffness

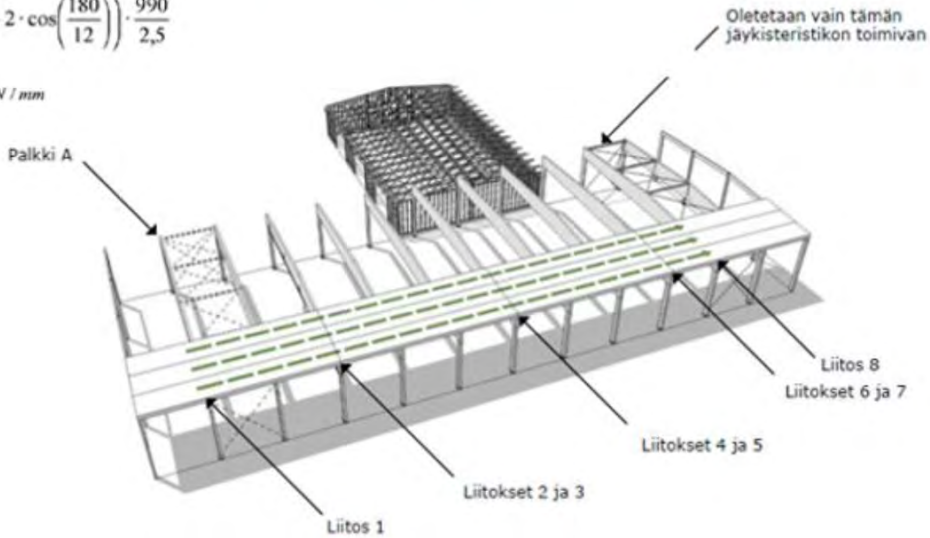
$N_d$	$F_i$	$M_{smax}$	$V_{smax}$	$\gamma$
1	$5.04 \cdot 10^4$	$2.44 \cdot 10^5$	742.736	$1.279 \cdot 10^{-4}$
$5 \cdot 10^4$	$1.004 \cdot 10^5$	$4.994 \cdot 10^5$	972.025	$2.617 \cdot 10^{-4}$
$10 \cdot 10^4$	$1.504 \cdot 10^5$	$7.694 \cdot 10^5$	$1.216 \cdot 10^3$	$4.032 \cdot 10^{-4}$
$1.5 \cdot 10^5$	$2.004 \cdot 10^5$	$1.055 \cdot 10^6$	$1.475 \cdot 10^3$	$5.53 \cdot 10^{-4}$
$2 \cdot 10^5$	$2.504 \cdot 10^5$	$1.358 \cdot 10^6$	$1.75 \cdot 10^3$	$7.119 \cdot 10^{-4}$
$2.5 \cdot 10^5$	$3.004 \cdot 10^5$	$1.68 \cdot 10^6$	$2.043 \cdot 10^3$	$8.806 \cdot 10^{-4}$
$3 \cdot 10^5$	$3.504 \cdot 10^5$	$2.023 \cdot 10^6$	$2.354 \cdot 10^3$	$1.06 \cdot 10^{-3}$

$$C \geq \left( 2 + 2 \cdot \cos\left(\frac{180}{m}\right) \right) \cdot \frac{N_d}{a}$$

$$C \geq \left( 2 + 2 \cdot \cos\left(\frac{180}{12}\right) \right) \cdot \frac{990}{2,5}$$

$$C = 1557 \text{ N/mm}$$

CONNECTION STIFFNESS REQUIREMENT



Palkin A kiepahdustuen jousijäykkyys

$$C = \frac{K_{\text{ser. jänän}}}{8} = \frac{18540}{8}$$

CONNECTION STIFFNESS VALUE

$$C = 2317 \text{ N/mm}$$

Figure 26. Connection stiffness requirement

Minimum spring stiffness C to be provided by each bracing member is:

$$C = k_s \frac{N_d}{a} = 2 \left[ 1 + \cos\left(\frac{\pi}{12}\right) \right] \frac{N_d}{a}$$

/17/

In the example portal frame there are 8 portal spaces so the connection stiffness is divided by it's number, in this case 9.

As the sandwich panels are spacing with  $a = 1000$  mm the required spring stiffness with different column compression forces from 50 kN to 300 kN are from 196 N/mm to 1180 N/mm

Table 5. The required spring stiffness according to different column forces

Nd	$C = 2 \left( 1 + \cos\left(\frac{\pi}{12}\right) \right) \frac{N_d}{a}$
1	$3.932 \cdot 10^{-3}$
$5 \cdot 10^4$	196.593
$10 \cdot 10^4$	393.181
$1.5 \cdot 10^5$	589.77
$2 \cdot 10^5$	786.359
$2.5 \cdot 10^5$	982.947
$3 \cdot 10^5$	$1.18 \cdot 10^3$

The stiffness value of 4 panel fastnings which follow each other in 9 series is depending the fastning stiffness  $k_v$  :

$$k_v = 2340 \quad C := 4 \cdot \frac{k_v}{9} = 1.04 \times 10^3 \quad k_v = 3600 \quad C := 4 \cdot \frac{k_v}{9} = 1.6 \times 10^3$$

The fastning with the stiffness  $k_v = 2340$  N/mm fullfills the criteria up to column normal force 250 kN and with the stiffness  $k_v = 3600$  N/mm even including the column normal force 300 kN.

The roof diaphragm and end wall diaphragms shall be designed with the identical way as the longitudinal wall presented. The conclusion is that the sandwich panel diaphragms could be the total or partial bracing solution for many typical steel portal frames. The interaction between the steel frame and

the sandwich panel diaphragms should be studied more to solve the exact share of each component.

## **SUMMARY**

The objective was to study the global stabilization of the whole building with sandwich panels. Typical framing solution and principles of stability design were presented.

This paper gives a survey about the results of EASIE Ensuring Advancement in Sandwich Construction through Innovation and Exploitation project. It produced information about e.g. the capacity of the sandwich panels, the capacity of fastenings, stabilizing of single steel members and guidelines for frameless buildings. The guidelines deal only with the stabilization of single steel members such as beams and columns but not the stabilization of the whole building frame.

The sandwich panel diaphragms could be used in addition for total or partial stabilization of buildings as the EASIE frameless building and this study shows. Steel portal frames could use sandwich panels for replacing the roof purling and wall rail braces. Sandwich panel diaphragms could as well replace partially or totally traditional bracing solutions e.g. roof and wall bracing trusses. The diaphragm solutions can be very cost efficient compared with the present practise.

The conclusion is that the sandwich panel diaphragms could be the total or partial bracing solution for many typical steel portal frames. The interaction between the steel frame and the sandwich panel diaphragms should be studied more to solve the exact share of each component.

## **REFERENCES**

- 1 Structural Bracing. Brian Chen Joseph Jura
- 2 Load and Resistance Factor Design Manual. American Institute of Steel Construction (AISC)
- 3 European Recommendations on the Stabilization of Steel Structures by Sandwich Panels 2013 CIB
- 4 EN 1990: 2002 + A1:2005 + A1:2005/AC:2010: Eurocode: Basis of structural design.
- 5 EN 1993-1-1:2005 + AC:2009: Eurocode 3: Design of steel structures - Part 1-1: General rules and rules for buildings.
- 6 EN 1993-1-3:2006 + AC:2009: Eurocode 3: Design of steel structures –

Part 1-3: General rules – Supplementary rules for cold-formed members and sheeting.

7 EN 14509:2006: Self-supporting double skin metal faced insulating panels – Factory made products – Specifications.

8 FprEN 14509:2013: Self-supporting double skin metal faced insulating panels – Factory made products – Specifications.

9 EASIE Ensuring Advancement in Sandwich Constructions Through Innovation and Exploitation <http://www.easie.eu/>

10 Column buckling with restraint from sandwich wall elements Hedman-Pétursson, Eva Doctoral Thesis / 2001-08-30

11 Preliminary European Recommendations for the Testing and design of Fastenings for Sandwich Panels 2009 ECCS 127

12 EASIE report No.: D3.3 – part 3 Connections of sandwich panels Best Practise in Steel Design. Research Fund for Coal and Steel

13 Industrial Buildings Frames, Bracings and Diaphragms. Risto Siirilä HUT

14 Jäykistys Tero Lahtela

15 Structural Timber Design to Eurocode 5 Jack Porteous Abby Kermani

16 Puurakenteiden jäykistysuunnittelun ohje VTT Markku Korttesmaa





The METNET network aims to enhance the development potential and the research and innovation capacities of regional innovation systems and wider communities of Europe. METNET provides an international innovation environment for its members and the possibility to expand their regional innovation networks internationally.

METNET seminars and workshops deal with technical aspects of metal construction as well as issues of concern to industry on management, planning and sustainability of projects.

This book covers papers presented and submitted for the tenth annual METNET seminar in October 2015 held at Budapest University of Technology and Economics BME. The seminar continued the METNET tradition of presenting scientific and development papers of high calibre.

PRINTED

ISBN 978-951-784-762-9  
ISSN 1795-4231  
HAMKin julkaisu 15/2015

ELECTRONIC

ISBN 978-951-784-763-6 (PDF)  
ISSN 1795-424X  
HAMKin e-julkaisu 30/2015

**HAMK**  
HÄMEEN AMMATTIKORKEAKOULU  
HÄME UNIVERSITY OF APPLIED SCIENCES